Function and structure of β1-3-glucan-degrading enzymes from the pink snow mold fungus, *Microdochium nivale*

(紅色雪腐病菌 *Microdochium nivale* 由来
β1-3-グルカン分解酵素の機能と構造に関する研究)

Hokkaido University, Graduate School of Agriculture,
Frontiers in Biosciences, Doctor course,
Tomoya Ota

CONTENTS

Abbreviations

BCA: copper-bicinchoninic acid

BSA: bovine serum albumin

Bz: benzoyl

BzCl: benzoyl chloride

Cel_n: cellooligosaccharide of DP*n*

C*m*-L*n*: the n^{th} loop of m^{th} coil

COSY: correlated spectroscopy

DIC: *N,N'*-diisopropylcarbodiimide

DMAP: 4-(dimethylamino)pyridine

DMF: *N,N*-dimethylformamide

DP: degree of polymerization

ESI: electrospray ionization

Et_3N: triethylamine

eq.: equivalent

FT: fourier transform

Gen_n: gentiooligosaccharide of DP*n*

GH: glycoside hydrolase family

HEPES: 4-(2-hydroxyethyl)-1-piperazineethanesulfonic acid

HMBC: heteronuclear multiple bond correlation

HPAEC-PAD: high-performance anion-exchange chromatography with pulsed amperometric detection

HSQC: heteronuclear single quantum coherence

Lam_n: laminarioligosaccharide of DP*n*

LC-MS/MS: liquid chromatography-tandem mass spectrometry

Lev: levulinyl

MS: mass spectrometry

MS4Å: 4Å molecular sieves

NIS: *N*-iodosuccinimide

NMR: nuclear magnetic resonance

PAGE: polyacrylamide gel electrophoresis

PD: potato dextrose

pNP: *p*-nitrophenol

pNP-Fuc: *p*-nitrophenyl β-D-fucopyranoside

pNP-Gal: *p*-nitrophenyl β-D-galactopyranoside

pNP-Glc: *p*-nitrophenyl β-D-glucopyranoside

pNP-Man: *p*-nitrophenyl β-D-mannopyranoside

pNP-Xyl: *p*-nitrophenyl β-D-xylopyranoside

RMSD: root mean square deviation

SDS-PAGE: sodium dodecyl sulfate polyacrylamide gel electrophoresis

Sop_2: sophorose

SPh: phenylthio

TBAF: tetrabutylammonium fluoride

TBDPS: *tert*-butyldiphenylsilyl

TBDPS-Cl: *tert*-butyldiphenylchlorosilane

TfOH: trifluoromethanesulfonic acid

THF: tetrahydrofuran

TLC: thin-layer chromatography

TMSEt: 2-(trimethylsilyl)ethyl

TMSEtOH: 2-(trimethylsilyl)ethanol

Tris: tris(hydroxymethyl)aminomethane

1. General introduction

1.1 β1-3-Glucan

β1-3-Glucan is a polysaccharide with β1-3-D-glucosidic main chain with various structures and distributes in various organisms. As examples, linear β1-3-glucans, curdlan and paramylon, are produced by bacteria and *Euglena gracilis*, respectively (Marchessault and Deslandes 1979), β1-3/1-6-glucans, scleroglucan (Rinaudo and Vincendon 1982) and laminarin (Liu *et al*. 2018), are contained in fungi and seaweeds, respectively, and β1-3/1-4-glucans are present in grass plants (Gómez *et al*. 1997). Several β1-3-glucans, especially β1-3/1-6-glucans from brown algae (Menshova *et al*. 2014; Liu *et al*. 2018) and fungi (Vetvicka and Yvin 2004; Brown and Gordon 2005; Chen and Seviour 2007; Zhang *et al*. 2011; Zhang *et al*. 2013), have been studied for their health benefits such as antitumor, anti-inflammatory, and immunostimulatory activities. In addition, β1-3/1-6-glucans are contained abundantly in fungal cell wall and extracellular polysaccharides that are estimated to contribute to fungal carbon metabolism, growth and survival strategy (Pitson *et al*. 1993). Despite their medical and microbiological importance, their structure-function relationships and degradation mechanisms are not yet fully understood due to their structural diversity. Laminarin from brown algae *Eisenia bicyclis* is composed of β1-3/1-6-linked main chain and β1-6-linked side chains (Menshova *et al*. 2014; Liu *et al*. 2018), scleroglucan from *Sclerotium* spp. and schizophyllan from *Schizophyllum commune*, which are extracellularly secreted, are composed of β1-3-linked main chain and β1-6-D-glucosidic side chains (Rinaudo and Vincendon 1982; Zhang *et al*. 2011; Zhang *et al*. 2013), and fungal cell wall glucan is composed of β1-3-linked main chain with branch of β1-3-glucan chains *via* β1-6-glucosidic linkages (Fontaine *et al*. 2000; Aimanianda *et al*. 2017).

1.2 β1-3-Glucan-degrading enzymes

Corresponding to the variation of β1-3-glucans, various β1-3-glucan-degrading enzymes are present in nature. They can be divided in three types, endo-type hydrolases (EC 3.2.1.6 and EC 3.2.1.39), exo-type hydrolases (EC 3.2.1.21 and EC 3.2.1.58), and phospholylases (EC 2.4.1.31 and EC 2.4.1.97). According to the sequence-based classification of glycoside-acting enzymes (Drula *et al*. 2022), β1-3-glucan-degrading enzymes are found in glycoside hydrolase family (GH) 1, GH2, GH3, GH5, GH8, GH9, GH16, GH17, GH30, GH39, GH55, GH64, GH81, GH94, GH116, GH128, GH131, GH132, GH148, GH149, GH152, GH157, GH158, GH161, GH175, and GH180 (Table 1-1). Of these families, endo-β-1,3-glucanases (EC 3.2.1.39) and endo-β-1,3(4)-glucanases (EC 3.2.1.6), which hydrolyze internal β1-3-linkages of β1-3-glucans, are present in GH5, GH8, GH9, GH16, GH17, GH55, GH64, GH81, GH128, GH132, GH148, GH152, GH157 and GH158 (Table 1-1). Exo-β-1,3-glucanase (EC 3.2.1.58) and β-glucosidase (EC 3.2.1.21), which generally hydrolyze the non-reducing terminal β1-3-linkage of β1-3-glucans and β-glucooligosaccharides, are present in GH1, GH2, GH3, GH5, GH16, GH17, GH30, GH39, GH55, GH116, GH128, GH131, GH132, GH175, and GH180 (Table 1-1). Laminaribiose phosphorylases (EC 2.4.1.31) are in GH94, and β1-3-glucan phosphorylases (EC 2.4.1.97) are in GH149 and GH161 (Table 1-1). The β1-3-glucans with a variety of structures are degraded by the combination of several enzymes listed above.

As mentioned in 1.1, filamentous fungi themselves and their growing environment contain β1-3-glucans, and they secrete various β1-3-glucan-degrading enzymes for their growth and carbon source acquisition. Fungal β1-3-glucan-degrading enzymes are categorized in GH1, GH3, GH5, GH16, GH17, GH30, GH39, GH55, GH64, GH81,

GH128, GH131, GH132, and GH152 (Table 1-1). By using several types of these β-1,3-glucanases with different types of reaction modes, fungi degrade and/or utilize surrounding β1-3-glucans (Pitson *et al*. 1993; Martin *et al*. 2006). Through synergistic action of exo- and endo-type enzymes with different modes of action, fungi effectively degrade the β1-3-glucans (Pitson *et al*. 1993).

1.3 Cell wall degradation of filamentous fungi

β1-3-Glucan is the core component of the fungal cell wall (Gow *et al*. 2017; Gow and Lenardon 2023), and filamentous fungi utilize the β1-3-glucan-degrading enzymes for softening the cell wall and their hyphal growth (Pitson *et al*. 1993; Mouyna *et al*. 2013). Mouyna *et al*. described the putative role of β-1,3-glucanases of *Aspergillus fumigatus* in cell wall remodeling (Mouyna *et al*. 2013). The *A. fumigatus* genome contains 29 genes encoding potential β-1,3-glucanases belonging to GH3, GH5, GH16, GH55 and GH81, and enzymes from each family are expressed during hyphal growth (Gibbons *et al*. 2012). It is suggested that cell wall β1-3-glucan is degraded by combinations of endo-β-1,3-glucanases (GH16 and GH81), exo-β-1,3-glucosidases (GH5 and GH55), and β-glucosidases (GH3).

1.4 Pink snow mold fungus, *Microdochium nivale*

M. nivale is a phytopathogenic ascomycete that infects grasses and cereals found in cool and temperate regions worldwide (Hoshino *et al.* 2009; Tronsmo *et al.* 2001). Under snow cover, it infects host plants, causing pink snow mold (Jamalainen 1974); under cool and humid conditions in the absence of snow, it may also cause fusarium patch on grasses (Tronsmo *et al.* 2001), and is one of the causal agents of fusarium head blight of cereals

(Mesterházy *et al*. 2005). *M. nivale* infects host plants in all seasons by a variety of inoculum, conidia, ascospores, and mycelia (Tronsmo *et al*. 2001). Under snow cover, the mycelia spread through the crown, leaf sheaths, and leaves of host plants, and penetrate into the host plant cells through the stomatal apparatus (Dubas *et al*. 2011).

Microdochium spp. includes plant pathogenic fungi such as *M. nivale* and *M. majas* (Jewell and Hsiang 2013; Marin-Felix *et al*. 2019), and endophytic fungi such as *M. bolleyi* (David *et al*. 2016; Marin-Felix *et al*. 2019). *M. nivale* was originally identified and named as *Lanosa nivalis* by Fries (1825) and reclassified as *Fusarium nivale* by Sorauer (1901) (Tronsmo *et al*. 2001; Jewell 2013). Based on the morphological differences of the conidia between this fungus and *Fusarium* spp., it was reclassified as *Gerlachia* spp. (Gams and Müller 1980). Finally, in 1983, Samuels and Hallett reclassified it as *M. nivale* (Samuels and Hallett 1983; Glynn *et al*. 2005). As these changes in classification indicate, *M. nivale* is regarded as the *Fusarium*-like fungus for a long time.

Despite its severe pathogenicity and damage to major crops, the physiology, particularly carbohydrate metabolism, of *M. nivale* is poorly understood. Cairns *et al*. revealed that this fungus utilizes a variety of carbohydrates from monosaccharides to polysaccharides by observing the growth of mycelia on the plate medium containing various carbohydrates as the sole carbon source (Cairns *et al*. 1995a). The same research group found an invertase from this mycelium grown on sucrose as the carbon source (Cairns *et al*. 1995b). An extracellular carbohydrate 1-oxidase from this fungus was also characterized (Xu *et al*. 2001; Kulys *et al*. 2001). It is known as lactose 1-oxidase based on its activity to lactose (Ahmad *et al*. 2004; Nordkvist *et al*. 2007). There are only these two reports about the characterized carbohydrate related enzymes purified from *M. nivale*,

and no reports about the characterized β1-3-glucan-degrading enzymes from this fungus. Although Hofgaard *et al*. and Gorshkov *et al*. reported about the extracellular activities of several plant cell wall-degrading enzymes from *M. nivale* (Hofgaard *et al*. 2006; Gorshkov *et al*. 2020), these enzymes themselves have not been identified and characterized.

1.5 Purpose of this study

β1-3-Glucans are important for fungal carbon source acquisition and growth. *M. nivale* possibly utilizes these glucans for its growth, but its β1-3-glucan-degrading enzymes have not been identified yet. In this study, the β1-3-glucan-degrading enzymes secreted by *M. nivale* during the growth phase are identified, and their enzymatic functions and structures are investigated. Chapter 2 describes the identification and characterization of β-glucosidase. Through this characterization, the preference of substrate in hydrolysis and products in transglucosylation and condensation are shown. In addition, the mechanism of substrate inhibition is assumed based on the effects of glycosides and monosaccharides on the reaction rates. Chapter 3 describes the identification and characterization of endo-β-1,3-glucanase. By nuclear magnetic resonance (NMR) analysis of the reaction products and the enzyme structure analysis, the molecular mechanism of the endo-type hydrolysis on laminarin is revealed. In chapter 4, related to the analysis of β1-3-glucan-degrading enzymes and the function-structure analysis of β1-3/1-6-glucans, the developed method to synthesize β1-3/1-6-glucooligosaccharide is described. Through this study, the biological roles of the β1-3-glucan-degrading enzymes are discussed based on the detailed characteristics of each enzyme.

Table 1-1. Glycoside hydrolase families containing β1-3-glucan-degrading enzymes

Enzyme type	EC number	Activity	Glycoside hydrolase families
Endo-type hydrolases	3.2.1.6	Endo-β-1,3(4)-glucanase	GH5, GH8, GH9, **GH16**, GH148
	3.2.1.39	Endo-β-1,3-glucanase	GH5, **GH16**, **GH17**, **GH55**, **GH64**, **GH81**, **GH128**, **GH152**, GH157, GH158
Exo-type hydrolases	3.2.1.21	β-glucosidase	**GH1**, GH2, **GH3**, **GH5**, GH16, **GH30**, **GH39**, GH116, **GH131**, GH175, GH180
	3.2.1.58	Exo-β-1,3-glucosidase	GH1, GH3, **GH5**, **GH17**, **GH55**, **GH128**, **GH131**, **GH132**
Phosphorylases	2.4.1.31	Laminaribiose phosphorylase	GH94
	2.4.1.97	β1-3-glucan phosphorylase	GH149, GH161

Bold letters show the families containing fungal β1-3-glucan-degrading enzymes.

1. Identification and characterization of an extracellular β-glucosidase from *M. nivale*

2.1 Introduction

β-Glucosidase (EC 3.2.1.21) hydrolyzes β-glucosides at the non-reducing end of substrates and releases β-D-glucose. The enzyme also catalyzes the reverse reaction of the hydrolysis (condensation) and transglucosylation to produce new glycosidic linkages (Crout and Vic 1998). β-Glucosidases are classified into GH1, GH2, GH3, GH5, GH16, GH30, GH39, GH116, GH131, GH175, and GH180. Of these families, GH3 contains β-glucosidases from bacteria, fungi, and plants. A representative GH3 β-glucosidase is barley HvExoI, which acts on various β-glucosides, such as β-glucans, aryl β-glucopyranosides, and β-glucooligosaccharides (Hrmova and Fincher 1997). GH3 β-glucosidases from filamentous fungi such as *Aspergillus* and *Trichoderma* have been also well studied as key enzymes in biomass degradation. They also act on a wide variety of substrates. Some GH3 β-glucosidases from plant pathogenic fungi are known to be involved in their pathogenicity. For example, plant antifungal saponins such as avenacin and α-tomatine undergo enzymatic hydrolysis to release their terminal D-glucose moieties resulting in reduction of their antifungal toxicity (Bowyer *et al*. 1995; Sandrock *et al*. 1995). Some are involved in degradation of plant cell walls (Walton 1994). β-Glucosidases, MoCel3A and MoCel3B, from the rice blast fungus *Magnaporthe oryzae* cooperate with endoglucanases to degrade plant cell wall polysaccharides, namely cellulose, β1-3/1-4-glucan, and β1-3-glucan (Takahashi *et al*. 2011). Recombinantly produced β-glucosidase UeBgl3A from the smut fungus, *Ustilago esculenta,* also showed hydrolytic activity towards barley β1-3/1-4-glucan in addition to β1-3- and 1-4-linked disaccharides (Nakajima *et al*. 2012).

Several three-dimensional structures of fungal GH3 β-glucosidases, such as *Aspergillus aculeatus* AaBGL1 (Suzuki *et al*. 2013), *Aspergillus fumigatus* AfβG (Agirre *et al*. 2016), *Aspergillus oryzae* AoβG (Agirre *et al*. 2016), *Hypocrea jecorina* HjCel3A (Karkehabadi *et al*. 2014), and *Neurospora crassa* NcCel3A (Karkehabadi *et al*. 2018), have been determined. They are mainly comprised of three domains, which are a $(\beta/\alpha)_8$-barrel-like domain, an α/β sandwich domain, and a fibronectin type III-like domain. Their active sites are formed in the interface of the first and second domains, as observed in barley HvExoI (Varghese *et al*. 1999; Suzuki *et al*. 2013). Subsite −1 residues Asp-92, Arg-156, Lys-189, His-190, Tyr-248, nucleophilic catalyst Asp-280, Trp-281, Ser-451, and acid/base catalyst Glu-509 (AaBGL1 numbering) are conserved and have hydrogen bonding and stacking interactions with the glucosyl moiety of substrates. The subsite +1 of most fungal GH3 β-glucosidases is commonly formed by some aromatic residues, although there are slight differences in the composing amino acids, e.g. Trp-68, Phe-305, and Tyr-511 in AaBGL1 (Suzuki *et al*. 2013; Karkehabadi *et al*. 2014; Karkehabadi *et al*. 2018). The aforementioned broad substrate specificity of GH3 β-glucosidases is attributed to the subsite +1 structure.

Isolates of *M. nivale* with high pathogenicity displayed higher extracellular β-glucosidase activity when they were grown with ryegrass cell wall as their carbon source (Hofgaard *et al*. 2006). From the genome data (Tsers *et al*. 2023), *M. nivale* has five putative extracellular β-glucosidases. One of them belongs to GH1, and the others belong to GH3. Although the knowledges described above suggest the involvement of GH3 β-glucosidase in fungal growth and pathogenicity, the *M. nivale* β-glucosidase itself has not previously been investigated to clarify its enzymatic properties and its protein sequence. In this chapter, the identification of the *M. nivale* GH3 extracellular β-glucosidase,

MnBG3A, and the enzymatic functions of its recombinant enzyme produced in *Komagataella pastoris* transformants are described. The substrate and product specificities in the reaction with oligosaccharide, and the effects of glycosides and monosaccharides on the reaction rates are reported.

2.2 Materials and methods

2.2.1 Purification of MnBG3A

M. nivale strain MCW222-7 was originally obtained from wheat in Memuro, Hokkaido, Japan and stored at −20°C. The hyphae of *M. nivale* MCW222-7, grown on potato dextrose (PD) agar medium (Becton, Dickinson and Company, Franklin Lakes, NJ, USA) at 4°C for 1 week, were cultured in 3 L of PD broth with vigorous shaking at 18°C for 4 weeks. The culture supernatant (2.6 L), obtained by centrifugation (6,000 ×*g*, 10 min, 4°C), was loaded onto a DEAE Sepharose Fast Flow column (Cytiva, Tokyo, Japan; 5.0 cm I.D. × 26 cm) equilibrated with 10 mM sodium phosphate buffer (pH 6.4). After non-adsorbed protein was eluted with the same buffer, adsorbed protein was eluted with a linear gradient of 0–500 mM sodium chloride. Active fractions collected were separated with a Butyl Sepharose 4 Fast Flow column (Cytiva; 2.8 cm I.D. × 12 cm) equilibrated with 10 mM sodium phosphate buffer (pH 7.0) containing 1.2 M ammonium sulfate. After washing with the same buffer, adsorbed protein was eluted with a linear gradient of 1.2–0 M ammonium sulfate. The active fractions collected were concentrated to 4 mL by ultrafiltration using Amicon Ultra YM30 (molecular weight cut off, 30,000; Merck Millipore, Billerica, MA, USA), and loaded on a Sephacryl S-200 column (Cytiva; 1.5 cm I.D. × 98 cm), equilibrated with 10 mM sodium phosphate buffer (pH 7.0) containing 0.1 M sodium chloride. An active fraction was stored at 4°C until analysis.

2.2.2 N-terminal amino acid sequence analysis of MnBG3A and liquid chromatography-tandem mass spectrometry (LC-MS/MS) analysis of tryptic peptides from MnBG3A

Purified MnBG3A (4.4 μg) was transferred to polyvinylidene difluoride membrane (Immobilon-P, Merck Millipore) with Trans-Blot SD Semi-Dry Transfer Cell (Bio-Rad, Hercules, CA, USA) from the sodium dodecyl sulfate polyacrylamide gel electrophoresis (SDS-PAGE) gel. The N-terminal amino acid sequence of the 94-kDa protein was analyzed by direct sequencing with Procise 492HT (Perkin Elmer, Waltham, MA, USA).

MnBG3A (0.88 μg) was separated by SDS-PAGE, followed by in-gel digestion using the In Gel Tryptic Digestion kit (Thermo Fisher Scientific, Waltham, MA, USA). The peptides were purified using the Pierce C18 Spin column (Thermo Fisher Scientific), and analyzed with LC-MS/MS Paradigm MS2 (Michrom BioResources, Auburn, CA, USA) under the following conditions: column, Zaplous α Pep-C18 (0.1 mm I.D. × 150 mm; AMR, Tokyo, Japan); elution, 35–90% acetonitrile linear gradient in 0.1% (v/v) formic acid; flow rate, 0.6 μL/min; MS, LTQ-Orbitrap XL (Thermo Fisher Scientific). Data were processed using the search software Proteome Discoverer (Thermo Fisher Scientific).

2.2.3 Whole genome sequencing of *M. nivale* and identification of the MnBG3A coding sequence

Genomic DNA of *M. nivale* YKP21-4, which was obtained from Dr. Fumihiro Terami [National Agriculture and Food Research Organization (NARO), Hokkaido Agricultural Research Center, Sapporo, Japan], was prepared using the Powersoil DNA isolation kit (Mo Bio, Carlsbad, CA, USA). Genomic DNA libraries were prepared with the Kapa HTP

gDNA Library Kit and sequenced using the Illumina HiSeq 2000 platform (Génome Québec, Montréal, Canada), to generate 100-bp paired-end reads. Reads were assembled with a range of Kmers (49–91), using three different programs: ABySS (Simpson *et al*. 2009), SOAP (Li *et al*. 2008), and Velvet (Zerbino and Birney 2008). After discarding scaffolds less than 100 bp long, the assembly with the highest N50 value was kept for further analysis. An annotated sequence data set (mn 13408) was created from the scaffolds using Augustus ver 3.0.2 (http://bioinf.uni-greifswald.de/augustus) based on the *Fusarium graminearum* gene model. To isolate a candidate gene for MnBG3A, a tblastn search of the mn13408 data set was carried out for N-terminal amino acid sequence of matured protein.

2.2.4 Construction of MnBG3A expression plasmid

From *M. nivale* cells grown at 18°C for 4 weeks, total RNA was prepared with TRIzol reagent (Thermo Fisher Scientific), and treatment with DNase I (Takara Bio, Kusatsu, Japan). cDNA was synthesized using Superscript III First-Strand Synthesis System for RT-PCR (Invitrogen, Carlsbad, CA, USA). The cDNA of MnBG3A was amplified by PCR using primers (5′-ATGCGCGCAACCTCGATCGC-3′, sense, and 5′-CTTGAGGTCAGCGCTGAGGG-3′, antisense) and KOD FX DNA polymerase (Toyobo, Osaka, Japan). The amplified DNA fragment was inserted into the site between the α-factor signal sequence and *c-myc* epitope sequence of pPICZαA (Invitrogen) using the In-Fusion HD Cloning Kit (Takara Bio) according to the manufacturer's method. The cloned DNA was sequenced using Big Dye Terminator v1.1 cycle Sequence Kit (Thermo Fisher Scientific) and Applied Biosystems 3130 Genetic Analyzer (Applied Biosystems, Foster City, CA, USA) with the primers:

5′ AOX primer Fw., 5′-GACTGGTTCCAATTGACAAGC-3′;

MnGH3_500s, 5′-TACTGGCGGCAGGAATTGGG-3′;

MnGH3_1050, 5′-ATCGGCACAGACGTACAGGA-3′;

MnGH3_1600, 5′-GCGACGACCTCATCAAGAAC-3′;

3′ AOX primer Rv., 5′-GCAAATGGCATTCAGACATCC-3′.

2.2.5 Preparation of recombinant MnBG3A

The pPICZαA derivative for the MnBG3A production was linearized at the *Pme*I site, and used for transformation of *K. pastoris* X-33 (Invitrogen; product name is *Pichia pastoris* X-33) by electroporation using Gene Pulser Xcell (Bio-Rad). Transformants were screened on YPDS agar plates [10 g/L yeast extract (Nacalai Tesque, Kyoto, Japan), 20 g/L peptone (Becton, Dickinson and Company), 20 g/L D-glucose, 1 M D-glucitol, and 20 g/L agar (Nacalai Tesque)] containing 100 mg/L Zeocin. The transformant was grown in 400 mL of BMGY medium [10 g/L yeast extract, 20 g/L peptone, 13.4 g/L yeast nitrogen base (w/o amino acids-w/ammonium sulfate, Thermo Fisher Scientific), 4 mg/L biotin, 10 g/L glycerol, and 0.1 M potassium phosphate buffer (pH 6.0)] at 30°C with vigorous shaking for 16 h, and the collected cell by centrifugation (6,000×*g*, room temperature, 20 min) were subsequently cultured in 2 L of BMMY medium (as BMGY, but with 1% v/v methanol replacing glycerol) at 30°C for 144 h. Methanol (20 mL) was added every 24 h. Proteins in the culture supernatant (1.8 L) were precipitated with a 90%-saturation solution of ammonium sulfate, collected by centrifugation (6,000×*g*, 4°C, 20 min), and dissolved in 500 mL of 10 mM sodium phosphate buffer (pH 7.0). The sample was subjected to chromatography on a Butyl Toyopearl 650M column (Tosoh, Tokyo, Japan; 2.8 cm I.D. × 24 cm) using the buffer containing 1.2 M ammonium sulfate

as a mobile phase. Non-adsorbed active fractions were collected and subjected to the same chromatography but using a mobile phase containing 1.6 M ammonium sulfate. Active proteins eluted with a linear gradient of decreasing in ammonium sulfate concentration were collected. After dialysis against 10 mM sodium phosphate buffer (pH 7.0), DEAE Sepharose Fast Flow column chromatography was performed as for the native enzyme. The pooled fractions were dialyzed against 10 mM sodium phosphate buffer (pH 7.0), concentrated by Amicon Ultra YM30, and stored at 4°C until analysis.

2.2.6 Protein assay

Protein concentration in the purification procedures was determined by A_{280} under the assumption that the extinction coefficient of a 1 mg/mL of protein solution is 1.00. The concentration of the purified recombinant MnBG3A was measured by amino acid analysis using a high-speed amino acid analyzer (L-8900; Hitachi, Tokyo, Japan) after complete hydrolysis of 28 μg of the sample, calculated based on the method (Pace *et al*. 1995), in 6 M HCl at 110°C for 24 h. The molecular mass of the subunit and MnBG3A in solution were determined by SDS-PAGE and blue native PAGE (Schägger *et al*. 1994), respectively. For the former, Rapid CBB Kanto (Kanto Chemical, Tokyo, Japan) was used for protein staining. For the latter, the Native PAGE Sample Prep Kit (Life Technologies, Carlsbad, CA, USA) and Native PAGE Novex 4–16% Bis-Tris Gels (Life Technologies) were used according to the manufacturer's instructions. As molecular mass standards, SDS-PAGE Molecular Weight Standards, Broad Range (Bio-Rad) and NativeMark Unstained Protein Standard (Invitrogen) were used for SDS-PAGE and blue native PAGE, respectively. Deglycosylated recombinant MnBG3A was prepared by heat denaturation of MnBG3A (0.42 μg) in 105 μL of 20 mM sodium acetate buffer (pH 5.0) at 100°C for

3 min, followed by incubation with 25 mU endoglycosidase H (Roche Diagnostics, Indianapolis, IN, USA) at 37°C for 18 h.

2.2.7 Standard enzyme assay

The reaction mixture (50 μL), consisting of 1 mM *p*-nitrophenyl β-D-glucopyranoside (pNP-Glc, Tokyo Chemical Industry, Tokyo, Japan), 40 mM sodium acetate buffer (pH 4.6), 0.2 mg/mL bovine serum albumin (BSA, Nacalai Tesque) and an appropriate concentration of enzyme, was incubated at 30°C for 10 min. The enzyme reaction was terminated by adding 100 μL of 1 M sodium carbonate, and liberated *p*-nitrophenol (pNP) was quantified based on the standard line of A_{400} at 0–180 μM pNP. Under these conditions, 1 U of enzyme was defined as the enzyme amount that produces 1 μmol of pNP in 1 min.

2.2.8 Effects of pH and temperature

The optimum pH was determined the same way as the standard activity assay, but the enzyme concentration was 1.92 nM and the reaction buffer was replaced by 80 mM Britton-Robinson buffer with pH values ranging between 2.0 to 10.0 adjusted by titrating a mixture of phosphoric acid, acetic acid, and glycine (80 mM each) with 0.5 M sodium hydroxide. The optimum temperature was measured as for activity but using 1.92 nM enzyme and temperature ranges between 10 to 70°C. For pH stability, the enzyme (19.2 nM) was kept in 25 mM Britton-Robinson buffer (pH 2.0–12.0) at 4°C for 24 h, and residual activity was measured. For the thermal stability, the enzyme (1.92 nM) in 67 mM sodium acetate buffer (pH 4.6) was kept at 30–55°C for 15 min. Three independent replications of each experiment were conducted.

2.2.9 Glycone specificity

pNP β-D-fucopyranoside (pNP-Fuc, Sigma, St. Louis, MO, USA), pNP β-D-galactopyranoside (pNP-Gal, Sigma), pNP-Glc, pNP β-D-mannopyranoside (pNP-Man, Sigma), and pNP β-D-xylopyranoside (pNP-Xyl, Sigma) were used as substrates for recombinant MnBG3A. The enzyme concentration was 1.92 nM for pNP-Glc and 192 nM for the other substrates. The reaction conditions were the same as the standard enzyme assay, but with 2 mM substrate and pH 5.0. Three independent replications of each experiment were conducted.

2.2.10 Kinetic analysis of the reaction with pNP-Glc

The velocities for pNP- and D-glucose-release were measured in a reaction mixture (250 μL) consisting of 0.05–5 mM pNP-Glc, 40 mM sodium acetate buffer (pH 5.0), 0.2 mg/mL BSA and 0.192 nM MnBG3A at 30°C. pNP was quantified based on the standard line of A_{400} at 0–100 μM pNP by measuring A_{400} after reaction aliquots (100 μL) were mixed with 50 μL of 2 M sodium carbonate. D-Glucose was quantified with a Glucose CII Test (Fujifilm Wako Pure Chemical, Osaka, Japan) (Huggett and Nixon 1957; Miwa *et al*. 1972) after aliquots (100 μL) were mixed with 50 μL of 4 M tris(hydroxymethyl)aminomethane (Tris)-HCl buffer (pH 7.0). To this solution, 20 μL of the glucostat reagent was added, and it was incubated at 37°C for 30 min. D-Glucose was quantified based on the standard line of A_{505} at 0–250 μM of D-glucose by measuring A_{505} of the solution. The substrate inhibition of pNP-releasing rates (Fig. 2-1A and B) was analyzed through regression with the rate equation (Eq. 1) by the Gauss-Newton method using R version 3.3.1 (Ihaka and Gentleman 1996).

Eq. 1 $v/[e]_0 = k_{cat}\,[S]/([S]^2 / K_{is} + [S] + K_m)$

where $k_{cat} = k_{+2}k_{+3} / (k_{+2} + k_{+3})$ and $K_m = (k_{-1} + k_{+2})k_{+3} / k_{+1}(k_{+2} + k_{+3})$.

K_{is} is $k_{-4}(k_{+2} + k_{+3}) / k_{+3}k_{+4}$ in Fig. 2-1A and $k_{-4}(k_{+2} + k_{+3}) / k_{+2}k_{+4}$ in Fig. 2-1B.

Inhibition of the pNP releasing velocity by D-glucose was analyzed using the same reaction conditions, but with 0.1–2 mM pNP-Glc and 0–50 mM D-glucose. Equations 2 and 3, theoretically obtained from the reaction schemes according to the steady-state kinetic models 2 and 3 (Fig. 2-1C and D), respectively, were used for the regression.

Eq. 2 $v/[e]_0 = k_{cat}\,[S] / ([S]^2/K_{is} + [S] + K_m[G]/K_{i1} + K_m)$

Eq. 3 $v/[e]_0 = k_{cat}\,[S] / ([S]^2/K_{is} + [S] + [G][S]/K_{i2} + K_m)$

where [S] and [G] are substrate and D-glucose concentrations, respectively.

Kinetic parameters k_{cat} and K_m are the same as defined above. K_{is} is $k_{-4}(k_{+2} + k_{+3}) / k_{+2}k_{+4}$. K_{i1} and K_{i2} are k_{-5}/k_{+5} in Fig. 2-1C and D, respectively. Three independent replications of each experiment were conducted.

2.2.11 Kinetic analysis for the hydrolysis of β-glucooligosaccharides

Reaction rates for sophorose (Sop_2, Sigma), laminarioligosaccharides [degree of polymerization (DP) 2–5; Lam_2–Lam_5, Megazyme, Bray, Ireland], cellobiose (Cel_2, Sigma), cellotriose (Cel_3, Megazyme), cellotetraose (Cel_4, Megazyme), and gentiobiose (Gen_2, Nacalai Tesque) were measured. For each substrate, a reaction mixture (100 μL) consisting of 0.08–0.4 mM substrate, 40 mM sodium acetate buffer (pH 5.0), 0.2 mg/mL BSA, and MnBG3A (1.92 nM for Sop_2 and 0.192 nM for the others) was incubated at 30°C for 10 min. Liberated D-glucose was measured as described above after aliquots (100 μL) were mixed with 50 μL of 4 M Tris-HCl buffer (pH 7.0). For the disaccharide reaction rates, half of the glucose-releasing rates were used. Nonlinear regression with

the Michaelis-Menten equation on [S]-*v* plots was done using Grafit version 7 (Erithacus Software, West Sussex, UK). Three independent replications of each experiment were conducted.

2.2.12 Transglucosylation with Gen_2 and Lam_2

A reaction mixture (50 μL) containing 20 mM Gen_2 or Lam_2, 40 mM sodium acetate buffer (pH 5.0), and 19.2 nM MnBG3A was incubated at 30°C. Aliquots (10 μL) were taken at 10, 30, 60, and 120 mins (Gen_2) or 3, 6, 9, 20, and 30 mins (Lam_2), and kept at 100°C for 3 min to terminate the reaction. One μL of each reaction solution was analyzed by thin-layer chromatography (TLC) using a Silica gel 60 F_{254} plate (Merck, Darmstadt, Germany) developed in 2-propanol:1-butanol:water 12:3:4 and 2:2:1 (v/v/v) for the products from Gen_2 and Lam_2, respectively, followed by detection with acetic acid:sulfuric acid:anisaldehyde 100:2:1 (v/v/v).

2.2.13 Condensation of D-glucose

A reaction mixture (100 μL) consisting of 2.1 M D-glucose, 10 mM sodium phosphate buffer (pH 7.0), and 9.6 μM MnBG3A was incubated at 30°C for 4 days. The reaction was terminated by heating the sample at 100°C for 3 min. Sugar composition was analyzed by TLC developed in 2-propanol:1-butanol:water 2:2:1 (v/v/v) as described in the section 2.2.12, and by high-performance anion-exchange chromatography with pulsed amperometric detection (HPAEC-PAD) using CarboPac PA-1 (4 mm I.D. × 250 mm; Thermo Fischer Scientific) in 0.4 M sodium hydroxide at 0.8 mL/min.

2.2.14 Allosteric effects of pNP-glycosides and monosaccharides on pNP-Glc hydrolysis

The pNP-releasing velocity was measured under the same reaction conditions described in the section 2.2.10, but 0.2 mM pNP-Glc in the presence of 0–2 mM pNP-glycoside (pNP-Gal, pNP-Man, and pNP-Xyl) or 0.1–2 mM pNP-Glc in the presence of 0–2 mM pNP-Xyl. pNP was quantified as described in the section 2.2.10. Equation 4, theoretically obtained from the reaction schemes according to the steady-state kinetic models (Fig. 2-2A and B), was used for the regression using Grafit version 7.

Eq. 4 $v/[e]_0 = k_{cat}\,[S] \,/\, \{[S]^2/K_{is} + ([pNP\text{-}Xyl]/K_{i3} + 1)\,[S] + K_m\}$

where [pNP-Xyl] is pNP-Xyl concentration.

Kinetic parameters k_{cat}, K_m, and K_{is} are the same as defined in Eq. 2 and 3 (2.2.10). K_{i3} is k_{-5}/k_{+5} (Fig. 2-2A and B). Three independent replications of each experiment were conducted.

The pNP-releasing velocity towards 0.1–2.5 mM pNP-Glc in the presence of 0–50 mM monosaccharides (D-galactose, D-xylose, and D-mannose) was measured under the conditions as described in the section 2.2.10. Equation 5, theoretically obtained from the reaction schemes (Fig. 2-2C and D), was used for the regression using Grafit version 7.

Eq. 5 $v/[e]_0 = (\alpha\,[MS] + k_{cat})\,[S] \,/\, \{[S]^2/K_{is} + (\beta\,[MS] + 1)\,[S] + \gamma\,[MS] + K_m\}$

where [MS] is monosaccharide concentration.

Kinetic parameters k_{cat}, K_m, and K_{is} are the same as defined above. α, β, and γ were shown from the scheme (Fig. 2-2C):

$\alpha = k_{+2}k_{+5}k_{+6}/(k_{+2}+k_{+3})(k_{-5}+k_{+6})$;

$\beta = k_{+5}(k_{+2}+k_{+6})/(k_{+2}+k_{+3})(k_{-5}+k_{+6})$;

$\gamma = (k_{-1}+k_{+2})k_{+5}k_{+6}/(k_{+2}+k_{+3})(k_{-5}+k_{+6})$.

α, β, and γ were shown from the scheme (Fig. 2-2D):

$\alpha = k_{+3}k_{+5}k_{+6}/(k_{+2}+k_{+3})(k_{-5}+k_{+6})$;

$\beta = k_{+3}(k_{+6}+k_{+7})/k_{+7}(k_{+2}+k_{+3})(k_{-5}+k_{+6})$;

$\gamma = k_{+3}k_{+5}k_{+6}/k_{+1}(k_{+2}+k_{+3})(k_{-5}+k_{+6})$.

Three independent replications of each experiment were conducted.

Based on the reaction schemes (Fig. 2-2C and D), the D-glucose releasing velocities from monosaccharide-unbound (v_1) and bound (v_2) intermediates were described as equations 6 and 7, and the ratio, v_2/v_1, was described as equation 8.

Eq. 6 $v_1 = k_{cat}\,[S] / \{[S]^2/K_{is} + (\beta\,[MS] + 1)\,[S] + \gamma\,[MS] + K_m\}$

Eq. 7 $v_2 = \alpha\,[MS]\,[S] / \{[S]^2/K_{is} + (\beta\,[MS] + 1)\,[S] + \gamma\,[MS] + K_m\}$

Eq. 8 $v_2/v_1 = \alpha\,[MS] / k_{cat}$

When the monosaccharide concentration is infinite, equation 5 can be transformed to equation 9.

Eq. 9 $v/[e]_0 = (\alpha/\beta)\,[S] / ([S] + \gamma/\beta)$

The k_{cat}, K_m, and k_{cat}/K_m converges to α/β, γ/β, and α/γ, respectively.

2.3 Results

2.3.1 Identification of extracellular β-glucosidase MnBG3A from *M. nivale*

The fermentation of *M. nivale* in PD broth (3 L) without additional inducer for 4 weeks at 18°C yielded 111 U of β-glucosidase in the culture supernatant. The enzyme MnBG3A was purified by three types of column chromatography: anion-exchange, hydrophobic interaction, and gel permeation. The activity was not separated and eluted in a single peak in each column chromatography, although the yield was low. The purified protein (0.110 mg, 0.833 U) showed specific activity of 7.57 U/mg and an almost single

band at 111 kDa on SDS-PAGE analysis (Fig. 2-3A). Partial amino acid sequences of MnBG3A, obtained by N-terminal sequencing by Edman degradation and LC-MS/MS analysis of tryptic peptides, was used to draw a candidate gene for MnBG3A from *M. nivale* genome sequence data. The 11 residues determined by the N-terminal sequencing were identical to Ala-32–Val-42 of the deduced amino acid sequence of the candidate gene for MnBG3A. The MS/MS spectra of the tryptic peptides closely matched the deduced sequence with 46% coverage of the entire protein sequence deduced from the cDNA sequence isolated from 4-week cultured *M. nivale* cells. The partial sequence of the MnBG3A-coding DNA is deposited in the DDBJ database under accession number LC723725. The whole sequence was defined here as Met-1 to Lys-876: the deposited sequence including additional N-terminal seven residues (Met-Arg-Ala-Thr-Ser-Ile-Ala) and C-terminal seven residues (Pro-Leu-Ser-Ala-Asp-Leu-Lys), which were included in PCR primer sequences.

The deduced protein sequence indicates that MnBG3A is an 845-residue protein (Ala-32–Lys-876) of theoretical molecular weight of 91,212, after the removal of Met-1–Arg-31 of the immature protein. It contains 13 possible *N*-glycosylation sites. A BLASTp search against non-redundant protein sequences revealed that MnBG3A is a GH3 protein with the highest identity (91%) to putative GH3 β-glucosidase A from *M. bolleyi* (NCBI ID KXJ94594.1). A high identity (60%) was also observed with well-characterized GH3 β-glucosidase AaBGL1 from *A. aculeatus* (Takada *et al*. 1998). In addition to the overall similarity, the essential residues conserved in the fungal GH3 enzymes were found in the MnBG3A sequence (Fig. 2-4): the catalytic nucleophile (Asp-295), the general acid/base (Glu-523), and amino acid residues involved in subsite −1 (Asp-107, Arg-171, Lys-204, His-205, Tyr-263, Trp-296, and Ser-464). The subsite +1 residues having hydrophobic

interaction with substrate in AaBGL1 were also found in MnBG3A (Trp-83, Phe-320, and Tyr-525).

2.3.2 Recombinant MnBG3A produced in *K. pastoris*

Recombinant MnBG3A (1,150 U) was produced in the 2-L culture supernatant after 144-h culture at 20°C by the *K. pastoris* transformant harboring a gene encoding the mature MnBG3A (Ala-32–Lys-876) with the plasmid-derived signal sequence of α-factor attached at the N-terminus. The enzyme (320 U, 7.04 mg) was purified by ammonium sulfate precipitation and column chromatographies. Specific activity of the recombinant MnBG3A (45.5 U/mg) was 6-fold higher than that of the native enzyme, possibly because of the low purity of the native enzyme. The purified enzyme showed a clear single band at 129 kDa on SDS-PAGE (Fig. 2-3B) and at 256 kDa on blue native PAGE (Fig. 2-3C). Digestion with endoglycosidase H decreased the molecular mass to 98 kDa on SDS-PAGE, which was close to the theoretical mass from the amino acid sequence of 91 kDa (Fig. 2-3B). These data suggested that recombinant MnBG3A was *N*-glycosylated and existed as dimer in solution. Recombinant MnBG3A showed the highest activity at pH 5.1 and 50°C (Fig. 2-5). The enzyme activity was ≥90% retained after incubation at pH values ranging between 5.1 and 10.0 (4°C for 24 h) and at temperatures ≤40°C (for 15 min) (Fig. 2-5).

2.3.3 Substrate specificity

The pNP-releasing velocity with 2 mM pNP β-glycosides (pNP-Glc, pNP-Man, pNP-Gal, pNP-Xyl, and pNP-Fuc) was measured. Recombinant MnBG3A acted only upon pNP-Glc and pNP-Xyl at reaction rates of 50.4 ± 1.9 s^{-1} and 0.200 ± 0.001 s^{-1},

respectively. The velocity for the other glycosides was not detectable (<0.0076 s^{-1}). In the reaction to pNP-Glc, pNP- and glucose-releasing velocities were almost identical at 0.05–5 mM concentrations of the substrate (Fig. 2-6A), indicating that MnBG3A catalyzed hydrolysis and no detectable transglycosylation under the conditions. However, a severe decrease in the velocities was observed in a higher range of substrate concentration, particularly over 0.3 mM (Fig. 2-6A). The rate equations for the substrate inhibition from two reaction schemes, involving the formation of the ESS complex and the E-Glc S complex (Fig. 2-1A and B), were of the same form (Eq. 1) and fitted well to the reaction rates with the following kinetic parameters: k_{cat}, 112 ± 4 s^{-1}; K_m, 0.0841 ± 0.0035 mM; and K_{is} (ESS- or E-Glc S-dissociation constant), 1.61 ± 0.13 mM; the parameter K_{is} is expressed as a combination of rate constants that vary with each scheme. The reaction of MnBG3A with pNP-Glc was inhibited also by D-glucose in a concentration-dependent manner (Fig. 2-6B). Two possible inhibition models involving the binding of D-glucose to free enzyme (competitive inhibition) (Fig. 2-1C) and to the D-glucosyl enzyme intermediate (uncompetitive inhibition) (Fig. 2-1D) were examined. The regression analysis indicated that the inhibition by D-glucose was competitive with kinetic parameters of k_{cat}, 105 ± 7 s^{-1}; K_m, 0.0786 ± 0.0104 mM; K_{is}, 2.01 ± 0.41 mM; and K_{i1} (E Glc-dissociation constant), 0.491 ± 0.016 mM. The k_{cat}, K_m, and K_{is} determined were consistent with the values from the reactions in the absence of D-glucose.

MnBG3A also hydrolyzed various β-glucooligosaccharides (Table 2-1). The reactions obeyed Michaelis-Menten kinetics in the substrate concentration range of 0.08–0.4 mM. Of the glucobioses tested, MnBG3A showed the highest k_{cat}/K_m to Lam_2 (β1-3; 1,410 $s^{-1}mM^{-1}$) followed by those to Gen_2 (β1-6, 720 $s^{-1}mM^{-1}$), Cel_2 (β1-4, 179 $s^{-1}mM^{-1}$), and Sop_2 (β1-2, 56.4 $s^{-1}mM^{-1}$) (Table 2-1). It showed the highest k_{cat}/K_m to the trisaccharide

Lam_3 of laminarioligosaccharides, whereas the highest k_{cat}/K_m was observed for Cel_4, the oligosaccharide with the longest chain length of the tested cellooligosaccharides.

2.3.4 Transglucosylation and condensation

MnBG3A was incubated with Gen_2 and Lam_2 at 20 mM, much higher than the concentrations used in the kinetic analysis, and the products were analyzed by TLC (Fig. 2-7A and B). In the reaction with Gen_2, gentiotriose (Gen_3) was detected as a product along with D-glucose (Fig. 2-7A). In the reaction with Lam_2, Gen_2 and D-glucose were predominantly produced with trace quantities of Lam_3 detected (Fig. 2-7B). This suggests that D-glucose, produced by hydrolysis in the early stage, served as acceptor of the transglucosylation. Therefore, transglucosylation of MnBG3A uses mainly Gen_2 and D-glucose as acceptors, and forms predominantly β1-6-linkages. MnBG3A was also incubated with 2.1 M D-glucose as the sole substrate for a longer time to analyze the condensation. Both the TLC and HPAEC-PAD analyses indicated the main production of Gen_2 (Fig. 2-7C and D). Although Cel_2 shows close retention time (3.8 min) to that of Gen_2 (3.7 min) in HPAEC-PAD chromatogram, the mobilities of them on TLC were clearly different (Fig. 2-7C). In the HPAEC-PAD chromatogram, two other peaks were found at 5.1 and 5.8 min of retention time, which corresponded to Sop_2 or Lam_2 and Gen_3, respectively (Fig. 2-7D). Quantification with the HPAEC-PAD indicated that Gen_2 reached a concentration of 89.5 mM in 4 days. The conversion ratio was 8.5% of the total conversion on a molar basis. The results of condensation also indicate that MnBG3A is highly β1-6-linkage specific in the formation of glycosidic linkages.

2.3.5 Effect of pNP β-glycoside on the hydrolytic velocity of pNP-Glc

Reaction velocity with 0.2 mM pNP-Glc of MnBG3A was measured in the presence of pNP β-glycoside. As described in 2.3.3, MnBG3A showed no or little activity to pNP-Gal, pNP-Xyl and pNP-Man, and the hydrolysis of these pNP β-glycosides can be ignored. pNP-Gal and pNP-Man showed almost no effect on the pNP-Glc hydrolytic velocity (Fig. 2-8A). A decrease in the reaction velocity was observed with increasing pNP-Xyl concentrations. In the presence of higher concentration of pNP-Xyl, the substrate inhibition in the pNP-Glc hydrolysis was less observed in the [S]-*v* plots (Fig. 2-8B). The rate equation (Eq. 4) from the reaction scheme including competitive binding of second pNP-Glc and pNP-Xyl (Fig. 2-2A and B) was well fitted to the reaction rates with the following kinetic parameters: k_{cat}, 88.1 ± 3.6 s^{-1}; K_m, 0.0776 ± 0.0065 mM; K_{is}, 1.34 ± 0.10 mM; and K_i (E-Glc pNP-Xyl- or ES pNP-Xyl-dissociation constant in Fig. 2-2A and B, respectively), 1.23 ± 0.03 mM.

2.3.6 Effect of monosaccharides on the hydrolytic velocity of pNP-Glc

Reaction velocities with pNP-Glc of MnBG3A were measured in the presence of monosaccharides. D-Galactose and D-xylose increased the velocity even in the range of substrate concentration occurring substrate inhibition (Fig. 2-9A and B). In contrast, D-mannose decreased the velocity in the low range of substrate concentration (Fig. 2-9C). Transglucosylation products using these monosaccharides as acceptors were not observed. The rate equation (Eq. 5) from the reaction scheme (Fig. 2-2C and D) including competitive binding of second pNP-Glc and monosaccharide, and hydrolysis through E-Glc MS or ES MS in Fig. 2-2C and D, respectively, was well fitted to the three reaction rates in the presence of monosaccharides. The kinetic parameters of k_{cat}, K_m, and K_{is} were

almost identical to those without any monosaccharides, and the other parameters (α, β and γ) were different by monosaccharides (Table 2-2). The ratio of v_2 to v_1 in the reaction schemes (Fig. 2-2C and D) is proportional to the monosaccharide concentration, and its proportionality constant is expressed by α/k_{cat}. These constants were 22, 29, and 5.5 M^{-1} under the presence of D-galactose, D-xylose, and D-mannose, respectively (Table 2-3). In addition, k_{cat}, K_m, and k_{cat}/K_m at an infinite concentration of monosaccharide were determined from α, β, and γ. k_{cat}, calculated as α/β, was 330, 220, and 54 s^{-1}, at an infinite concentration of D-galactose, D-xylose, and D-mannose, respectively (Table 2-3). K_m, calculated as γ/β, was 0.48, 0.35, and 0.82 mM, respectively, and k_{cat}/K_m, calculated as α/γ, was 690, 630, 66 $s^{-1}mM^{-1}$, respectively (Table 2-3).

2.4 Discussion

In this chapter, extracellular GH3 β-glucosidase MnBG3A from *M. nivale*, was identified. Characterization of the enzyme was done mainly using recombinant enzyme produced in the *K. pastoris* transformant. The sequence comparison indicated that MnBG3A is 91% identical to putative GH3 β-glucosidase A from *M. bolleyi* and 60% identical to AaBGL1, one of the most well-studied fungal GH3 β-glucosidase in terms of its function and structure. MnBG3A was very similar to AaBGL1 in its enzymatic functions, particularly substrate specificity to various pNP β-glycosides and β-glucobioses, and in terms of its chain length preferences for cellooligosaccharides and laminarioligosaccharides (Baba *et al*. 2015). These functional similarities are explained by the high structural similarity, particularly the highly conserved subsites −1 and +1-forming residues as shown in the multiple sequence alignment (Fig. 2-4).

Differences between MnBG3A and AaBGL1 were observed in terms of the

inhibitions of MnBG3A by both pNP-Glc and D-glucose, which are more severe than those of AaBGL1. MnBG3A was inhibited by pNP-Glc with a K_{is} value of 1.6 mM, but AaBGL1 followed Michaelis-Menten equation with 0.1–1.2 mM pNP-Glc, and substrate inhibition was not observed (Suzuki *et al*. 2013). Higher inhibition by D-glucose was also exhibited by MnBG3A. The K_i value is significantly lower in MnBG3A (0.491 mM) than AaBGL1 (K_i 9.99 mM; Baba *et al*. 2015).

The decrease of reaction rate by both substrate and product have been reported in some fungal GH3 β-glucosidases. In *Penicillium brasilianum* BGL and *A. oryzae* AoCel3A, the rate decreases by substrate and product were observed. The K_i values of *P. brasilianum* BGL and *A. oryzae* AoCel3A for product inhibition by D-glucose were 2.3 and 2.9 mM, respectively (Krogh *et al*. 2010; Langston *et al*. 2006). However, the decline of the pNP-generating rates at a higher range of pNP-Glc concentration in the AoCel3A-catalyzing reaction was explained by transglucosylation kinetics (Langston *et al*. 2006). Before this report, a similar rate decrease in Lam_2 hydrolysis by a GH3 β-glucosidase of the white-rot fungus *Phanerochaete chrysosporium* was demonstrated to follow the hydrolysis-transglucosylation reaction scheme (Kawai *et al*. 2004). In the reaction scheme, after the formation of the D-glucosyl enzyme intermediate through the cleavage of substrate, water and substrate are bound to the intermediate in a competitive manner. Therefore, the higher concentration of substrate gives higher transglucosylation, but if the rate constant for the synthesis of the transglucosylation product from the D-glucosyl enzyme-substrate complex is low, the overall reaction rate decreases with increasing substrate concentration. When this rate constant is zero, the reaction scheme is as shown in Fig. 2-1B and gives the same inhibition equation (Eq. 1). Considering the similarity of all of the GH3 β-glucosidases, the substrate inhibition of MnBG3A occurs probably not

via simple ESS formation (Fig. 2-1A), but rather the formation of the D-glucosyl enzyme intermediate and pNP-Glc complex (Fig. 2-1B). The second pNP-Glc is considered to bind at subsites +1 and +2 of the D-glucosyl enzyme intermediate, but in a non-productive manner in MnBG3A. This mechanism explains the substrate inhibition weakened by the addition of pNP-Xyl and monosaccharides. According to the model illustrated in Fig. 2-10, the second pNP-Glc competes with the water molecule which is the substrate in hydrolysis. As pNP-Xyl binds to the D-glucosyl enzyme intermediate like the second pNP-Glc, pNP-Xyl cancels the substrate inhibition (Fig. 2-10). Inhibition of the hydrolysis by pNP-Xyl is considered to be preferential because the inhibition constant for pNP-Xyl, K_{i3} (1.23 mM), was smaller than K_{is} (1.34 mM). In the case of monosaccharides, they also compete with the binding of the second pNP-Glc. However, the hydrolysis from the monosaccharide complex progresses with different reaction rates. The differences in reaction rates are suggested to be caused by the differences in competitiveness with the water molecule, as illustrated in Fig. 2-10. The actual binding forms of glycosides and monosaccharides have not been elucidated.

MnBG3A catalyzed β1-6 transglucosylation using D-glucose and Gen_2 as acceptors. The enzyme also produced Gen_2 from D-glucose in the condensation reaction. As for AaBGL1, transglucosylation and condensation were not thoroughly analyzed, but Gen_2 was detected in small amounts in the reaction with 25 mM Cel_2 or Lam_2 (Baba *et al*. 2015). The generation of β1-6-linkages through transglucosylation was also reported in several other fungal GH3 β-glucosidases. In the transglucosylation of Cel_2 by AnBGL, 6^{II}-*O*-β-D-glucosyl cellobiose was produced initially, and after 5 mM and more D-glucose accumulated, Gen_2 was produced (Seidle and Huber 2005). In the reaction with Lam_2 of *P. chrysosporium* PcBgl1A, only 6^{II}-*O*-β-D-glucosyl laminaribiose was generated as the

transglucosylation product (Kawai *et al*. 2004). The enzymes described above commonly produce the β1-6-linkages, but the selectivity for D-glucose and the disaccharides as acceptor substrates differs of the enzymes. As the subsite +1 formed by some aromatic residues is common, the different acceptor preferences suggest structural differences in subsite +2. In MnBG3A, binding of the reducing-end D-glucosyl moiety of Gen_2 in subsite +2 was suitable for the nonreducing-end D-glucosyl moiety to bind in subsite +1 for the formation of β1-6-linkages. The binding of Lam_2 in subsite +2, however, placed the nonreducing-end D-glucosyl moiety in an orientation not suitable for the linkage formation. The inhibition and transglucosylation with pNP-Glc mentioned above also support the difference in subsite +2 of MnBG3A compared to the other enzymes. No complex structure indicating subsite +2 has been determined yet, which makes it difficult to predict which residues are involved in the activity at this subsite.

As observed in AaBGL1, MnBG3A has higher β1-3-linkage specificity in hydrolysis though it has broad substrate specificity. The substrate preference of MnBG3A is suitable for its involvement in degradation of cellulose through Cel_2 hydrolysis, and also in degradation of hemicellulosic β1-3-glucan and β1-3/1-4-glucan, as mentioned for the *M. oryzae* GH3 β-glucosidases, MoCel3A and MoCel3B (Takahashi *et al*. 2011). *M. bolleyi*, which encodes a putative enzyme with the highest identity to MnBG3A identified in a BLASTp search, is generally known as an endophyte of grasses and grows in root cells of healthy plants (David *et al*. 2016). GH3 β-glucosidase A is probably required for plant cell invasion and proliferation of the fungus. The broad substrate specificity of MnBG3A is suitable for these physiological roles. In addition, the transglucosylation activity of MnBG3A implies that another possible role of MnBG3A is the production of Gen_2, which is known as an inducer of cellulolytic enzymes in *Penicillium purpurogenum* (Kurasawa

et al. 1992; Suto and Tomita 2001). This would be beneficial for plant infection and the proliferation of *M. nivale*.

In summary, *M. nivale* was shown to possess the GH3 β-glucosidase MnBG3A, which has similar characteristics to fungal GH3 β-glucosidases. Given the pathogenic nature of this fungus, MnBG3A is likely responsible for degrading β-glucooligosaccharides generated from cellulose and/or hemicelluloses by β-glucanases. In addition, this enzyme might be involved in the induction of cellulases through the production of a possible inducer, Gen_2, by transglucosylation in *M. nivale.*

Table 2-1. Kinetic parameters of recombinant MnBG3A

Substrate	k_{cat} (s^{-1})	K_m (mM)	k_{cat}/K_m ($s^{-1}mM^{-1}$)	K_{is} [c] (mM)	K_{il} [d] (mM)
pNP-Glc [a]	112 ± 4	0.0841 ± 0.0035	1,330	1.61 ± 0.13	n.a.
pNP-Glc [b]	105 ± 7	0.0786 ± 0.0104	1,350	2.01 ± 0.41	0.491 ± 0.016
Sophorose	80.1 ± 3.0	1.42 ± 0.07	56.4	n.a.	n.a.
Lainaribiose	133 ± 2	0.0951 ± 0.0092	1,410	n.a.	n.a.
Laminaritriose	144 ± 7	0.0792 ± 0.0086	1,830	n.a.	n.a.
Laminaritetraose	138 ± 6	0.108 ± 0.010	1,290	n.a.	n.a.
Laminaripentaose	159 ± 3	0.292 ± 0.006	544	n.a.	n.a.
Cellobiose	67.0 ± 6.5	0.379 ± 0.063	179	n.a.	n.a.
Cellotriose	96.2 ± 4.1	0.104 ± 0.016	945	n.a.	n.a.
Cellotetraose	80.0 ± 2.2	0.0735 ± 0.0081	1,090	n.a.	n.a.
Gentiobiose	136 ± 3	0.188 ± 0.008	720	n.a.	n.a.

a, parameters calculated from Eq. 1. b, parameters in the presence of 0–50 mM D-glucose, calculated from Eq. 2. n.a., not analyzed. c, ESS- or E-Glc S-dissociation constant, referring to Fig. 2-1A and B, respectively. d, E Glc-dissociation constant, referring to Fig. 2-1C.

Table 2-2. Kinetic parameters of recombinant MnBG3A under the presence of monosaccharides

MS	k_{cat} (s^{-1})	K_m (mM)	K_{is} (mM)	α ($s^{-1}mM^{-1}$)	β (M^{-1})	γ
none	112 ± 4	0.0841 ± 0.0035	1.61 ± 0.13	n.a.	n.a.	n.a.
Gal	128 ± 5	0.109 ± 0.006	1.18 ± 0.14	2.84 ± 0.63	8.62 ± 3.80	0.00415 ± 0.00085
Xyl	127 ± 4	0.110 ± 0.013	1.32 ± 0.11	3.63 ± 0.73	16.2 ± 6.1	0.00559 ± 0.00068
Man	111 ± 4	0.0802 ± 0.0044	1.51 ± 0.12	0.610 ± 0.404	11.4 ± 5.8	0.00935 ± 0.00091

n.a., not analyzed.

Table 2-3. Kinetic parameters of recombinant MnBG3A affecting on the changes of reaction rates by monosaccharides

MS	α/k_{cat} (M^{-1})	α/β (s^{-1})	γ/β (mM)	α/γ ($s^{-1}mM^{-1}$)
Gal	22	330	0.48	690
Xyl	29	220	0.35	630
Man	5.5	54	0.82	66

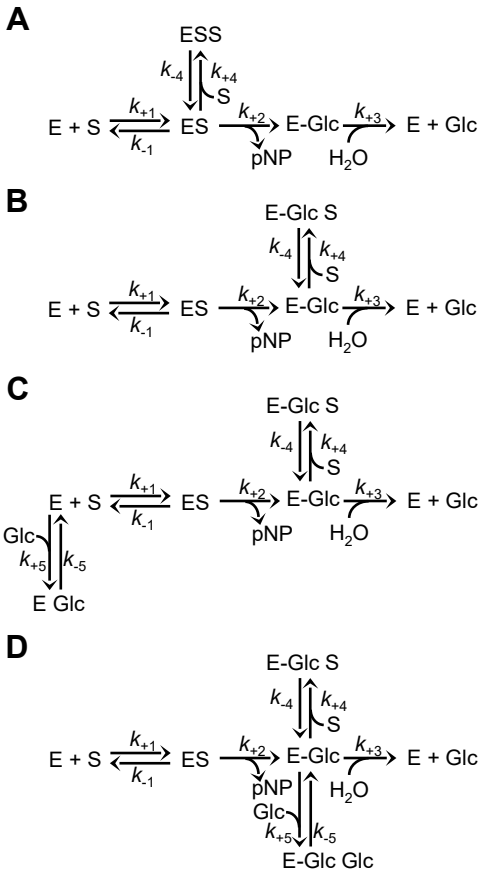

Fig. 2-1. Reaction schemes for hydrolysis of pNP-Glc
(A) The scheme of substrate inhibition of the simple ESS formation. (B) The scheme of substrate inhibition of the formation of the D-glucosyl enzyme intermediate and pNP-Glc complex. (C) The scheme of competitive inhibition by D-glucose. (D) The scheme of uncompetitive inhibition by D-glucose. “E”, enzyme; “S”, substrate; “ES”, ES complex; “ESS”, inactive complex of enzyme and two substrates; “E-Glc”, the D-glucosyl enzyme intermediate; “E-Glc S”, the complex of the D-glucosyl enzyme intermediate and substrate; “E Glc”, enzyme-D-glucose complex; “Glc”, D-glucose; “E-Glc Glc”, the complex of the D-glucosyl enzyme intermediate and D-glucose.

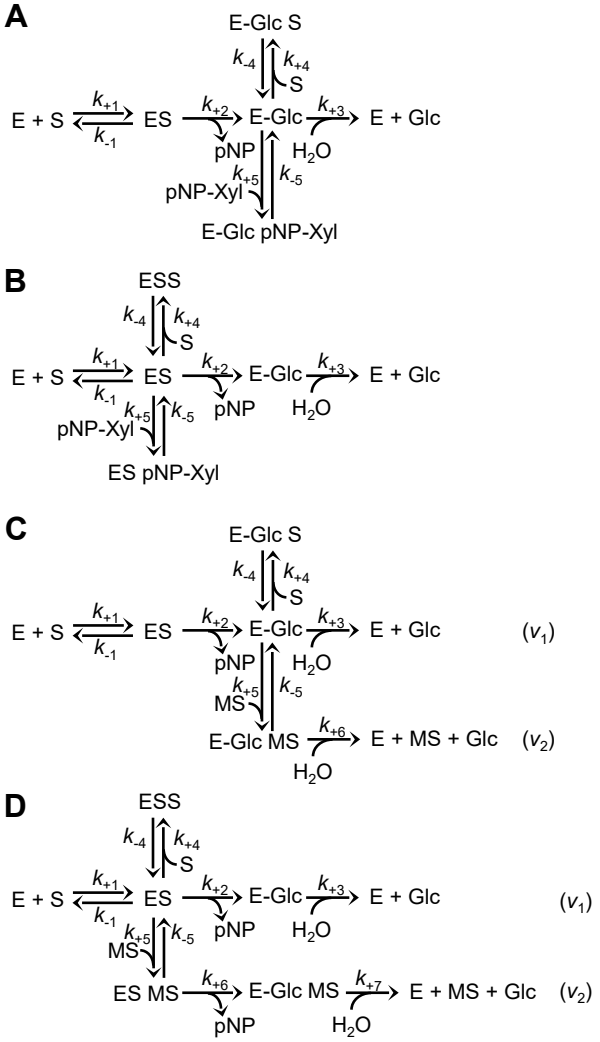

Fig. 2-2. Reaction schemes for hydrolysis of pNP-Glc in the presence of pNP-Xyl or monosaccharide

(A) The scheme of substrate and pNP-Xyl inhibition of the formation of the D-glucosyl enzyme intermediate and pNP-Glc or pNP-Xyl complex. (B) The scheme of substrate and pNP-Xyl inhibition of the formation of the ES complex and pNP-Glc or pNP-Xyl complex. (C) The scheme of monosaccharide and pNP-Glc competitively binding to the D-glucosyl enzyme intermediate, and hydrolysis proceeds from the monosaccharide complex. (D) The scheme of monosaccharide and pNP-Glc competitively binding to the ES complex, and hydrolysis proceeds from the monosaccharide complex. "E", enzyme; "S", substrate; "ES", ES complex; "ESS", inactive complex of enzyme and two substrates; "E-Glc", the D-glucosyl enzyme intermediate; "E-Glc S", the complex of the D-glucosyl enzyme intermediate and substrate; "E Glc", enzyme-D-glucose complex; "Glc", D-glucose; "ES Glc", the complex of ES complex and D-glucose; "E-Glc pNP-Xyl", the complex of the D-glucosyl enzyme intermediate and pNP-Xyl; "ES pNP-Xyl", the complex of ES complex and pNP-Xyl; "E-Glc MS", the complex of the D-glucosyl enzyme intermediate and monosaccharide; "ES MS", the complex of ES complex and monosaccharide.

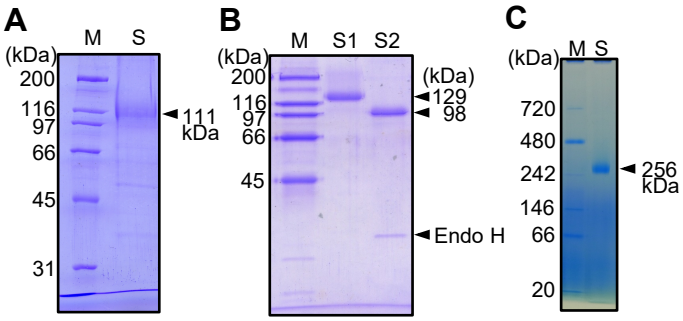

Fig. 2-3. SDS-PAGE and blue native PAGE of purified native and recombinant MnBG3A

Purified MnBG3A (1.0 μg for SDS-PAGE and 5.0 μg for blue native PAGE) was analyzed. (A) SDS-PAGE of native MnBG3A; (B) SDS-PAGE of recombinant MnBG3A; (C) blue native PAGE of recombinant MnBG3A. Protein was stained with CBB. Lane M, size markers. Lane S, purified MnBG3A. Lane S1, purified MnBG3A. Lane S2, Endo H treated MnBG3A.

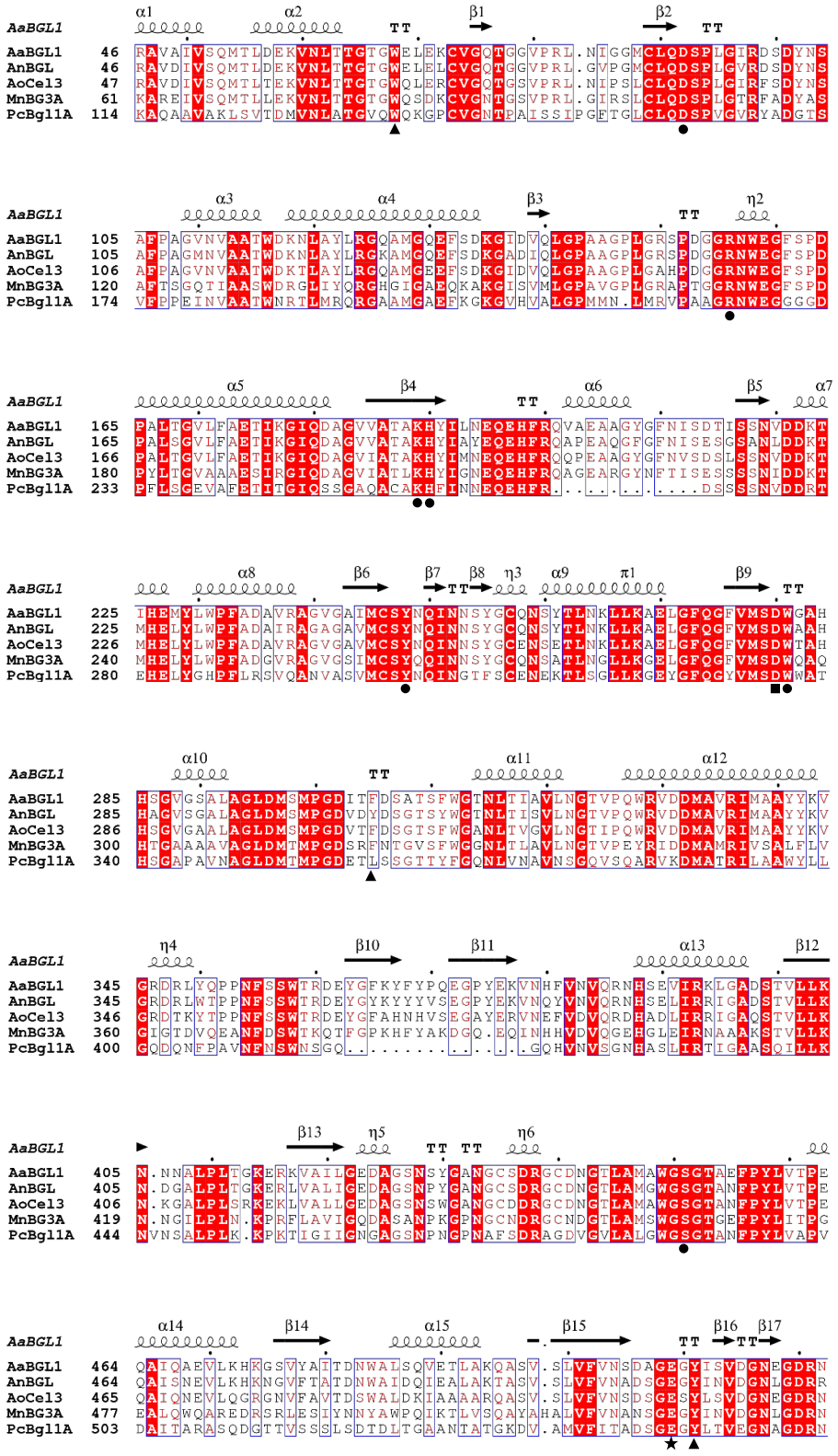

Fig. 2-4. Multiple alignment of partial amino acid sequences of MnBG3A and other fungal GH3 β-glucosidases

The amino acid sequence of AaBGL1, AnBGL, AoCel3, MnBG3A, and PcBgl1A were aligned with MAFFT ver. 7 (Katoh *et al.* 2019). The results of alignment were visualized using ESPript 3.0 (Robert and Gouet 2014). Circles and triangles indicate the residues at subsites −1 and +1, respectively. Square indicates catalytic nucleophile and star indicates catalytic acid/base.

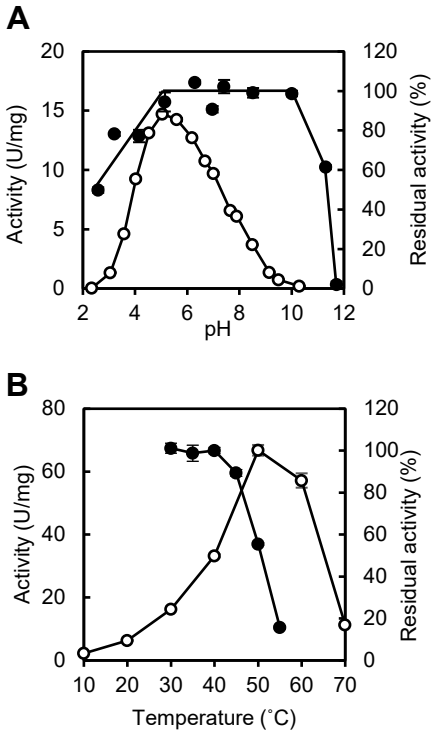

Fig. 2-5. Effects of pH and temperature on activity and stability of recombinant MnBG3A
Open and closed circles show activity and stability, respectively. (A) Effect of pH on recombinant MnBG3A. Stability was evaluated by residual activity after incubation at 4˚C for 24 h in the various pH conditions. (B) Effect of temperature on recombinant MnBG3A. Stability was evaluated by residual activity after incubation for 15 min at the various temperatures. Values are average of the values from three independent experiments, and error bars indicate their standard deviation.

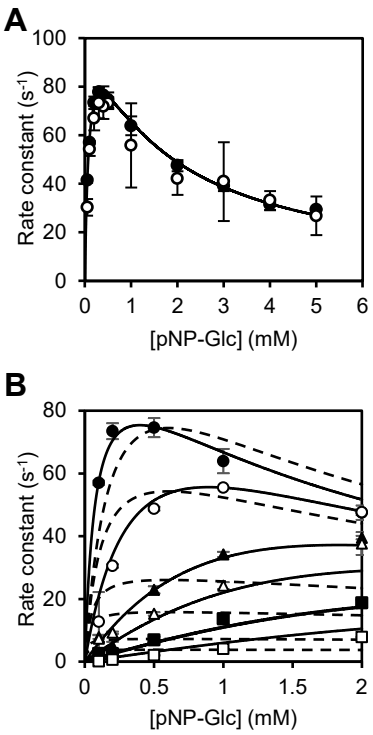

Fig. 2-6. [S]-*v* plot of MnBG3A for the hydrolysis of pNP-Glc

Values and error bars are mean and standard deviation for three independent experiments. (A) Reaction with pNP-Glc. Closed circles, pNP-releasing velocity; open circles, D-glucose-releasing velocity; line, theoretical line for pNP release. (B) Hydrolysis of pNP-Glc in the presence of various concentration of D-glucose. Closed circles, 0 mM; open circles, 2 mM; closed triangles, 10 mM; open triangles, 20 mM; closed squares, 50 mM; open squares, 100 mM. Theoretical lines from Eq. 2 (solid line) and Eq. 3 (broken line) were fitted to the experimental values.

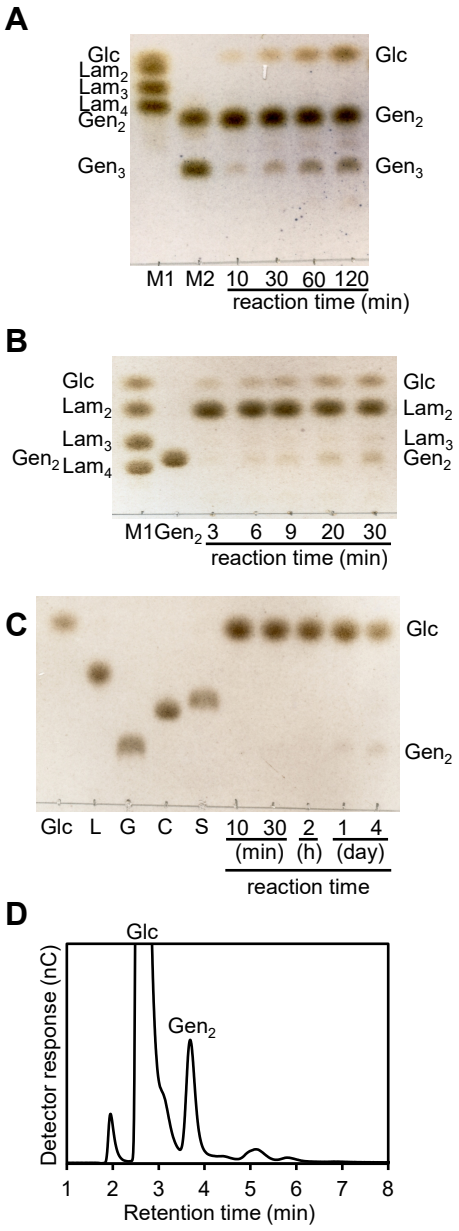

Fig. 2-7. TLC and HPAEC-PAD analysis of MnBG3A reaction products from Gen_2, Lam_2, and D-glucose

MnBG3A (19.2 nM) was incubated with 20 mM Gen_2 (A) and Lam_2 (B) for the indicated time and analyzed by TLC. MnBG3A (9.6 μM) was incubated with 2.1 M D-glucose for indicated time (C) and 4 days (D). Lane M1, D-glucose and laminarioligosaccharides; Lane M2, gentiooligosaccharides; Lane L, Lam_2; Lane G, Gen_2; Lane C, Cel_2; Lane S, Sop_2.

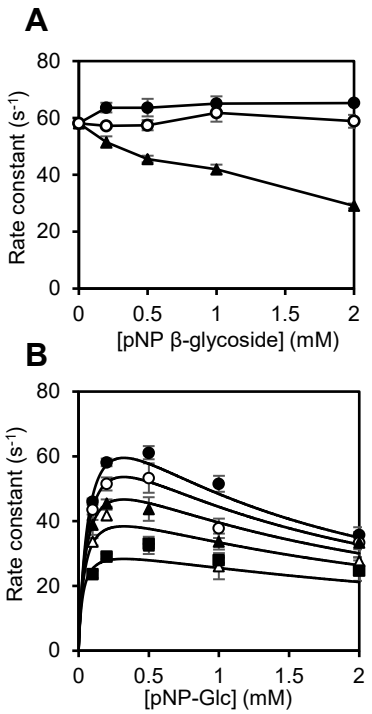

Fig. 2-8. Effect of pNP β-glycosides on the hydrolysis of pNP-Glc
Values and error bars are mean and standard deviation for three independent experiments. (A) Reaction with pNP-Glc in the presence of pNP β-glycoside. Closed circles, pNP-Gal; open circles, pNP-Man; closed triangles, pNP-Xyl. (B) Hydrolysis of pNP-Glc in the presence of various concentration of pNP-Xyl. Closed circles, 0 mM; open circles, 0.2 mM; closed triangles, 0.5 mM; open triangles, 1 mM; closed squares, 2 mM. Theoretical lines from Eq. 4 was fitted to the experimental values.

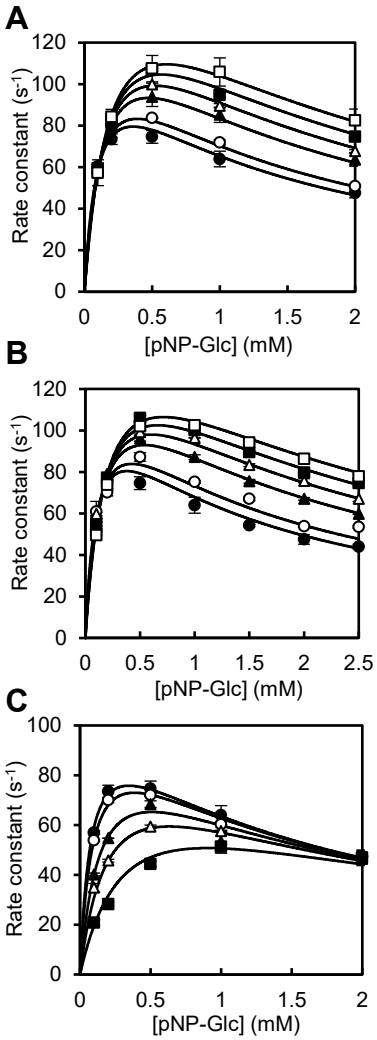

Fig. 2-9. Effect of monosaccharides on the hydrolysis of pNP-Glc
Values and error bars are mean and standard deviation for three independent experiments. Reactions with pNP-Glc in the presence of D-galactose (A), D-xylose (B), and D-mannose (C). (A and B) Closed circles, 0 mM; open circles, 5 mM; closed triangles, 20 mM; open triangles, 30 mM; closed squares, 40 mM; open squares, 50 mM. (C) Closed circles, 0 mM; open circles, 2 mM; closed triangles, 10 mM; open triangles, 20 mM; closed squares, 50 mM. Theoretical lines from Eq. 5 was fitted to the experimental values.

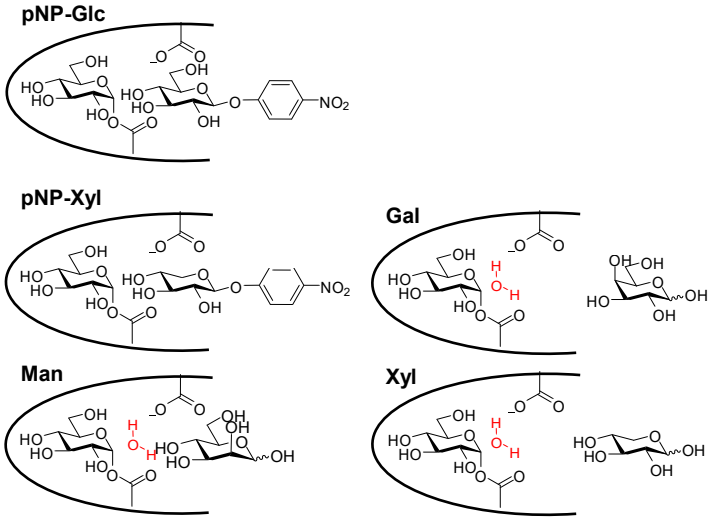

Fig. 2-10. Schematic binding mode of pNP β-glycosides and monosaccharides.
Predicted pNP β-glycoside- and monosaccharide-binding mode to the D-glucosyl enzyme intermediate.

3. Function and structure of an extracellular endo-β-1,3-glucanase from *M. nivale*

3.1 Introduction

Endo-β-1,3-glucanases (EC 3.2.1.6 or 3.2.1.39) are found in bacteria, fungi, plants, and marine organisms. β1-3-Glucans are present in nature such as linear β1-3-glucans, curdlan and paramylon (Marchessault and Deslandes 1979); β1-3/1-6-glucans, laminarin (Liu *et al*. 2018; Fig. 3-1) and scleroglucan (Rinaudo and Vincendon 1982); and β1-3/1-4-glucan (Gómez *et al*. 1997). Endo-β-1,3-glucanases hydrolyze them to release D-glucose and/or oligosaccharides. In the carbohydrate-active enzymes database (Drula *et al*. 2022), endo-β-1,3-glucanases are distributed in GH5, GH8, GH9, GH16, GH17, GH55, GH64, GH81, GH128, GH152, GH157, and GH158.

GH55 contains bacterial and fungal inverting exo-β-1,3-glucosidase (often called as exo-β-1,3-glucanase, EC 3.2.1.58), endo-β-1,3-glucanase (EC 3.2.1.39), and hesperidin 6-*O*-α-L-rhamnosyl-β-glucosidase (EC 3.2.1.168). Fungal GH55 β-1,3-glucanases are physiologically involved in conidial maturation and germination in *A. fumigatus* (Millet *et al*. 2019) and mycoparasitism in *Trichoderma harzianum* (de la Cruz *et al*. 1995) through the hydrolysis of β1-3/1-6-glucans in the cell walls. Both exo-β-1,3-glucosidases and endo-β-1,3-glucanases degrade laminarin and are called as laminarinases. Laminarin is diverse β1-3/1-6-glucan derived from brown algae. Typical laminarin from *E. bicyclis* consists of a β1-3- and β1-6-linked linear main chain and β1-6-linked branching D-glucosyl, gentiobiosyl, and gentiotriosyl residues (Liu *et al*. 2018) (Fig. 3-1). Endo-type enzymes degrade internal β1-3-linkages of the main chain of laminarin and produce predominantly reducing sugars (oligosaccharide products) (de la Cruz *et al*. 1995; Nobe *et al*. 2003; Nobe *et al*. 2004), but scissile linkages have not been clarified yet. Exo-β-1,3-glucosidases degrade β1-3-glucosidic linkages from non-reducing ends of the main

chains even in the presence of branches, resulting in the liberation of D-glucose and gentiooligosaccharides (Kasahara *et al*. 1992; Martin *et al*. 2006; Ooi *et al*. 2009).

Three-dimensional structures of GH55 exo-β-1,3-glucosidases have been determined so far in two fungal enzymes, *P. chrysosporium* exo-β-1,3-glucosidase PcLam55A (Ishida *et al*. 2009) and *Chaetomium thermophilum* CtLam55 (Papageorgiou *et al*. 2017), and a bacterial one, *Streptomyces* sp. SirexAA-E SacteLam55A (Bianchetti *et al*. 2015). These enzymes commonly have an overall structure, consisting of two β-helical domains (N- and C-domains) connected by a polypeptide linker. Both the β-helical domains contain 12 coils, each of which is composed of three β-strands and three loops (the n^{th} loop of m^{th} coil is called as C*m*-L*n*). The active site is located at the interface of the N- and C-domains. The Glu residue (equivalent to Glu-502 of SacteLam55A) in C8-L3 of the C-domain serves as a general acid catalyst with the help of the adjacent Tyr residue (Tyr-505 of SacteLam55A) in the orientation by a hydrogen bond. The proposed proton relay network of four amino acid residues (Thr-149, Gln-174, Ser-198, and Glu-480 in SacteLam55A) activates a water molecule, which attacks the anomeric carbon of the substrate from the other side of the scissile β-glucosidic bond (Bianchetti *et al*. 2015). For the exo-type reaction by the exo-β-1,3-glucosidases, the non-reducing end D-glucosyl moiety of laminarioligosaccharide substrates interacts extensively in subsite –1 with Thr-149, Trp-446, Asp-449, Glu-480, and His-481 of SacteLam55A (Bianchetti *et al*. 2015). In addition, the aromatic block, composed of the three conserved aromatic residues (Phe-152, Trp-444, and Trp-446 in SacteLam55A), caps the substrate-binding cleft, resulting in the formation of the dead-end structure of subsite –1 (Bianchetti *et al*. 2015). Furthermore, in the structures of fungal exo-β-1,3-glucosidases, a potential pocket accommodating the 6-*O*-linked branch moiety on the non-reducing terminal D-glucosyl moiety has been

found in the proximity of subsite –1 (Ishida *et al*. 2009; Papageorgiou *et al*. 2017). This is essential for the successive hydrolysis of β1-3-linkage of β1-3/1-6-glucans from their non-reducing ends. Exo-β-1,3-glucosidases show high preference for long-chain laminarioligosaccharides (Martin *et al*. 2006; Ishida *et al*. 2009; Papageorgiou *et al*. 2017), and have an extended substrate-binding cleft with six or more subsites at the domain interface (Ishida *et al*. 2009; Papageorgiou *et al*. 2017; Bianchetti *et al*. 2015). In the cleft of SacteLam55A, two aromatic residues, Tyr-194 and Trp-196, provide stacking interactions that are important for the high preference for long-chain substrates, although they are not conserved in GH55 enzymes (Ishida *et al*. 2009).

Despite the progress made in understanding exo-acting enzymes on the basis of protein structure, the mechanism of the endo-acting mode of endo-β-1,3-glucanases on laminarin remains ambiguous. It is noteworthy that the sequence similarity suggests that endo-β-1,3-glucanases share with the exo-acting β-1,3-glucosidases not only the catalytic residues, but also amino acid residues forming subsite –1 and the aromatic block (Fig. 3-2).

In this chapter, the endo-wise action of GH55 endo-β-1,3-glucanase is described. MnLam55A was identified from extracellular proteins of *M. nivale*. The recombinant MnLam55A catalyzed endo-acting hydrolysis by initially cleaving the non-reducing end of laminarioligosaccharide moieties adjacent to β1-6-linkages in the laminarin main chain. Through protein structure determination together with structural comparison and the docking analysis, it was found that this enzyme had the subsite –2 structure suitable for the binding of a β1-6-linked D-glucosyl moiety and the extended cleft that is expected to form minus subsites. The high conservation of the associated residues in GH55 endo-β-1,3-glucanases supports the idea that these structures are common for the endo-acting

hydrolysis by GH55 endo-β-1,3-glucanases.

3.2 Materials and methods

3.2.1 Identification of MnLam55A from the culture supernatant of *M. nivale*

M. nivale strain MCW222-7 was grown on PD agar medium and cultured in PD broth (0.8 L) as described in section 2.2.1. Culture supernatant (0.7 L), collected by centrifugation (6,000×*g*, 10 min, 4°C), was loaded on a DEAE Sepharose Fast Flow column (2.8 cm I.D. × 25 cm) equilibrated with 10 mM sodium phosphate buffer (pH 7.0). Non-adsorbed protein was eluted by the same buffer, and ammonium sulfate was added up to 1.2 M. The sample was separated on a Butyl Sepharose Fast Flow 4 column (Cytiva; 2.8 cm I.D. × 16 cm) equilibrated with 10 mM sodium phosphate buffer (pH 7.0) containing 1.2 M ammonium sulfate. After washing the column with the same buffer, adsorbed protein was eluted with a linear gradient of 1.2–0 M ammonium sulfate. Active fractions were concentrated to 3 mL by ultrafiltration using Amicon Ultra YM30, and loaded on a Sephacryl S-200 column (1.5 cm I.D. × 98 cm), equilibrated with 10 mM sodium phosphate buffer (pH 7.0) containing 0.1 M sodium chloride. Active fractions were collected. The purified enzyme (2.4 μg) was separated by SDS-PAGE. The single protein band of MnLam55A (68 kDa) was cut out and in-gel tryptic digest was performed as described in section 2.2.2. Data were processed using the search software Proteome Discoverer with a draft genome sequence of *M. nivale* (2.2.3).

3.2.2 Preparation of recombinant MnLam55A in *K. pastoris*

The cDNA of MnLam55A was amplified from a cDNA pool, prepared from total RNA of 4-week-cultured *M. nivale* cells (2.2.4), by PCR using primers (5′-

ATGGTCAGACTCCCTGCCCT-3′, sense; and 5′-AGGGGTATATCTGCCGACAA -3′, antisense) and KOD FX DNA polymerase. N-terminal of matured protein was predicted based on the Signal P ver. 5.0 (Almagro Armenteros *et al*. 2019). The amplified DNA fragment was inserted into pPICZαA (between α-factor signal sequence and *c-myc* epitope sequence) using In-Fusion HD Cloning Kit. The cloned DNA was sequenced as described in section 2.2.4 but with primers:

5′ AOX primer Fw.;

Mn55_pZaA_if_F,

5′-AGAAAAGAGAGGCTGAAGCTTCGCCCGTCGCCGGCCACGA-3′;

MnGH55A_250, 5′-ACCATCAGCAGCACAATCTTCATG-3′;

MnGH55A_600, 5′-AGAATGTCCTCGTCCGTGTCGGGC-3′;

MnGH55A_850, 5′-GCTCGTGGATGCGAGGTCGATCAA-3′;

MnGH55A_1150, 5′-ATTATGCCGCCAACACCGTTGCCG-3′;

MnGH55A_1350, 5′-CGGCCTGTCGTCAAGGTCGGTAAC-3′;

MnGH55A_1700, 5′-TGAGAATGTGTGGAACTGGGTTGC-3′;

3′ AOX primer Rv.

The *Sac*I-linearized plasmid was introduced into *K. pastoris* X-33 by electroporation. The transformant was cultured following section 2.2.5, but using 600 mL of BMGY medium and 1.2 L of BMMY medium containing 2% methanol. During the 96 h incubation in BMMY, methanol (24 mL) was added every 24 h. MnLam55A was purified from the culture supernatant (1.1 L). Proteins were precipitated with 90% saturated ammonium sulfate, dissolved in 10 mM sodium phosphate buffer (pH 7.0, 140 mL), and separated with a Butyl Toyopearl 650M column (2.8 cm I.D. × 16 cm) as described in section 2.2.5. Active fractions were dialyzed against 10 mM sodium phosphate buffer (pH 7.0) and

separated with DEAE Sepharose Fast Flow column (2.8 cm I.D. × 16 cm) equilibrated with 10 mM sodium phosphate buffer (pH7.0). Non-adsorbed protein, eluted by the same buffer, was dialyzed against 10 mM glycine-NaOH buffer (pH 9.0) and separated with DEAE Sepharose Fast Flow column (2.8 cm I.D. × 16 cm) equilibrated with 10 mM glycine-NaOH buffer (pH 9.0). Elution of adsorbed protein was performed with a linear gradient of 0–0.5 M sodium chloride (400 mL). The active fraction was dialyzed against 10 mM glycine-NaOH buffer (pH 9.0), concentrated as described in section 3.2.1, and stored at 4°C until analysis. Protein concentration of the purified enzyme was determined by amino acid analysis as described in section 2.2.6. N-terminal amino acid sequence was analyzed as described in section 2.2.2.

3.2.3 Standard enzyme assay

Production of reducing sugar from laminarin from *E. bicyclis* (Nacalai Tesque) was measured. A reaction mixture (100 μL) consisting of 4 mg/mL laminarin, 40 mM sodium acetate buffer (pH 5.1), 0.2 mg/mL BSA, and appropriate concentration of enzyme was incubated at 30°C for 12 min. Reaction mixture (10 μL) was taken every 3 min, and reducing sugar was quantified by measuring A_{560} according to the copper-bicinchoninic acid (BCA) method (Fox and Robyt 1991). One U of enzyme activity was defined as enzyme amount that produces 1 μmol of reducing sugar equivalent to D-glucose in 1 min under these conditions.

3.2.4 Effect of pH and temperature

The optimum pH was determined from reaction rates at various pH values. The reaction solutions were prepared as in the standard assay, but 80 mM Britton-Robinson

buffer (pH 3.5–7.0) was used. The stable pH range was determined by residual activity after incubation of 348 nM MnLam55A in 20 mM Britton-Robinson buffer (pH 2.5–12.0) at 4°C for 24 h. The optimum temperature was determined by the reaction rates in the standard assay but 10–70°C. The stable temperature range of MnLam55A was determined from residual activity after incubation of 174 nM MnLam55A in 67 mM sodium acetate buffer (pH 5.1) at 30–65°C for 20 min. The range in which the enzyme retained ≥95% of the original activity was regarded as stable range. Three independent replications of each experiment were conducted.

3.2.5 Time course of the reaction with laminarin

To analyze the initial products, the reaction with laminarin was performed using a low concentration of the enzyme for a short period. A reaction mixture consisting of 4 mg/mL laminarin, 40 mM sodium acetate buffer (pH 5.6), 0.2 mg/mL BSA and 13.9 nM MnLam55A, was incubated at 30°C for 15 min. The reaction was terminated by heating at 100°C for 3 min. Reducing sugar was quantified as described in section 3.2.3, and sugar content was analyzed by HPAEC-PAD under the conditions described in section 2.2.13 but with linear gradient of 0–250 mM sodium acetate in 0.2 M NaOH for 30 min. For NMR analysis, the reaction solutions (740 μL) at 0 and 15 min were lyophilized, and dissolved in D_2O. ^{1}H NMR, correlated spectroscopy (COSY) 2D-NMR, ^{13}C NMR, heteronuclear single quantum coherence (HSQC) 2D-NMR, and heteronuclear multiple bond correlation (HMBC) 2D-NMR spectra were measured using Avance Neo (Bruker, Billerica, MA, USA). Data were analyzed using TopSpin version 3.6.2 (Bruker).

The progress of the reactions was monitored as follows: a reaction mixture of 10 mg/mL laminarin, 11 mM sodium acetate buffer (pH 5.6), 0.05 mg/mL BSA and 870 nM

MnLam55A was incubated at 30°C for 25.5 h. Aliquots (100 μL) taken at several timepoints were heated at 100°C for 3 min. Sugar content of the samples was analyzed by TLC using a Silica gel 60 F_{254} plate developed with 2-propanol:1-butanol:water = 12:3:4 (v/v/v), followed by detection as described in section 2.2.12, and HPLC using Aminex HPX-42A Carbohydrate column (Bio-Rad; 7.8 mm I.D. × 300 mm; 75°C) with water at 0.5 mL/min, and a refractive index detector, RI-2031 Plus (Jasco, Tokyo, Japan).

From the reaction products, the trisaccharide and tetrasaccharide products were prepared. A reaction (10 mL) was made as above but with 174 nM MnLam55A for 24 h. The reaction solution was heated at 100°C for 3 min. The trisaccharide and tetrasaccharide were separated from the sample (10 mL) by gel-filtration column chromatography using Toyopearl HW-40S (Tosoh; 5 cm I.D. × 100 cm) with water under 1.8 mL/min, and analyzed by electrospray ionization (ESI)-mass spectrometry (MS) using Exactive Plus (Thermo Fisher Scientific) and NMR as described above.

3.2.6 Reaction with laminarioligoasccharides

A reaction mixture (50 μL) of 10 mM laminarioligosaccharides (DP2–6; Megazyme), 10 mM sodium acetate buffer (pH 5.6), 0.2 mg/mL BSA, and 17.4 nM MnLam55A was incubated at 30°C for 180 min. Aliquots (10 μL) taken at several timepoints were heated at 100°C for 3 min. The samples were analyzed by TLC as described in section 3.2.5. Progress of initial reactions was monitored by analyzing samples (3–12 min, every 3 min) with HPAEC-PAD as described in the section 3.2.5.

MS analysis of laminaripentaose-hydrolyzed products in H_2O and $H_2{}^{18}O$ was performed as follows: the reaction was made in a mixture (25 μL) of 2 mM laminaripentaose, 40 mM sodium acetate buffer (pH 5.6), 0.2 mg/mL BSA, and 139 nM

MnLam55A in H_2O or 99.2% (v/v) $H_2{}^{18}O$ (Sigma) at 30°C for 30 min. The samples were heated at 100°C for 3 min, dried, and analyzed by ESI-MS as described in the section 3.2.5.

3.2.7 Substrate specificity of MnLam55A

The hydrolysis rate was determined for the following β1-3-glucans: laminarin, scleroglucan (Biosynth, Staad, Switzerland), curdlan (Fujifilm Wako Pure Chemical), paramylon (Sigma), and barley β1-3/1-4-glucan (Sigma). The reactions were made in a mixture (100 μL) of 1 mg/mL β1-3-glucan, 40 mM sodium acetate buffer (pH 5.6), 0.2 mg/mL BSA, and MnLam55A (1.86 nM for laminarin and 186 nM for the others) at 30°C for 15 min. The reaction for the kinetic analysis with laminarin was done in a reaction mixture (100 μL) of 0.2–2 mg/mL (6.4–64 μM; calculated based on the average molecular weight by measuring reducing sugar using BCA method) laminarin, 40 mM sodium acetate buffer (pH 5.6), 0.2 mg/mL BSA, and 3.48 nM MnLam55A, at 30°C for 12 min. Reducing sugar was measured as described in section 3.2.3. For laminarioligosaccharides (DP3–6), reactions were similar to those for laminarin but containing 2–10 mM laminarioligosaccharides and 34.8 nM MnLam55A, at 30°C for 10 min. Release of D-glucose was quantified with a Glucose CII Test (Huggett and Nixon 1957; Miwa *et al*. 1972) after aliquots (25 μL) of the reaction mixtures were heated at 100°C for 3 min and mixed with 50 μL of 2 M Tris-HCl buffer (pH 7.0). Non-linear regressions with the Michaelis-Menten equation on [S]-*v* plots were performed using Grafit version 7. For laminarihexaose, linear regression was performed to calculate k_{cat}/K_m. Three independent replications of each experiment were conducted.

3.2.8 Crystallization and data collection

Crystal of MnLam55A was prepared by the sitting drop vapor-diffusion method as follows: the drop (1.5 μL) was prepared by mixing 5.1 mg/mL MnLam55A in 10 mM 4-(2-hydroxyethyl)-1-piperazineethanesulfonic acid (HEPES)-NaOH buffer (pH 7.0) and 10 mM D-glucose with the same volume of reservoir solution consisting of 0.1 M HEPES-NaOH buffer (pH 7.0), 1 M disodium succinate and 10 mg/mL polyethylene glycol monomethyl ether 2000. Crystallization was observed within 37 days at 20°C. Crystals were picked up from the crystallization solution and flash-cooled. Diffraction data were collected on a beamline BL45XU at SPring-8 (Hyogo, Japan). The data sets were indexed, integrated, scaled, and merged using the XDS program suite (Kabsch 2010). The asymmetric unit of MnLam55A contained two molecules. Estimated Matthews coefficient and solvent content (Matthews 1968) were 3.09 $Å^3Da^{-1}$ and 60.2%, respectively. The data collection and processing statistics are summarized in Table 3-1.

3.2.9 Structure solution and refinement

The structure of MnLam55A was determined by the molecular replacement method with the program AutoMR in the PHENIX program package (Adams *et al*. 2010; McCoy *et al*. 2007). The model structure constructed by ColabFold (Mirdita *et al*. 2022) was used as the search model. The refinement process was carried out using the program phenix.refine in conjunction with interactive fitting and rebuilding based on $2F_o-F_c$ and F_o-F_c electron densities using COOT (Adams *et al*. 2010; Emsley and Cowtan 2004). Water molecules were constructed based on electron densities. The crystal was pseudomerohedrally twinned with the twin operator (−h, −l, −k). The final refinement statistics and geometry defined by MOLPROBITY (Chen *et al*. 2010) are shown in Table

3-1. The atomic coordinates and structure factors were deposited in the Protein Data Bank (http://www.wwpdb.org/; PDB ID, 8JHH). All structure figures were generated by PyMOL ver. 2.6.0a0 (Schrödinger, LLC, New York, NY, USA).

3.2.10 Docking simulation

A docking simulation was performed by AutoDock Vina (ADT version 1.5.6) (Trott and Olson 2010) to estimate the binding mode of MnLam55A to the laminarin main chain. The structure of 6^{III}-*O*-D-glucosyl laminaritriose was constructed by BIOVIA Discovery Studio Visualizer (Dassault Systèmes BIOVIA, San Diego, CA, USA). In the simulation, water and glycerol molecules in the structure of MnLam55A were removed. The 6^{III}-*O*-D-glucosyl laminaritriose was docked into the active site of MnLam55A using the grid box with a spacing of 1 Å and dimension of 40×40×114, centered at positions of 0 (x), 0 (y), and 0 (z).

3.3 Results

3.3.1 Identification of MnLam55A

MnLam55A (0.182 mg, specific activity of 16.8 U/mg) was purified to homogeneity from the culture supernatant of *M. nivale*, cultured for 4 weeks at 18°C. The purified enzyme showed a single band of 68 kDa on SDS-PAGE (Fig. 3-3A). The tryptic digests of MnLam55A were subjected to LC-MS/MS analysis to identify the *MnLam55A* gene from the *M. nivale* genome. The MS/MS spectra of the tryptic digests matched the deduced sequence with 47% coverage of the entire sequence of the putative GH55 protein (DDBJ accession number: LC773407). The N-terminal 19 residues (Met to Ala) in the deduced sequence were a putative cleavable signal sequence, and the next Ser (Ser-1) was

the N-terminal residue of the mature protein. A Web BLASTp search of MnLam55A against non-redundant protein sequences showed the highest identity at 87% to glucan endo-1,3-β-glucosidase BGN13.1 from *M. bolleyi* (NCBI ID: KXJ95237.1). Among characterized GH55 enzymes, the highest identity at 64% was found for LamAI from *Trichoderma viride* U-1 (Nobe *et al*. 2003; Nobe *et al*. 2004). In the phylogenetic analysis of characterized GH55 enzymes, MnLam55A fell into a clade of fungal endo-β-1,3-glucanases together with LamAI (Fig. 3-3B). MnLam55A possesses all of the highly conserved residues of GH55 enzymes for the formation of the catalytic site and subsite −1 as follows: the general acid catalyst, Glu-614; its interacting residue, Tyr-617; the proton relay network activating substrate water, Glu-140, Gln-172, Ser-203, and Glu-591; the subsite −1 forming residues, Glu-140, Trp-552, Asp-557, Glu-591, and His-592; and the aromatic block, Phe-143, Trp-552, and Trp-554 (Fig. 3-2).

Recombinant MnLam55A was extracellularly produced in a *K. pastoris* transformant harboring the gene encoding MnLam55A with the N-terminal signal sequence of α-factor replacing the original signal sequence. N-terminal amino acid sequence analysis showed that the recombinant MnLam55A is started from Ser-1, and the whole sequence of recombinant MnLam55A is expected as Ser-1 to Pro-752. In 1.2 L of the culture broth, 491 U of laminarinase activity was produced after 96 h of cultivation. Purified recombinant MnLam55A (5.57 mg, 94.4 U) showed 16.9 U/mg of specific activity and a single band of 67 kDa on SDS-PAGE, consistent with those of the native enzyme (Fig. 3-3A). The apparent molecular mass on SDS-PAGE was lower than the calculated mass (80 kDa) from amino acid sequences. This smaller apparent molecular mass on SDS-PAGE was also reported in other fungal GH55 endo-β-1,3-glucanases BGN13.1 from *T. harzianum* (de la Cruz *et al*. 1995) and lamAI from *T. viride* (Nobe *et al*. 2004), and is

understood as anomalous migration due to the negative interaction to the gel matrix. Recombinant MnLam55A showed the highest activity at pH 5.6 and 50°C (Fig. 3-4A and B). This enzyme retained ≥95% of the original activity after incubation in a pH range of 4.3–9.3 (4°C, 24 h) and at ≤45°C (for 20 min) (Fig. 3-4A and B).

3.3.2 Time course of laminarin hydrolysis by MnLam55A

The reaction products from laminarin were monitored. At the early stage of the reaction, total molar concentration of reducing sugars was 4-fold higher than the sum of those of D-glucose, gentiobiose and gentiotriose, which were possibly released from non-reducing end of laminarin through exo-acting hydrolysis (Fig. 3-5A). This result suggests that MnLam55A has both endo- and exo-acting activities on laminarin, but acts it mainly in an endo-acting manner. Using 62.5-fold higher concentration of enzyme, the reaction approached the complete digestion of laminarin (Fig. 3-5B and C). D-Glucose and oligosaccharides with DP of 2–4 were gradually accumulated with decrease of laminarin (DP ≥10). After 25.5 h of reaction, 90% of laminarin was degraded to monosaccharide and oligosaccharides of DP2–4 (Fig. 3-5B). The disaccharide, one of the complete degradation products accumulated in the reaction, migrated similarly to the gentiobiose standard in the TLC analysis. The trisaccharide and tetrasaccharide were isolated by gel-filtration column chromatography, and their chemical structures were analyzed by ESI-MS and NMR. In MS spectra of the trisaccharide and the tetrasaccharide, $[M+Na]^+$ ion peaks of *m/z* 527.16 and 689.21 were detected, respectively. From the NMR analysis, the chemical shifts from ^{13}C NMR spectra of the trisaccharide (Table 3-2) and the tetrasaccharide (Table 3-3) matched those of gentiotriose (Usui *et al*. 1973) and gentiotetraose (Fujimoto *et al*. 2009), respectively. MnLam55A catalyzed hydrolysis of

laminarin mainly in the endo-acting manner at the early stage of the reaction, and almost completely hydrolyzed laminarin to D-glucose and gentiooligosaccharides (DP2–4) through its exo-acting activity.

3.3.3 Determination of initially cleaved linkage of laminarin

In order to determine the initial cleavage site of laminarin, NMR analysis of early reaction products from laminarin was performed. ^{1}H NMR spectra (0.0–9.9 ppm) of reaction mixture at 0 min was shown in Fig. 3-6A and B. COSY 2D-NMR spectrum of laminarin showed four correlation peaks between 1-H and 2-H, which corresponded to the four D-glucosyl residues: a, Glc1→6; b, →3Glc1→6; c, →6Glc1→3; and d, →3Glc1→3 (a–d shown in Fig. 3-6C). In addition to these peaks, two correlation peaks derived from the newly produced residues (α and β) were observed in the COSY 2D-NMR spectrum of the 15-min reaction product (Fig. 3-6D). The HMBC 2D-NMR spectra of this reaction product showed the clear correlation peak of 1-C from a and b and 6-H from α and β (δ_H 4.19→δ_C 103.4), although those of 1-H from a and b and 6-C from sugar residues α and β (δ_H 4.50→δ_C 69.4) were covered by other peaks (Fig. 3-6E). The correlation peaks of 3-C from α and β and proton signals from any other D-glucosyl residues were not observed (Fig. 3-6E). These results indicated that α and β were 6-*O*-β-glycosylated D-glucose residues at the reducing end (→6Glc).

Differences of the integration ratio to the sum of the integrations of each 1-H signal between 0- and 15-min reaction solutions were calculated (Fig. 3-6F). The 1-H signals of a and b were obtained by ^{1}H NMR analysis at 27°C, while those of c and d were conducted at 60°C to avoid overlapping the large signal of H_2O (Fig. 3-6G and H, respectively). Anomeric proton signals of sugar residues, a–d, are shown as a1–d1, respectively, and 1-

H signals of the reducing end residue of the reaction products are shown as α1 and β1. The ratio of c1 decreased the most, and it was followed by d1 and b1 (Fig. 3-6F). The signal of a1 slightly increased, and that of α1+β1 significantly increased. The sum of the decreasing ratio of b1 and d1 was almost equal to that of c1, and the increasing ratio of a1 was almost equal to the decreasing ratio of b1. These results indicated that MnLam55A cleaved the β1-3-linkages between sugar residues c and b/d (non-reducing end 6-*O*-glycosylated β1-3-glucosidic linkage of β1-3-linked laminarioligosaccharide portions of laminarin), and produced the oligosaccharides harboring 6-*O*-β-glycosylated D-glucose residues at reducing end (α and β) (Fig. 3-6I).

3.3.4 Reaction products from laminarioligosaccharides

Reactions of MnLam55A with laminarioligosaccharides (DP2–6) were analyzed. MnLam55A degraded laminaritriose and longer laminarioligosaccharides, but not laminaribiose (Fig. 3-7A). At the early stage of the reactions with laminarioligosaccharides (DP4–6), D-glucose was most commonly produced (Fig. 3-7B–D), indicating the dominant exo-type hydrolysis of laminarioligosaccharides. To identify the terminal of the substrates releasing D-glucose, MS analysis of the products from laminaripentaose hydrolyzed in H_2O and $H_2{}^{18}O$ was performed. A mass peak of *m/z* 181.06, corresponding to $[M-H]^-$ of ^{18}O-containing D-glucose, was observed only in the spectrum of the reaction with $H_2{}^{18}O$ (Fig. 3-7E and F). In contrast, the mass peak corresponding to $[M-H]^-$ of ^{18}O-containing laminaritetraose was not observed. The weak mass signal at *m/z* 667.22, two units higher than that of laminaritetraose, was observed in both the reactions with H_2O and $H_2{}^{18}O$ and was considered to be the natural isotope of laminaritetraose (Fig. 3-7G and H).

3.3.5 Substrate specificity of MnLam55A

Reaction velocities for various β-glucans and laminarioligosaccharides (DP2–6) were measured. MnLam55A acted on laminarin (44.8 ± 6.3 s^{-1}), but not on scleroglucan (β1-3/1-6-glucan, β1-3-linked main chain with β1-6-D-glucosyl branches), curdlan (liner β1-3-glucan), paramylon (liner β1-3-glucan), and barley β1-3/1-4-glucan (<0.110 s^{-1}). MnLam55A showed 1,400-fold higher k_{cat}/K_m to laminarin (5,920 $s^{-1}mM^{-1}$) than laminarioligosaccharides of DP3, which showed the highest k_{cat}/K_m (4.21 $s^{-1}mM^{-1}$) of the laminarioligosaccharides (Table 3-4). These differences of k_{cat}/K_m between laminarin and laminarioligosaccharides were caused by the extremely low K_m (0.00947 mM) to laminarin (Table 3-4).

3.3.6 Three-dimensional structure of MnLam55A

The crystal structure of MnLam55A was determined in unliganded form at 2.4 Å resolution. The solved structure contains two molecules of MnLam55A in the asymmetric unit. The entire structure consists of two β-helical domains of 3-solenoid connected by a linker (Fig. 3-8A). Each domain is composed of 12 coils, containing three strands and three loops as observed in GH55 exo-β-1,3-glucosidases (Fig. 3-8A). Root mean square deviation (RMSD) for Cα atoms of MnLam55A and GH55 exo-β-1,3-glucosidases is 1.38 Å and 1.25 Å to fungal enzymes, PcLam55A (PDB ID: 3EQO) and CtLam55 (PDB ID: 5M60), respectively, and 2.79 Å to bacterial one, SacteLam55A (PDB ID: 4PEW). Thus, the whole structure of MnLam55A is more similar to the fungal enzymes than to the bacterial one. The active site and substrate binding site of MnLam55A were compared with those of PcLam55A (PDB ID: 3EQO) and SacteLam55A (PDB ID: 4TZ1) (Fig. 3-

8B). In MnLam55A, the catalytic site and subsite −1 are formed by Glu-140, Gln-172, Ser-203, Trp-552, Asp-557, Glu-591, His-592, Glu-614, and Tyr-617, the aromatic block is formed by Phe-143, Trp-552, and Trp-554, and subsite +1 is formed by Gln-225, Tyr-617, Phe-677, and Phe-678. These residues are spatially conserved well with those of exo-β-1,3-glucosidases (Fig. 3-8B). Residues forming subsite +2 of MnLam55A are Gln-225 and Trp-738, which are spatially placed at similar positions of the corresponding residues of exo-β-1,3-glucosidases, although their orientation is less conserved compared to the residues at subsites −1 and +1 (Fig. 3-8B). As the plus subsites for the binding of longer oligosaccharides, the aromatic residues suggested in SacteLam55A (Trp-196 at subsite +2 and Tyr-194 at subsite +5) and those on the putative substrate binding groove in PcLam55A (Tyr-135, Phe-199, and Trp-245) are not observed in MnLam55A. Docking simulation of MnLam55A with 6^{III}-*O*-D-glucosyl laminaritriose was performed to predict a binding mode of the non-reducing end β1-6-linked Glc^{IV} group to the enzyme. In the docked model, Glc^{III} of the ligand was accommodated at subsite −1 where the non-reducing end D-glucosyl residue of laminaritriose was predicted as shown in Fig. 3-8B. The Glc^{IV} residue was accommodated in possible subsite −2, corresponding to the expected space in the fungal GH55 exo-β-1,3-glucosidases (Ishida *et al*. 2009; Papageorgiou *et al*. 2017) (Fig. 3-8C). His-558 was suitably located to interact with Glc^{IV} in subsite −2 (Fig. 3-8D and E). In the structure of PcLam55A (PDB ID: 3EQO), the corresponding His-576 was similarly located, but more residues seemed to be involved in the formation of the pocket-shaped subsite −2 (Fig. 3-8F, G and H). In contrast, MnLam55A possesses no equivalent residues, particularly to Ser-583 of PcLam55A, mainly due to the differentially oriented C6-L3. The 3-hydroxy group of Glc^{IV} in the MnLam55A structure was located in an open space on an extended cleft structure (Fig. 3-

8C and D). This cleft is formed at the interface of the two domains: C6-L3 in the C-domain (main chain of Gly-559, Thr-560 and Glu-561) to one side, and C4-L1 and C2-L1 of the N-domain involving Leu-141, Arg-138, Thr-135, Glu-74, and Trp-75 for the other (Fig. 3-8E). The extended cleft was expected to form the minus subsites beyond subsite −2.

3.4 Discussion

β-1,3-Glucanases are distributed among various organisms, and degrade β1-3-glucans with various structures (Pitson *et al*. 1993). GH55 contains exo-β-1,3-glucosidases and endo-β-1,3-glucanases acting on laminarin (Drula *et al*. 2022). The dead-end structure of subsite –1 is regarded to be indispensable for the exo-type reaction of exo-β-1,3-glucosidases (Ishida *et al*. 2009; Papageorgiou *et al*. 2017; Bianchetti *et al*. 2015), but the sequence comparison suggests that the residues are conserved in endo-acting enzymes in this family (de la Cruz *et al*. 1995; Nobe *et al*. 2003; Nobe *et al*. 2004). In this chapter, the mechanism for laminarin degradation by GH55 endo-β-1,3-glucanase was described. Firstly, the cleavage site in laminarin was determined by functional analyses. MnLam55A has highly similar amino acid sequences to fungal GH55 endo-β-1,3-glucanases (Fig. 3-2 and 3-3B), and exhibited endo-type action in the reaction with laminarin (Fig. 3-5A) but no activity with β1-3-glucans containing no β1-6-linkages in the main chain, whereas typical endo-β-1,3-glucanases in families other than GH55 randomly degrade the β1-3-glucans (Reese and Mandels 1959; Horikoshi *et al*. 1963). This indicates that β1-6-linkages in the main chain of laminarin are essential for the hydrolysis by MnLam55A, and MnLam55A is clearly discriminated from the typical endo-β-1,3-glucanases. NMR analysis of the initial products from laminarin showed that

MnLam55A predominantly hydrolyzed β1-3-linkages at the non-reducing end of the laminarioligosaccharide moiety adjacent to β1-6-linkage in the laminarin main chain, and produced products containing gentiobiose residues at the reducing end (Fig. 3-6I). As this enzyme almost completely degraded laminarin to D-glucose and gentiooligosaccharides (Fig. 3-5) and showed exo-type action in the reaction with laminarioligosaccharides (Fig. 3-7), this enzyme was suggested to cleave laminarin by the endo-acting hydrolysis first, followed by successive exo-acting hydrolysis of every β1-3-linkage regardless of the presence of β1-6-linked branching moieties from the non-reducing ends, as observed in GH55 exo-β-1,3-glucosidases (Kasahara *et al*. 1992; Martin *et al*. 2006; Ooi *et al*. 2009; Ishida *et al*. 2009). The lack of remaining 3-*O*-β-D-glucosyl gentiooligosaccharides after complete degradation of laminarin (Fig. 3-5C) suggested that MnLam55A hydrolyzes the β1-3-D-glucosidic linkage when linked to gentiooligosaccharides, although laminaribiose is not a substrate of this enzyme. MnLam55A acted similarly on non-reducing terminal β1-3-D-glucosidic linkages of laminarioligosaccharides and laminarioligosaccharide moieties of laminarin, but with very different k_{cat}/K_m values (Table 3-4). MnLam55A much preferred laminarin over the oligosaccharides, even though the k_{cat}/K_m values to longer oligosaccharides are lower than triose (Table 3-4). These results suggest that the long non-reducing end part of laminarin from the scissile β1-3-D-glucosidic linkage provides high binding affinity. Beyond subsites −1 and −2 which accommodated β1-6-linked gentiobiose moieties, further minus subsites were expected for binding the β1-3/1-6-glucan of laminarin main chain in the hydrolysis by MnLam55A.

This work provides the first ternary structure of endo-acting GH55 β-1,3-glucanases. The structure indicates that MnLam55A shares with the GH55 exo-β-1,3-glucosidases (Ishida *et al*. 2009; Papageorgiou *et al*. 2017; Bianchetti *et al*. 2015) not only overall

structure but also the residues forming the catalytic site and subsite −1 including the aromatic block (Fig. 3-8B). The exo-type action of MnLam55A on laminarioligosaccharides and laminarioligosaccharide moieties in the main chain of laminarin is attributed to the structure for exo-acting enzymes. The possible subsite −2 structure of MnLam55A was probed by the docking study with 6^{III}-*O*-D-glucosyl laminaritriose (Fig. 3-8C). The space accommodating the non-reducing end D-glucosyl residue (Glc^{IV}) was equivalent to the pocket structure in fungal GH55 exo-β-1,3-glucosidases for binding of the β1-6-branching moiety of substrate (Ishida *et al*. 2009; Papageorgiou *et al*. 2017), whereas the corresponding space was not present in the structure of bacterial GH55 exo-β-1,3-glucosidase SacteLam55A (Bianchetti *et al*. 2015). The possible binding residue in subsite −2, His-558 of MnLam55A, is conserved well in the fungal GH55 exo-β-1,3-glucosidases and endo-β-1,3-glucanases (Fig. 3-2 and Fig. 3-8C–H). PcLam55A, however, additionally has Asn-147, Ser-583, and Gln-585 involved in the formation of the closed pocket structure, preventing 3-*O*-glycosylated D-glucosyl group from binding to subsite −2 (Fig. 3-8F, G and H). On the contrary, MnLam55A has an open cleft, extending from subsite −2 toward the non-reducing part-binding site, and the 3-hydroxy group of the D-glucosyl residue in subsite −2 points to an open space on the cleft in the docking model (Fig. 3-8D). Thus, this cleft possibly forms minus subsites beyond subsite −2 to accommodate the laminarin main chain linked to 3-O of the D-glucosyl residue bound to subsite −2. The cleft-forming residues of N-domain, Trp-75, Thr-135, and Leu-141 of MnLam55A, are conserved well in other endo-β-1,3-glucanase sequences, which suggests their importance for the formation of minus subsites. Another structure directly involved in the formation of this cleft in MnLam55A is C6-L3 of the C-domain, whereas the corresponding loop of GH55 exo-β-1,3-glucosidases are

differentially located close to subsite −2 to form the closed pocket shape structure (Fig. 3-8C–H). The difference in the C6-L3 localization is presumably caused by the structural difference of the adjacent C5-L3 (Fig. 3-8C–H). C5-L3 of MnLam55A is shorter than the corresponding loops of fungal exo-type enzymes (Fig. 3-2). The smaller size of C5-L3 in the structure probably allows the localization of C6-L3 appropriately for the formation of the extended cleft and possible subsites (illustrated in Fig. 3-9). In addition to the conservation of the cleft-forming residues in primary structures, the comparable lengths of the C5-L3 loops in fungal endo-β-1,3-glucanases suggest that the extended cleft possibly involved in the formation of minus subsites, observed in MnLam55A, is shared by GH55 endo-β-1,3-glucanases (Fig. 3-2). It is noteworthy that the bacterial exo-acting enzymes such as SacteLam55A possess even shorter C5-L3 than MnLam55A (Fig. 3-2), but SacteLam55A has no space for subsite −2 due to the occupation of the space by Phe-143, Trp-144, and Gln-150 in the ternary structure of SacteLam55A. Based on these facts, GH55 enzymes can be divided into three groups: group 1, bacterial exo-β-1,3-glucosidases, which have only subsite −1 as a minus subsite (Fig. 3-10A); group 2, fungal exo-β-1,3-glucosidases, which have subsites −1 and −2 (Fig. 3-10B); and group 3, fungal endo-β-1,3-glucanases, which have subsites −1 and −2, and more minus subsites (Fig. 3-10C). The sequences around the C5-L3 loop are aligned in Fig. 3-10D. The lengths of C5-L3 are clearly different in each group. The putative GH55 enzymes listed in group 3 of Fig. 3-10D seems to be endo-β-1,3-glucanases based on the trend of the length of C5-L3.

The endo-acting MnLam55A, like other GH55 endo-β-1,3-glucanases, showed the greatest preference for laminaritriose of laminarioligosaccharides (Table 3-4), whereas GH55 exo-β-1,3-glucosidases prefer the longer ones (Martin *et al*. 2006; Ishida *et al*.

2009). All of them commonly show very low or undetectable activity to laminaribiose (Fig. 3-7A) (Nobe *et al*. 2004; Martin *et al*. 2006; Ishida *et al*. 2009; Papageorgiou *et al*. 2017; Bianchetti *et al*. 2015). The trisaccharide requirement for activity commonly observed in the GH55 enzymes is probably due to the well-conserved structure of subsites −1 and +1, with a little difference in the subsite +2-forming residues (Fig. 3-2 and 3-8B). Laminaritriose is probably required for productive binding. In contrast, some aromatic residues such as Trp-196 and Tyr-194 in SacteLam55A at subsites +2 and +5, respectively (Bianchetti *et al*. 2015), and Tyr-135, Phe-199, and Trp-245 on the long groove in PcLam55A (Ishida *et al*. 2009) are involved in the formation of the plus subsites, but MnLam55A lacks these aromatic residues. This probably causes the different preference for long-chain laminarioligosaccharides.

In conclusion, it was found that endo-acting hydrolysis of MnLam55A cleaves the β1-3-linkages at the non-reducing end of the laminarioligosaccharide moiety adjacent to β1-6-linkages in the laminarin main chain with significantly higher affinity than exo-wise hydrolysis of laminarioligosaccharides. Crystal structure determination and the docking analysis revealed that MnLam55A shares with fungal GH55 exo-β-1,3-glucosidases overall structures and subsites −2 to +2, including the binding mode of the gentiobiose moiety in subsites −1 and −2, but the possible substrate-binding cleft extending from subsite −2 was found in MnLam55A structure for the first time. The relevant structures are similar in other GH55 endo-β-1,3-glucanases. Based on these findings, the substrate binding modes in GH55 endo-acting β-1,3-glucanases are presented (Fig. 3-9).

Table 3-1. Summary of crystallization conditions, data collection, and refinement statistics.

	MnLam55A
Data collection	
PDB ID	8JHH
Beamline	SPring-8 BL45XU
Space group	$I2_12_12_1$
Unit cell parameters a, b, c, (Å)	89.2, 211.0, 211.2
Unit cell parameters α, β, γ, (º)	90, 90, 90
Wavelength (Å)	1.0000
Resolution range (Å)	50.0-2.40 (2.55-2.40)
Total No. of reflections	467,996 (77,596)
No. of unique reflections	77,596 (12,330)
R_{meas} (%)	27.1 (98.9)
R_{merge} (%)	24.8 (90.0)
R_{pim} (%)	11.0 (43.1)
$\langle I/\sigma(I) \rangle$	6.48 (1.68)
Wilson B-factor (Å^2)	27.6
$CC_{1/2}$	98.8 (78.1)
Completeness (%)	99.8 (99.2)
Redundancy	6.03 (5.87)
Refinement	
No. reflections used in refinement	77,596
No. reflection used for R_{free}	3,879
R_{work}/R_{free} (%)	16.3/19.4
Twin operator	$-h, -l, -k$
Twin fraction (%)	36.8
CC*	99.5 (79.4)
CC_{work}	88.6 (60.0)
CC_{free}	85.3 (50.6)
No. of atoms	
Macromolecules	11,322
Ligand/ion	3
Water	236
B-factors (Å^2)	
Macromolecules	22.4
Ligand/ion	23.9
Water	31.2
Protein residues	1,470
RMSD from ideal	
Bond lengths (Å)	0.004
Bond angles (°)	0.63
Clashscore	3.77
Ramachandran	
Favored (%)	95.4
Allowed (%)	4.4
Outliers (%)	0.2

Values in parentheses are for the highest resolution shell.

Table 3-2 Chemical shifts of gentiotriose in ^{13}C NMR spectra.

Residue [a]	Number	δ_C (ppm)	δ_{Cref} (ppm) [b]
Iα	1	92.9	93.4
	2	72.2	73.1
	3	73.5	74.3
	4	70.3	71.2
	5	71.2	71.2
	6	69.6	70.0 or 70.2
Iβ	1	96.8	97.3
	2	74.8	75.5
	3	76.3	76.8
	4	70.4	71.2
	5	75.7	76.1
	6	69.8	70.0 or 70.2
II	1	103.5 or 103.6	103.7
	2	73.8 or 73.9	74.6
	3	76.5	77.1
	4	70.3	71.2
	5	75.8	76.1
	6	69.3	70.0 or 70.2
III	1	103.5 or 103.6	103.7
	2	73.8 or 73.9	74.6
	3	76.5	77.1
	4	70.2	71.0
	5	76.7	77.1
	6	61.5	62.4

[a] Roman numbers indicate the positions of D-glucosyl residue counted from the reducing-end.
[b] δ_{Cref} is reported data by Usui *et al*. (Usui *et al*. 1973).

Table 3-3 Chemical shifts of gentiotetraose in ^{13}C NMR spectra.

Residue [a]	Number	δ_C (ppm)	δ_{Cref} (ppm) [b]
Iα	1	92.9	94.9
	2	72.2	74.2
	3	73.5	75.5
	4	70.3	72.2
	5	71.2	73.2
	6	69.6	71.6
Iβ	1	96.8	98.8
	2	74.8	76.8
	3	76.4	78.5
	4	70.4	72.3
	5	75.7	77.6
	6	69.8	71.8
II and III	1	103.5–103.8	105.5 and 105.8
	2	73.8 or 73.9	75.8
	3	76.5	78.4
	4	70.3	72.2
	5	75.8	77.8
	6	69.4	71.6 and 71.4
IV	1	103.5–103.8	105.7
	2	73.8 or 73.9	75.9
	3	76.5	78.5
	4	70.2	72.4
	5	76.7	78.7
	6	61.5	63.5

[a] Roman numbers indicate the positions of D-glucosyl residue counted from the reducing-end.
[b] δ_{Cref} is reported data by Fujimoto *et al*. (Fujimoto *et al*. 2009).

Table 3-4. Kinetic parameters of recombinant MnLam55A

substrate	k_{cat} (s^{-1})	K_m (mM)	k_{cat}/K_m ($s^{-1}mM^{-1}$)	Relative k_{cat}/K_m
laminaritriose	24.3 ± 2.4	5.86 ± 1.03	4.21	7.11×10^{-4}
laminaritetraose	17.4 ± 1.3	4.68 ± 0.89	3.79	6.40×10^{-4}
laminaripentaose	13.1 ± 1.5	5.02 ± 1.07	2.65	4.48×10^{-4}
laminarihexaose	n.a.	n.a.	0.497	8.40×10^{-5}
laminarin	56.1 ± 5.2	0.00947 ± 0.00162	5,920	1

n.a., not analyzed.

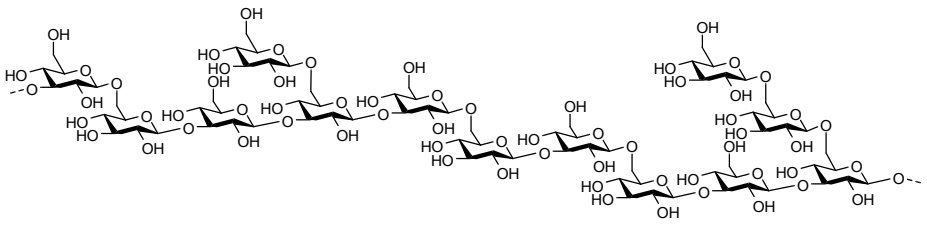

Fig. 3-1. Estimated chemical structure of laminarin from *E. bicyclis*
The chemical structure of laminarin was illustrated based on the report by Liu *et al*. (Liu *et al*., 2018).

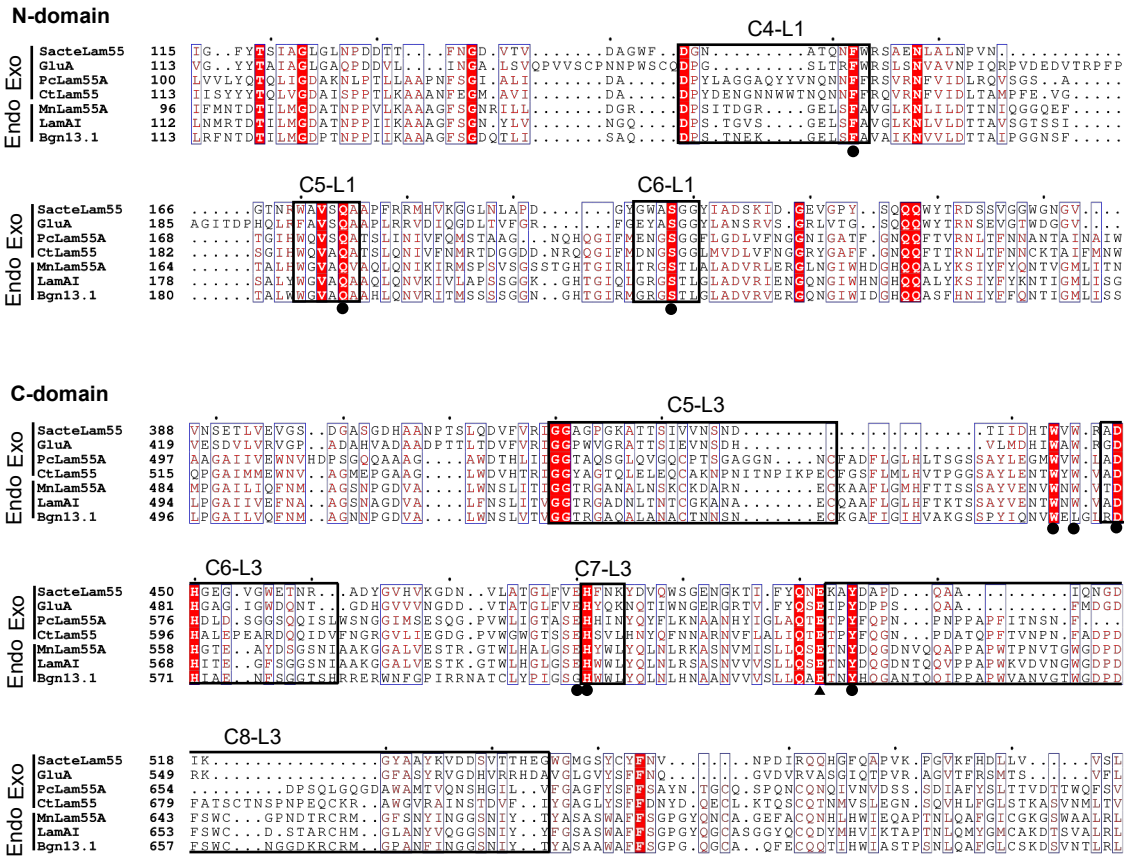

Fig. 3-2 Comparison of partial sequences of characterized GH55 enzymes.
The amino acid sequences were aligned with MAFFT ver. 7 (Katoh *et al*. 2019). The result of alignment was visualized using ESPript 3.0 (Robert and Gouet 2014). Closed circles indicate highly conserved residues in GH55 enzymes; a closed triangle indicates general acid catalyst; squares with thick borders indicate the loops.

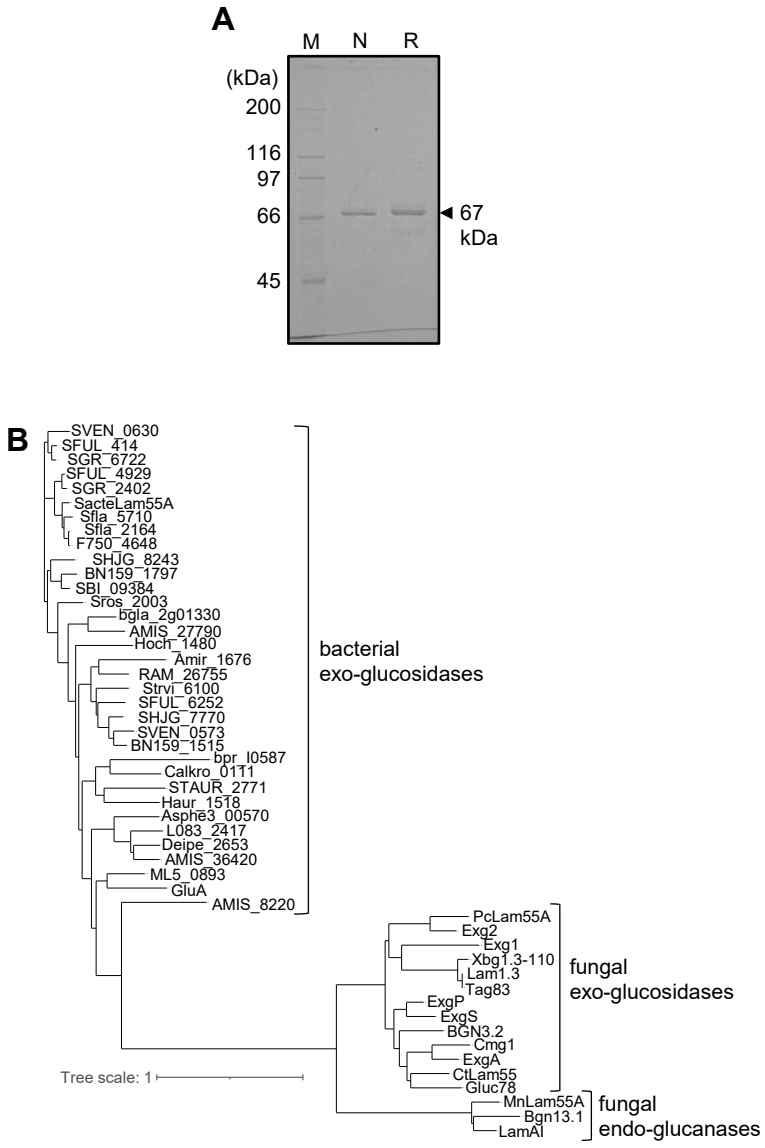

Fig. 3-3. Identification of MnLam55A.
(A) SDS-PAGE of native and recombinant MnLam55A. Lane M, protein markers; lane N, native MnLam55A; lane R, recombinant MnLam55A. (B) Phylogenetic tree of characterized GH55 enzymes was made by MAFFT ver. 7 (Katoh *et al*. 2019) and visualized by iTOL ver. 6 (Letunic and Bork 2021).

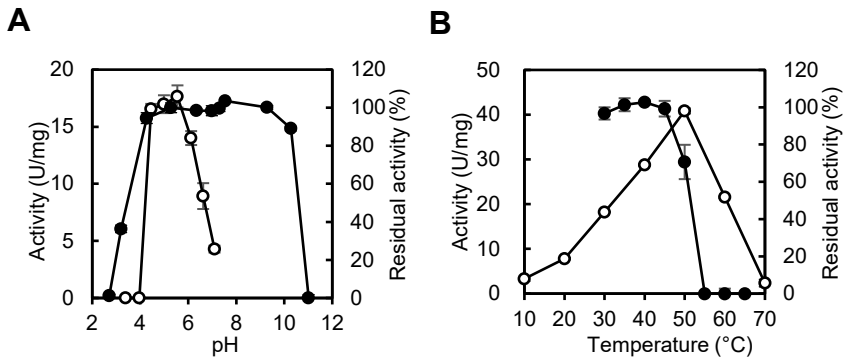

Fig. 3-4. Effect of pH and temperature on the activity of MnLam55A.
(A) Effect of pH on recombinant MnLam55A activity. Open and closed circles show activity and stability, respectively. (B) Effect of temperature on recombinant MnLam55A activity. Open and closed circles show activity and stability, respectively.

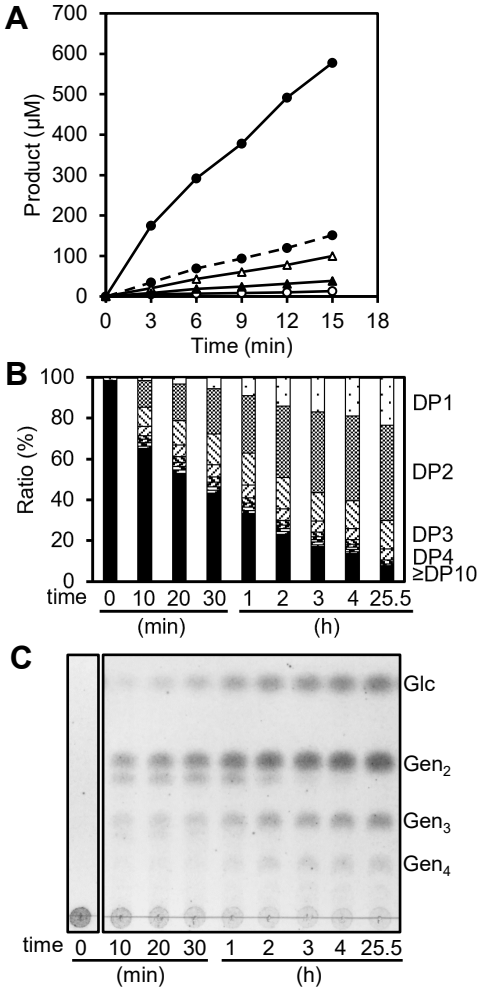

Fig. 3-5. Progress of reaction product formation from laminarin by MnLam55A.
(A) Time course of increase in initial reaction products from 4 mg/mL laminarin. Solid line with closed circles shows the concentrations of reducing sugars, and broken line with closed circles shows the concentrations of the sum of D-glucose, gentiobiose and gentiotriose. Open circles, closed triangles, and open triangles show D-glucose, gentiotriose and gentiobiose, respectively. (B) Time course of DP of the products from 10 mg/mL laminarin. Percentage was based on the weight ratio. (C) TLC of the same samples shown in panel B. Glc, D-glucose; Gen_n, gentiooligosaccharide of DP*n*.

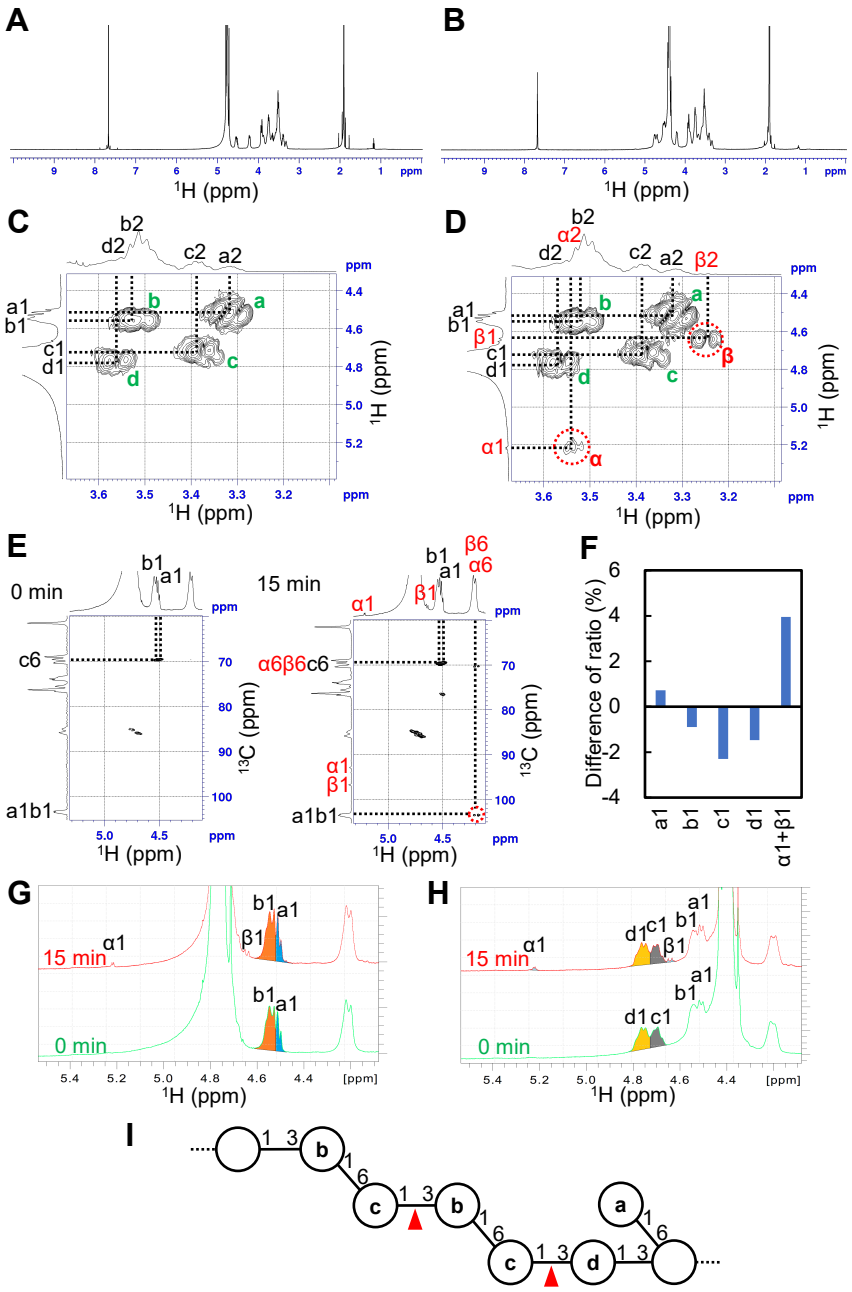

Fig. 3-6. NMR analysis of initial reaction products of MnLam55A with laminarin.
(A and B) ^{1}H NMR spectra (0.0–9.9 ppm) of reaction mixture at 0 min shown in Fig. 3-5A recorded at 27˚C (A) and 60˚C (B). (C) COSY 2D-NMR spectrum of reaction mixture at 0-min of Fig. 3-5A. Correlation peaks indicated as a–d are corresponded to labeled D-glucosyl residues in the model figure of laminarin. (D) COSY 2D-NMR spectrum of reaction mixture at 15 min of Fig. 3-5A. (E) HMBC 2D-NMR spectra of reaction mixture at 0 and 15 min of Fig. 3-5A. (F) The difference of integration ratio of 1-H proton signals colored in G and H. (G and H) ^{1}H NMR spectra of reaction mixture at 0 and 15 min shown in Fig. 3-5A recorded at 27˚C (G) and 60˚C (H). (I) The determined endo-acting cleavage sites in laminarin by MnLam55A.

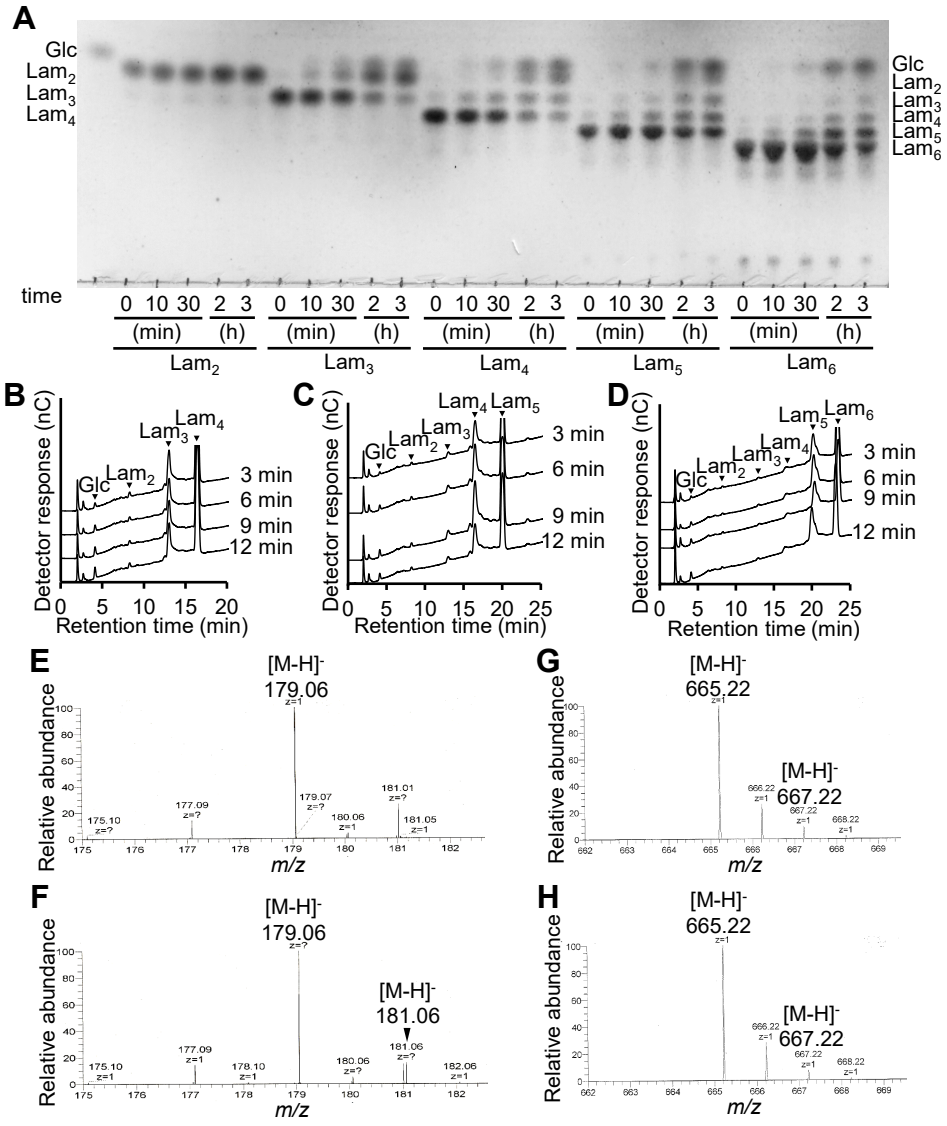

Fig. 3-7. Reaction of MnLam55A with laminarioligosaccharide.
(A) TLC analysis of MnLam55A reaction products. MnLam55A (17.4 nM) was incubated with 10 mM laminarioligosaccharides (DP2–6). Lam$_n$, laminarioligosaccharide of DPn. (B–D) HPAEC-PAD analysis of MnLam55A initial products. MnLam55A (17.4 nM) was incubated with 10 mM laminaritetraose (B), laminaripentaose (C), or laminarihexaose (D). (E–H) ESI-MS spectra of reaction products from 2 mM laminaripentaose in H_2O or $H_2{}^{18}O$. The mass peak of *m/z* 181.01 in both E and F is from a contaminating compound.

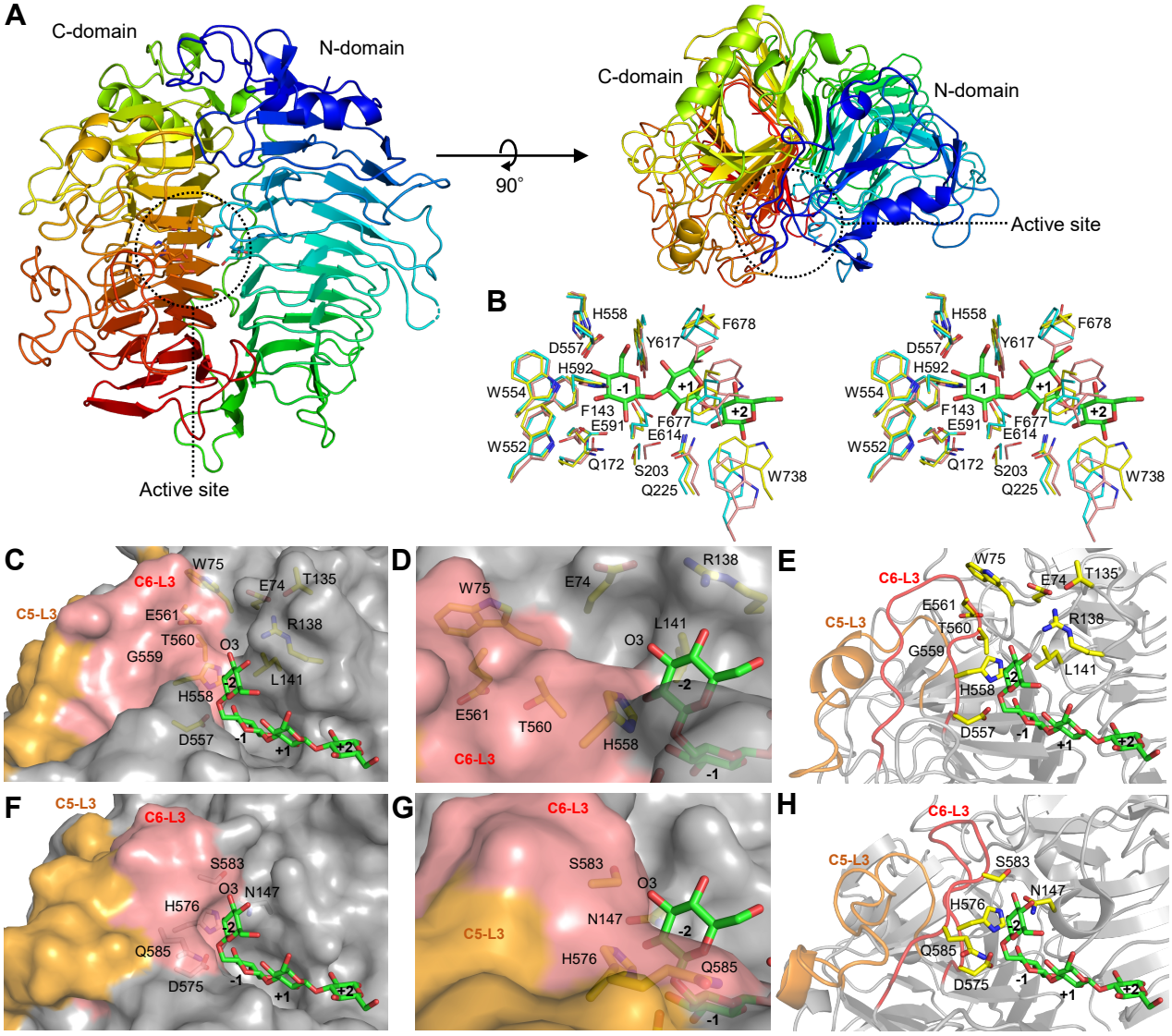

Fig. 3-8. Three-dimensional structure of MnLam55A.
(A) The crystal structure of MnLam55A was determined in unliganded form at 2.4 Å resolution. (B) Stereo-view of the structure around subsites −1 to +2. The residues of MnLam55A (yellow), PcLam55A (PDB ID: 3eqo; cyan) and SacteLam55A (PDB ID: 4TZ1; pink) and laminaritriose from 4TZ1 were shown. (C–E) 6^{III}-*O*-D-glucosyl laminaritriose docked MnLam55A structure using AutoDock Vina. (F–H) The corresponding structure of PcLam55A. The ligand is from the docking model of MnLam55A.

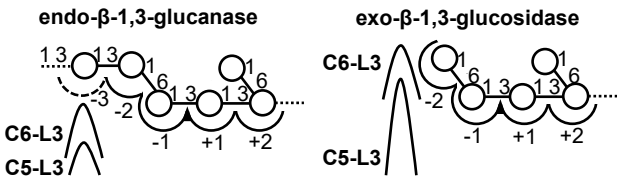

Fig. 3-9. Substrate-binding mode of GH55 enzymes.
Predicted substrate-binding mode of exo-β-1,3-glucosidases and endo-β-1,3-glucanases.

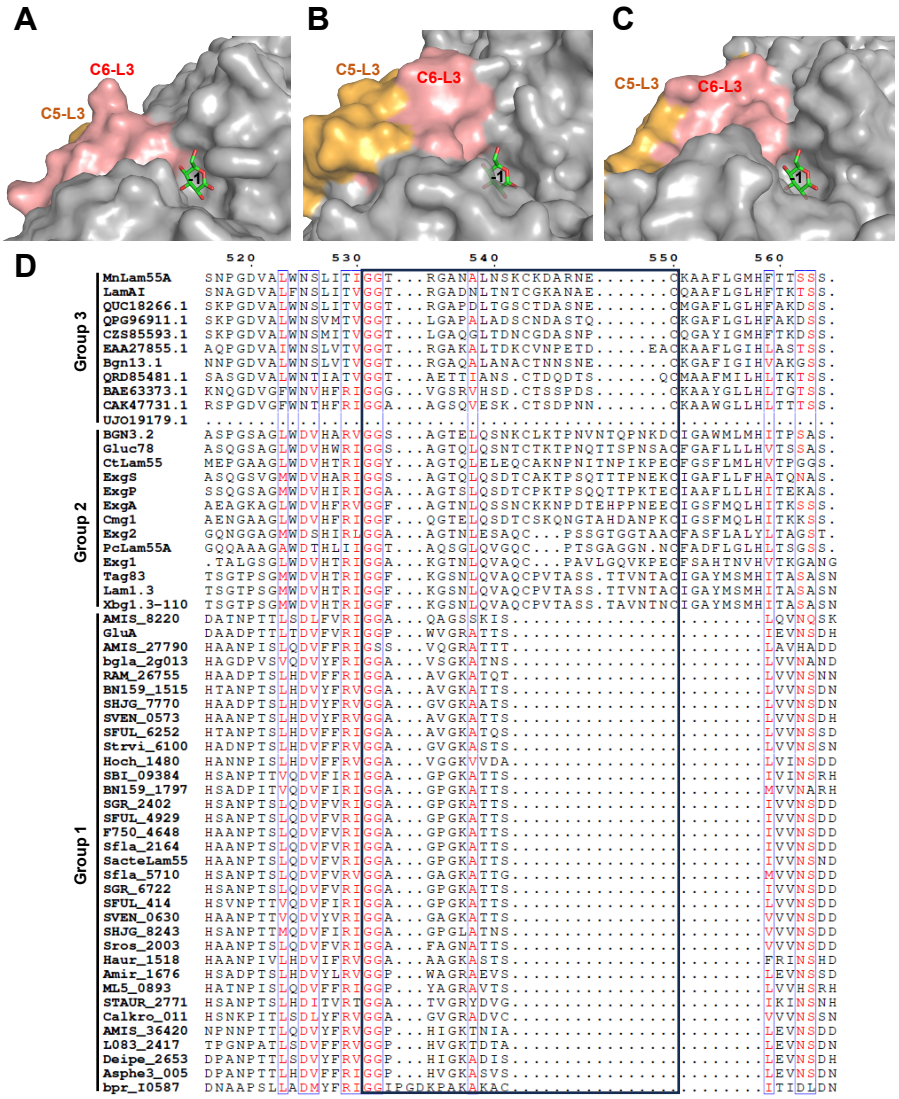

Fig. 3-10. Structural comparison of GH55 enzymes.
(A) Bacterial exo-β-1,3-glucosidase with gluconolactone from 3EQO (SacteLam55A; PDB ID: 4PEY). (B) Fungal exo-β-1,3-glucosidase (PcLam55A; PDB ID: 3EQO). (C) Fungal endo-β-1,3-glucanase (MnLam55A) with gluconolactone from 3EQO. (D) The amino acid sequences of characterized GH55 enzymes and several putative GH55 endo-β-1,3-glucanases were aligned with MAFFT ver. 7 (Katoh *et al*. 2019). The result of alignment was visualized using ESPript 3.0 (Robert and Gouet 2014). Squares with thick borders indicate the C5-L3 loop.

3. Chemical synthesis of three monomeric units for the synthesis of β1-3/1-6-glucooligosaccharides

4.1 Introduction

As described in chapter 1, β1-3/1-6-glucan has a variety of structures. Fungal β1-3/1-6-glucans such as *Schizophyllum commune* schizophyllan and *Lentinula edodes* lentinan have a main chain comprising only β1-3-glucosidic linkages and side chains comprising β1-6-glucosides (Zhang *et al*. 2011; Zhang *et al*. 2013). *E. bicyclis* laminarins contain β1-6-glucosidic linkages in the β1-3-glucan main chain and single D-glucosyl as well as gentiooligosaccharyl residues in their side chain (Menshova *et al*. 2014; Liu *et al*. 2018).

β1-3/1-6-Glucans have various health benefits and are known to act as antitumor, anti-inflammatory, and immunostimulatory agents (Vetvicka and Yvin 2004; Brown and Gordon 2005; Chen and Seviour 2007; Zhang *et al*. 2011; Zhang *et al*. 2013; Menshova *et al*. 2014; Liu *et al*. 2018). Their functionality is related to their structure (Pang *et al*. 2005; Chen and Seviour 2007; Zhang *et al*. 2013; Menshova *et al*. 2014; Liu *et al*. 2018), but the relationship is not yet fully understood. To investigate their structure-dependent bioactivity, oligosaccharides that accurately represent portions of the β1-3/1-6-glucan structures are needed. Furthermore, due to their structural diversity, the degradation scheme of β1-3/1-6 glucans is complex and still needs to be determined. For further functional and structural analysis of the enzymes acting on β1-3/1-6-glucans including GH3 and GH55 enzymes, the oligosaccharides with the partial structures of laminarin are desired.

Laminarioligosaccharides containing β1-6-linked D-glucosyl branches (Takeo and Tei 1986; Du *et al*. 2000; Yang and Kong 2000; Ning *et al*. 2003; Tanaka *et al*. 2003; Yang and Kong 2005; Adamo *et al*. 2011; Tanaka *et al*. 2012; Miyagawa *et al*. 2015),

laminaribiosyl branches, and gentiotetraosyl branches (Zeng and Kong 2003; Zhao *et al*. 2003; Zhou *et al*. 2021) have been synthesized through chemical routes. Of these, 6^{I},6^{III}-di-*O*-D-glucosyl laminaritetraose demonstrated its antitumor activity (Ning *et al*. 2003). Conversely, the synthesis of β1-3-linked glucooligosaccharides containing β1-6-linkages in the main chain is limited (Takeo *et al*. 1986; Adamo *et al*. 2011; Miyagawa *et al*. 2015), and none of the synthetic routes of them include the synthesis of internal β1-6-linkages or the development of monomeric units suitable for it. The enzymatic synthesis is also limited to 6-*O*-glucosylation of laminarioligosaccharides at the non-reducing end (Kawai *et al*. 2004; Smaali *et al*. 2004). To synthesize the oligosaccharides with the partial structure of *E. bicyclis* laminarin main chain, another method is required. The synthesis of β1-3- and β1-6-linkages in desired order requires suitable monomeric units. In this chapter, the design of three monomeric units and the effective function of these units for the sequential synthesis of β1-3- and β1-6-linkages are described. One serves as a β1-3-specific acceptor for the first glycosylation, and the other two units as donors for glycosylation to produce β1-3- and β1-6-specific acceptors. The 3-specific introduction of the orthogonal protecting group proceeded highly efficiently. The monomeric unit for the synthesis of β1-6-linkage was synthesized in short steps. These three units were derived from the same starting compound. The synthesis of a derivative of the tetrasaccharide Glcβ1-6Glcβ1-3Glcβ1-3Glc (compound **1**; Fig. 4-1) using the three units is demonstrated.

4.2 Materials and methods

4.2.1 General

Wakogel C-200 (Fujifilm Wako Pure Chemical) and Silica gel 60N (Kanto

Chemical) was used for silica gel column chromatography. The reaction progress and collected fractions were monitored and checked by TLC using a Silica gel 60 F_{254} plate (Merck). Plates were visualized by UV detection, treated with a detection reagent (as described in the section 2.2.12 or 20% (v/v) sulfuric acid in EtOH), and heated. For NMR analysis, samples were dissolved in $CDCl_3$ and analyzed with an Avance Neo (Bruker). An Exactive Plus (Thermo Fisher Scientific) was used for ESI-Fourier transform (FT)-MS analysis. The data were collected in positive and negative ion modes. A JASCO P-2200 polarimeter (Jasco) was used for optical rotation analysis.

4.2.2 Phenylthio β-D-glucopyranoside (compound **2**)

Compound **2** was synthesized from D-glucopyranose as reported previously (Roy *et al*. 2008). To a stirred solution of sodium acetate [1.1 equivalent (eq.) 50.0 g, 610 mmol] in acetic anhydride (7.6 eq., 400 mL, 4.24 mol) was added D-glucopyranose (1 eq., 100 g, 555 mmol) at 110°C, and the reaction mixture was further stirred for 10 min at 110°C. The reaction was terminated by adding crashed ice and cold water, and the solution was stirred at room temperature for the crystallization. The solid portion was filtrated, washed by water, and dried in vacuo.

To a stirred solution of a part of the collected sample (1 eq., 60.1 g, 154 mmol) in dry dichloromethane (353 mL) were added thiophenol (1.1 eq., 17.4 mL, 169 mmol) and boron trifluoride·diethyl ether complex (2 eq., 39.0 mL, 308 mmol), and the reaction mixture was further stirred for 17.5 h at room temperature. The samples were extracted with water and chloroform, followed with saturated sodium hydrogen carbonate and chloroform, and the chloroform layer was concentrated in vacuo. To a stirred solution of all sample in MeOH (500 mL) was added sodium methoxide until the pH of the solution

reached 10, and the reaction mixture was further stirred for 16 h at room temperature. The reaction was terminated by adding acetic acid until the pH reached 5, and the samples were extracted with toluene and water, and water layer was concentrated in vacuo and cooled at 0°C for the crystallization. Compound **2** (16.0 g, 38%) was obtained.

4.2.3 Introduction of a 3-position-specific levulinyl (Lev) group to compound **2** under three conditions (a, b, and c)

Preparation of levulinic acid anhydride (for use in a, b, and c): To a stirred solution of levulinic acid (4.4 eq., 188 mg, 1.61 mmol) in dry dichloromethane (2 mL) was added *N,N'*-diisopropylcarbodiimide (DIC) (2.2 eq., 102 mg, 807 μmol), and the reaction mixture was further stirred for 40 min at 0°C. The solution was concentrated in vacuo, and the residue was dissolved in dry *N,N*-dimethylformamide (DMF) (4 mL).

Conditions a: To a stirred solution of compound **2** (1 eq., 100 mg, 367 μmol) and 4-(dimethylamino)pyridine (DMAP) (0.1 eq., 4.48 mg, 36.7 μmol) in DMF (2 mL) was added a solution of levulinic acid anhydride (2.2 eq., 805 μmol) in DMF (2 mL), and the reaction mixture was further stirred for 3.5 h at 0°C.

Conditions b: To a stirred solution of compound **2** (1 eq., 1.00 g, 3.67 mmol) in pyridine (2 mL) was added a solution of levulinic acid anhydride (2.2 eq., 8.05 mmol) in DMF (20 mL), and the reaction mixture was further stirred for 15.5 h at 0°C.

Conditions c: To a stirred solution of compound **2** (1 eq., 100 mg, 367 μmol) in DMF (2 mL) were added pyridine (1.1 eq., 32.7 μL, 2.02 mmol) and a solution of levulinic acid anhydride (2.2 eq., 805 μmol) in DMF (2 mL), and the reaction mixture was stirred for 21.5 h at 0°C, and for further 74.5 h at 27°C.

In all the above conditions (a, b, and c), the reaction was terminated by adding

crushed ice, and in case of the condition b, the volatile components of the solution were removed in vacuo, and the resulting residue was purified by silica gel column chromatography using $CHCl_3$/MeOH (19/1, v/v) as a mobile phase and further separated *via* silica gel column chromatography using ethyl acetate as the mobile phase to give pure compounds **3**, **4** and **5** and the mixture of compounds **4** and **6**. Chemical structures of compounds **3**, **4** and **5** were elucidated by NMR data. The synthesized compounds were used as standards in following HPLC analysis. Compound **6** was assumed to be phenyl 4-*O*-levulinyl-1-thio-β-D-glucopyranoside, but the structure was not determined due to the small amounts of isolated compound. The reaction yield of compounds **3**, **4**, **5**, and **6** are 16%, 16%, 7%, and 5%, respectively under conditions a, 18%, 11%, 10%, and 5% under conditions b, and 7%, 28%, 6%, and 10% under conditions c (Fig. 4-2, 4-3). Compound **3**; ^{1}H NMR (400 MHz, $CDCl_3$): δ 2.15 (s, 3H, Me of Lev), 2.57 (t, 2H, J 6.3 Hz, $COC\underline{H}_2CH_2COCH_3$), 2.72 (t, 2H, J 6.4 Hz, $COCH_2C\underline{H}_2COCH_3$), 3.38 (t, 1H, $J_{1,2}$ = $J_{2,3}$ 9.4 Hz, H-2), 3.41 (t, 1H, $J_{3,4}$ = $J_{4,5}$ 9.8 Hz, H-4), 3.50 (ddd, 1H, $J_{4,5}$ 9.7 Hz, $J_{5,6}$ 5.2 Hz, $J_{5,6'}$ 2.5 Hz, H-5), 3.56 (t, 1H, $J_{2,3}$ = $J_{3,4}$ 8.8 Hz, H-3), 4.30 (dd, 1H, $J_{5,6}$ 5.1 Hz, J_{gem} 12.2 Hz, H-6), 4.35 (dd, 1H, $J_{5,6'}$ 2.2 Hz, J_{gem} 11.9 Hz, H-6′), 4.59 (d, 1H, $J_{1,2}$ 9.7 Hz, H-1), 7.22–7.51 (m, 5H, Ph); ^{13}C NMR (100 MHz, $CDCl_3$): δ 27.9 ($CO\underline{C}H_2CH_2COCH_3$), 29.9 (Me of Lev), 38.0 ($COCH_2\underline{C}H_2COCH_3$), 63.8 (C-6), 69.7 (C-4), 72.1 (C-2), 77.5 (C-5), 77.7 (C-3), 87.7 (C-1), 127.7, 128.9, 132.0, 132.9, 173.1 ($\underline{C}OCH_2CH_2COCH_3$), 207.8 ($COCH_2CH_2\underline{C}OCH_3$); HMBC 2D-NMR (400 MHz, $CDCl_3$), δ 4.30 (H-6) and 4.35 (H-6′) →173.1 ($\underline{C}OCH_2CH_2COCH_3$), indicates 6-OH was protected by Lev. Compound **4**; ^{1}H NMR (400 MHz, $CDCl_3$): δ 2.18 (s, 3H, Me of Lev), 2.60 (m, 2H, $COC\underline{H}_2CH_2COCH_3$), 2.82 (m, 2H, $COCH_2C\underline{H}_2COCH_3$), 3.47 (ddd, 1H, $J_{4,5}$ 9.6 Hz, $J_{5,6}$ 4.7 Hz, $J_{5,6'}$ 3.3 Hz, H-5), 3.47 (t, 1H, $J_{1,2}$ 9.6 Hz, $J_{2,3}$ 9.3 Hz, H-2), 3.66 (t, 1H, $J_{3,4}$ = $J_{4,5}$ 9.5 Hz, H-4), 3.81 (dd,

1H, $J_{5,6}$ 4.8 Hz, J_{gem} 12.0 Hz, H-6), 3.94 (dd, 1H, $J_{5,6'}$ 3.3 Hz, J_{gem} 12.0 Hz, H-6′), 4.65 (d, 1H, $J_{1,2}$ 9.8 Hz, H-1), 5.01 (t, 1H, $J_{2,3} = J_{3,4}$ 9.2 Hz, H-3), 7.25–7.59 (m, 5H, Ph); ^{13}C NMR (100 MHz, $CDCl_3$): δ 28.3 ($CO\underline{C}H_2CH_2COCH_3$), 29.8 (Me of Lev), 38.5 ($COCH_2\underline{C}H_2COCH_3$), 62.5 (C-6), 69.2 (C-4), 70.4 (C-2), 79.6 (C-5), 79.6 (C-3), 88.1 (C-1), 128.3, 129.1, 131.6, 132.8, 173.7 ($\underline{C}OCH_2CH_2COCH_3$), 208.4 ($COCH_2CH_2\underline{C}OCH_3$); HMBC 2D-NMR (400 MHz, $CDCl_3$), δ 5.01 (H-3) →173.7 ($\underline{C}OCH_2CH_2COCH_3$), indicates 3-OH was protected by Lev. Compound **5**; ^{1}H NMR (400 MHz, $CDCl_3$): δ 2.21 (s, 3H, Me of Lev), 2.61 (m, 2H, $COC\underline{H}_2CH_2COCH_3$), 2.89 (m, 2H, $COCH_2C\underline{H}_2COCH_3$), 3.47 (m, 1H, H-5), 3.61 (t, 1H, $J_{3,4} = J_{4,5}$ 9.4 Hz, H-4), 3.72 (t, 1H, $J_{2,3} = J_{3,4}$ 8.8 Hz, H-3), 3.81 (dd, 1H, $J_{5,6}$ 5.0 Hz, J_{gem} 12.2 Hz, H-6), 3.94 (m, 1H, H-6′), 4.74 (d, 1H, $J_{1,2}$ 10.1 Hz, H-1), 4.82 (t, 1H, $J_{1,2} = J_{2,3}$ 9.4 Hz, H-2), 6.98–7.54 (m, 5H, Ph); δ 4.82 (H-2) indicates 2-OH was protected by Lev.

HPLC analysis: A portion of each sample was dissolved in acetonitrile and analyzed by HPLC, employing a COSMOSIL Cholester column (4.6 mm I.D. × 250 mm; Nacalai Tesque), with elution at a linear gradient of 5–100% acetonitrile for 40 min at room temperature, at a flow rate of 1 mL/min, and detection at A_{254}.

4.2.4 Phenyl 3-*O*-levulinyl-1-thio-β-D-glucopyranoside (compound **4**) and phenyl 2,4,6-tri-*O*-benzoyl-3-*O*-levulinyl-1-thio-β-D-glucopyranoside (compound **7**)

To a stirred solution of compound **2** (1 eq., 14 g, 51.4 mmol) in DMF (280 mL) were added pyridine (1.1 eq., 4.6 mL, 56.6 mmol) and levulinic acid anhydride in DMF (280 mL), and the reaction mixture was further stirred for 110 h at 23°C. The reaction was terminated by adding ice water, the volatile components of the solution were removed in vacuo, and the resulting residue was purified by silica gel column chromatography using

$CHCl_3$/MeOH (19/1, v/v) as the mobile phase and further separated *via* the same column chromatography to give a mixture of compounds **4** and **5**. To a stirred solution of this mixture (1 eq., 8.71 g, 22.5 mmol) in pyridine (26 mL) was added benzoyl chloride (BzCl) (6 eq., 15.6 mL, 135 mmol), and the reaction mixture was further stirred for 1 h at room temperature. The reaction was terminated by adding ice water, and the solution was extracted with 2 M HCl and chloroform. The volatile components of the organic layer were removed in vacuo, and the resulting residue was purified by silica gel column chromatography using toluene/ethyl acetate (10/1, v/v) as the mobile phase to give pure compound **7** (5.17 g, 14%). $[\alpha]_D^{27}$ +14.0 (c 1.25, $CHCl_3$); ^{1}H NMR (400 MHz, $CDCl_3$): δ 1.86 (s, 3H, Me of Lev), 2.32 (m, 2H, $COC\underline{H}_2CH_2COCH_3$), 2.41 (m, 2H, $COCH_2C\underline{H}_2COCH_3$), 4.12 (ddd, 1H, $J_{4,5}$ 10.0 Hz, $J_{5,6}$ 6.0 Hz, $J_{5,6'}$ 2.8 Hz, H-5), 4.44 (dd, 1H, J_{gem} 12.2 Hz, $J_{5,6}$ 6.0 Hz, H-6), 4.65 (dd, 1H, J_{gem} 12.2 Hz, $J_{5,6'}$ 2.8 Hz, H-6′), 4.98 (d, 1H, $J_{1,2}$ 10.0 Hz, H-1), 5.34 (t, 1H, $J_{1,2} = J_{2,3}$ 9.8 Hz, H-2), 5.46 (t, 1H, $J_{3,4} = J_{4,5}$ 9.8 Hz, H-4), 5.68 (t, 1H, $J_{2,3} = J_{3,4}$ 9.5 Hz, H-3), 7.10–8.13 (m, 20H, 4Ph); ^{13}C NMR (100 MHz, $CDCl_3$): δ 28.0 ($CO\underline{C}H_2CH_2COCH_3$), 29.2 (Me of Lev), 37.8 ($COCH_2\underline{C}H_2COCH_3$), 63.2 (C-6), 69.3 (C-4), 70.4 (C-2), 73.8 (C-3), 76.2 (C-5), 86.1 (C-1), 128.3, 128.4, 128.49, 128.52, 128.54, 128.8, 128.9, 129.3, 129.6, 129.8, 129.97, 130.00, 130.2, 131.8, 133.1, 133.2, 133.5, 133.6, 133.7, 165.1 (C=O of benzoyl [Bz]), 165.2 (C=O of Bz), 166.1 (C=O of Bz), 171.8 ($\underline{C}OCH_2CH_2COCH_3$), 205.4 ($COCH_2CH_2\underline{C}OCH_3$); HMBC 2D-NMR (400 MHz, $CDCl_3$), δ 5.68 (H-3) →171.8 ($\underline{C}OCH_2CH_2COCH_3$), indicates 3-OH was protected by Lev, 5.34 (H-2) →165.1 (C=O of Bz), 5.46 (H-4) →165.1 (C=O of Bz), and 4.44 (H-6) and 4.65 (H-6′) →166.1 (C=O of Bz) indicate 2-, 4- and 6-OH were protected by Bz; ESI-FT-MS, calculated for $C_{38}H_{34}O_{10}SNa^+$ $(M + Na)^+$: 705.1765, found *m/z*: 705.1769.

4.2.5 2-(Trimethylsilyl)ethyl 2,4,6-tri-*O*-benzoyl-3-*O*-levulinyl-β-D-glucopyranoside (compound **8**)

Compound **7** (1 eq., 1.00 g, 1.43 mmol) was mixed with activated 4Å molecular sieves (MS4Å) (1.0 g) and *N*-iodosuccinimide (NIS) (3 eq., 0.966 g, 4.29 mmol), and dissolved in dry dichloromethane/acetonitrile (1/1, v/v) (20 mL) under argon gas. After adding 2-(trimethylsilyl)ethanol (TMSEtOH) (2 eq., 410 μL, 2.86 mmol), the solution was cooled to −40°C. To the stirred solution was added trifluoromethanesulfonic acid (TfOH) (1 eq., 127 μL, 1.43 mmol), and the solution was stirred for 2 h at −40°C. The reaction was terminated by adding triethylamine (Et_3N) (700 μL). The reaction mixture was filtered through Celite, extracted with sodium thiosulfate and chloroform, the volatile components of the obtained chloroform layer were removed in vacuo, and the resulting residue was purified by silica gel column chromatography using ethyl acetate/*n*-hexane (1/2, v/v) as the mobile phase to give pure compound **8** (449 mg, 44%).

The unreacted portion of compound **7** (1 eq., 269 mg, 385 μmol) was mixed with MS4Å (269 mg) and NIS (3 eq., 260 mg, 1.16 mmol), and dissolved in dry dichloromethane/acetonitrile (1/1, v/v) (5.4 mL) under argon gas. After adding TMSEtOH (2 eq., 110 μL, 770 μmol), the solution was cooled to −40°C. To the stirred solution was added TfOH (1 eq., 34 μL, 385 μmol), and the solution was stirred for 2 h at −40°C. The reaction was terminated by adding Et_3N (190 μL). Compound **8** (95 mg, 35%) was obtained by purification according to the same procedure described above. $[\alpha]_D^{27}$ +17.4 (c 1.03, $CHCl_3$); ^1H NMR (400 MHz, $CDCl_3$): δ −0.04 (s, 9H, 3Me of 2-(trimethylsilyl)ethyl [TMSEt]), 0.91 (ddd, 1H, J_{gem} 13.9 Hz, $J_{H\text{-}2,H\text{-}1}$ 10.2 Hz, $J_{H\text{-}2,H\text{-}1'}$ 5.8 Hz, H-2 of TMSEt), 0.98 (ddd, 1H, J_{gem} 13.9 Hz, $J_{H\text{-}2',H\text{-}1'}$ 10.5 Hz, $J_{H\text{-}2',H\text{-}1}$ 6.6 Hz, H-2′ of TMSEt), 1.93 (s, 3H, Me of Lev), 2.39 (m, 2H, $COC\underline{H}_2CH_2COCH_3$), 2.49 (m, 2H,

$COCH_2C\underline{H}_2COCH_3$), 3.66 (td, 1H, $J_{gem} = J_{H\text{-}1,H\text{-}2}$ 10.1 Hz, $J_{H\text{-}1,H\text{-}2'}$ 6.6 Hz, H-1 of TMSEt), 4.04 (ddd, 1H, J_{gem} 10.5 Hz, $J_{H\text{-}1',H\text{-}2'}$ 9.6 Hz, $J_{H\text{-}1',H\text{-}2}$ 5.8 Hz, H-1′ of TMSEt), 4.13 (ddd, 1H, $J_{4,5}$ 9.0 Hz, $J_{5,6}$ 5.6 Hz, $J_{5,6'}$ 3.3 Hz, H-5), 4.52 (dd, 1H, J_{gem} 12.1 Hz, $J_{6,5}$ 5.6 Hz, H-6), 4.65 (dd, 1H, J_{gem} 12.0 Hz, $J_{6',5}$ 3.3 Hz, H-6′), 4.83 (d, 1H, $J_{1,2}$ 7.9 Hz, H-1), 5.40 (dd, 1H, $J_{2,3}$ 9.7 Hz, $J_{2,1}$ 7.9 Hz, H-2), 5.55 (t, 1H, $J_{3,4} = J_{4,5}$ 9.6 Hz, H-4), 5.70 (t, 1H, $J_{2,3} = J_{3,4}$ 9.6 Hz, H-3), 7.42–8.08 (m, 15H, 3Ph); ^{13}C NMR (100 MHz, $CDCl_3$): δ −1.5 (3Me of TMSEt), 17.9 (C-2 of TMSEt), 28.1 ($CO\underline{C}H_2CH_2COCH_3$), 29.3 (Me of Lev), 37.8 ($COCH_2\underline{C}H_2COCH_3$), 63.3 (C-6), 67.6 (C-1 of TMSEt), 69.9 (C-4), 71.9 (C-2), 72.1 (C-5), 72.8 (C-3), 100.5 (C-1), 128.35, 128.40, 128.5, 129.0, 129.6, 129.65, 129.71, 129.89, 129.94, 133.1, 133.2, 133.5, 165.1 (C=O of Bz), 165.3 (C=O of Bz), 166.1 (C=O of Bz), 171.9 ($\underline{C}OCH_2CH_2COCH_3$), 205.3 ($COCH_2CH_2\underline{C}OCH_3$); HMBC 2D-NMR (400 MHz, $CDCl_3$), δ 3.66 (H-1 of TMSEt) and 4.04 (H-1′ of TMSEt) →100.5 (C-1), indicates 1-OH was protected by TMSEt; ESI-FT-MS, calculated for $C_{37}H_{42}O_{11}SiNa^+$ $(M + Na)^+$: 713.2389, found *m/z*: 713.2372.

4.2.6 2-(Trimethylsilyl)ethyl 2,4,6-tri-*O*-benzoyl-β-D-glucopyranoside (compound **9**)

To a stirred solution of compound **8** (528 mg, 747 μmol) in pyridine (10 mL) was added a solution of 1 M hydrazine monohydrate in pyridine/acetic acid (3/2, v/v) (10 mL), and the reaction mixture was further stirred for 5 min at room temperature. Ethyl acetate (100 mL) and 2 M HCl (150 mL) were added at 0°C, and the mixture was stirred for 10 min at 0°C. The samples were then extracted using ethyl acetate, the volatile components of the ethyl acetate layer were removed in vacuo, and the resulting residue was purified by silica gel column chromatography using toluene/ethyl acetate (10/1, v/v) as the mobile phase to give pure compound **9** (397 mg, 87%). ^{1}H NMR (400 MHz, $CDCl_3$): δ −0.08 (s,

9H, 3Me of TMSEt), 0.87 (ddd, 1H, J_{gem} 13.9 Hz, $J_{H\text{-}2,H\text{-}1}$ 10.3 Hz, $J_{H\text{-}2,H\text{-}1'}$ 5.7 Hz, H-2 of TMSEt), 0.95 (ddd, 1H, J_{gem} 13.9 Hz, $J_{H\text{-}2',H\text{-}1'}$ 10.4 Hz, $J_{H\text{-}2',H\text{-}1}$ 6.4 Hz, H-2′ of TMSEt), 2.85 (d, 1H, $J_{OH,3}$ 6.0 Hz, 3-OH), 3.62 (td, 1H, $J_{gem} = J_{H\text{-}1,H\text{-}2}$ 9.9 Hz, $J_{H\text{-}1,H\text{-}2'}$ 6.5 Hz, H-1 of TMSEt), 4.00 (m, 1H, H-1′ of TMSEt), 4.04 (m, 1H, H-5), 4.11 (td, 1H, $J_{2,3} = J_{3,4}$ 9.2 Hz, $J_{3,OH}$ 6.0 Hz, H-3), 4.45 (dd, 1H, J_{gem} 12.0 Hz, $J_{5,6}$ 5.8 Hz, H-6), 4.64 (dd, 1H, J_{gem} 12.0 Hz, $J_{5,6'}$ 3.0 Hz, H-6′), 4.75 (d, 1H, $J_{1,2}$ 7.7 Hz, H-1), 5.19 (dd, 1H, $J_{2,3}$ 9.3 Hz, $J_{1,2}$ 7.8 Hz, H-2), 5.38 (t, 1H, $J_{3,4} = J_{4,5}$ 9.4 Hz, H-4), 7.37–8.08 (m, 15H, 3Ph); ^{13}C NMR (100 MHz, $CDCl_3$): δ −1.5 (3Me of TMSEt), 18.0 (C-2 of TMSEt), 63.5 (C-6), 67.5 (C-1 of TMSEt), 71.9 (C-5), 72.6 (C-4), 74.2 (C-3), 75.1 (C-2), 100.3 (C-1), 128.4, 128.5, 129.2, 129.6, 129.67, 129.72, 129.9, 133.1, 133.3, 133.5, 166.1 (C=O of Bz), 166.2 (C=O of Bz), 166.3 (C=O of Bz).

4.2.7 Phenyl 4,6-*O*-benzylidene-1-thio-β-D-glucopyranoside (compound **10**)

Compound **10** was synthesized from compound **2** as reported previously (Roy *et al*. 2008). To a stirred solution of compound **2** (1 eq., 8.00 g, 29.4 mmol) in DMF (72.8 mL) was added benzaldehyde dimethyl acetal (3 eq., 13.2 mL, 88.2 mmol) and *p*-toluenesulfonic acid monohydrate until the pH reached 3, and the reaction mixture was further stirred for 7 days at room temperature. The reaction was terminated by adding Et_3N until the pH reached 10, the sample was extracted with ethyl acetate and water, and the volatile components of the solution were removed in vacuo. The DMF was eliminated by co-evaporation with toluene. The sample was crystallized by ethyl acetate and *n*-hexane, filtered, and dried up in vacuo to give pure compound **10** (3.03 g, 29%).

4.2.8 Phenyl 4,6-*O*-benzylidene-3-*O*-(*tert*-butyldiphenylsilyl)-1-thio-β-D-glucopyranoside (compound **11**)

To a stirred solution of compound **10** (1 eq., 1.90 g, 5.27 mmol) in DMF (20 mL) was added *tert*-butyldiphenylchlorosilane (TBDPS-Cl) (1.5 eq., 2.06 mL, 7.91 mmol), and the reaction mixture was stirred at 0°C. Imidazole (3 eq., 1.08 g, 15.8 mmol) was added, and the solution was kept for 8 days at 4°C. The reaction was terminated by adding ice water. After stirring at room temperature for a few minutes, the supernatant was removed by decantation. The precipitate was washed by addition of 2 M HCl and decantation of the supernatant (twice). The precipitate was then washed with water, and finally dissolved in MeOH. To this solution was added water, forming a precipitate of compound **11**. Compound **11**, partly contained in the supernatant, was extracted twice with *n*-hexane and mixed with the precipitate. Compound **11** (3.17 g, quant.) was yielded. $[\alpha]_D^{27}$ −13.7 (c 1.00, $CHCl_3$); ^{1}H NMR (500 MHz, $CDCl_3$): δ 0.99 (s, 9H, 3Me of *tert*-butyldiphenylsilyl [TBDPS]), 2.33 (d, 1H, $J_{2,OH}$ 2.6 Hz, 2-OH), 3.30 (td, 1H, $J_{4,5} = J_{5,6}$ 9.7 Hz, $J_{5,6'}$ 4.9 Hz, H-5), 3.55 (t, 1H, $J_{3,4} = J_{4,5}$ 9.3 Hz, H-4), 3,58 (ddd, $J_{2,OH}$ 2.4 Hz, $J_{1,2}$ 10.9 Hz, $J_{2,3}$ 8.0 Hz, H-2), 3.68 (t, 1H, $J_{5,6} = J_{gem}$ 10.3 Hz, H-6), 3.82 (dd, 1H, $J_{2,3}$ 8.2 Hz, $J_{3,4}$ 9.1 Hz, H-3), 4.26 (dd, 1H, $J_{5,6'}$ 5.0 Hz, J_{gem} 10.4 Hz, H-6′), 4.53 (d, 1H, $J_{1,2}$ 9.8 Hz, H-1), 5.24 (s, 1H, $O_2C\underline{H}Ph$), 7.01–7.72 (m, 20H, 4Ph); ^{13}C NMR (126 MHz, $CDCl_3$): δ 19.6 (C of TBDPS), 26.9 (3Me of TBDPS), 68.5 (C-6), 70.5 (C-5), 73.9 (C-2), 76.8 (C-3), 80.7 (C-4), 88.6 (C-1), 101.4 ($O_2\underline{C}HPh$), 126.2, 127.3, 127.5, 127.7, 127.8, 128.1, 128.7, 129.0, 129.5, 129.6, 132.2, 132.6, 133.2, 133.6, 134.8, 135.2, 135.8, 136.0, 136.9; ESI-FT-MS, calculated for $C_{35}H_{38}O_5SSiNa^+$ $(M + Na)^+$: 621.2101, found *m/z*: 621.2088.

4.2.9 Phenyl 2-*O*-benzoyl-4,6-*O*-benzylidene-3-*O*-(*tert*-butyldiphenylsilyl)-1-thio-β-D-glucopyranoside (compound **12**)

To a stirred solution of compound **11** (1 eq., 2.43 g, 4.05 mmol) in pyridine (50 mL) was added BzCl (3 eq., 1.42 mL, 12.2 mmol), and the reaction mixture was stirred for 7 days at 60°C. The reaction was terminated by adding ice water, and the volatile components of the solution were removed in vacuo. The remaining pyridine was removed by co-evaporation with toluene. The resulting residue was dissolved in chloroform and purified by silica gel column chromatography. Benzoic acid was removed using ethyl acetate/*n*-hexane/acetic acid (5/95/2, v/v/v) as the mobile phase, and compound **12** (1.46 g, 51%) was obtained by elution with toluene. $[\alpha]_D^{27}$ −2.93 (c 1.00, $CHCl_3$); ^{1}H NMR (500 MHz, $CDCl_3$): δ 0.75 (s, 9H, 3Me of TBDPS), 3.34 (td, 1H, $J_{4,5} = J_{5,6}$ 9.7 Hz, $J_{5,6'}$ 4.9 Hz, H-5), 3.68 (t, 1H, $J_{3,4} = J_{4,5}$ 9.3 Hz, H-4), 3.70 (t, 1H, $J_{5,6} = J_{gem}$ 10.3 Hz, H-6), 4.04 (t, 1H, $J_{2,3} = J_{3,4}$ 8.8 Hz, H-3), 4.26 (dd, 1H, J_{gem} 10.4 Hz, $J_{5,6'}$ 4.9 Hz, H-6′), 4.74 (d, 1H, $J_{1,2}$ 10.1 Hz, H-1), 5.12 (s, 1H, $O_2C\underline{H}Ph$), 5.42 (t, 1H, $J_{1,2} = J_{2,3}$ 8.7 Hz, H-2), 6.81–7.98 (m, 25H, 5Ph); ^{13}C NMR (126 MHz, $CDCl_3$): δ 19.3 ($OSi(Ph)_2\underline{C}Me_3$), 26.6 (3Me of TBDPS), 68.4 (C-6), 70.5 (C-5), 73.6 (C-2), 74.9 (C-3), 80.9 (C-4), 87.5 (C-1), 101.6 ($O_2\underline{C}HPh$), 126.3, 127.1, 127.2, 127.7, 127.8, 128.18, 128.21, 128.7, 128.9, 129.0, 129.3, 129.4, 129.8, 130.1, 132.1, 133.0, 133.2, 134.0, 135.6, 136.2, 136.6, 165.4 (C=O of Bz); HMBC 2D-NMR (500 MHz, $CDCl_3$), δ 5.42 (H-2) →165.4 (C=O of Bz), indicates 2-OH was protected by Bz; ESI-FT-MS, calculated for $C_{42}H_{42}O_6SSiNa^+$ $(M + Na)^+$: 725.2364, found *m/z*: 725.2356.

4.2.10 2-(Trimethylsilyl)ethyl 2-*O*-benzoyl-4,6-*O*-benzylidene-3-*O*-(*tert*-butyldiphenylsilyl)-β-D-glucopyranoside (compound **13**)

Compound **12** (1 eq., 858 mg, 1.22 mmol) was mixed with MS4Å (860 mg) and NIS (3 eq., 824 mg, 3.66 mmol) and dissolved in dry dichloromethane/acetonitrile (1/1, v/v) (20 mL) under nitrogen. After adding TMSEtOH (2 eq., 350 μL, 2.44 mmol), the solution was cooled to −40°C. To the solution was added TfOH (1 eq., 108 μL, 1.22 mmol), and the reaction mixture was kept for 1 h at −40°C. The reaction was terminated by adding Et_3N (858 μL). Compound **13** (505 mg, 59%) was obtained by purification according to the same procedure as applied to compound **8**, however, using toluene as the mobile phase for the silica gel column chromatography. $[\alpha]_D^{27}$ −36.0 (c 1.00, $CHCl_3$); ^{1}H NMR (500 MHz, $CDCl_3$): δ −0.12 (s, 9H, 3Me of TMSEt), 0.73–0.85 (m, H-2 and H-2′ of TMSEt), 0.78 (s, 9H, 3Me of TBDPS), 3.29 (td, 1H, $J_{4,5} = J_{5,6}$ 9.7 Hz, $J_{5,6'}$ 4.9 Hz, H-5), 3.47 (td, 1H, J_{gem} 10.1 Hz, J 6.4 Hz, H-1 of TMSEt), 3.67 (t, 1H, $J_{3,4} = J_{4,5}$ 9.1 Hz, H-4), 3.71 (t, 1H, $J_{5,6} = J_{gem}$ 10.1 Hz, H-6), 3.89 (ddd, 1H, J_{gem} 10.4 Hz, J 5.7 Hz, J 10.6 Hz, H-1′ of TMSEt), 4.04 (t, 1H, $J_{2,3} = J_{3,4}$ 9.0 Hz, H-3), 4.25 (dd, 1H, $J_{5,6'}$ 4.9 Hz, J_{gem} 10.4 Hz, H-6′), 4.48 (d, 1H, $J_{1,2}$ 8.0 Hz, H-1), 5.12 (s, 1H, $O_2C\underline{H}Ph$), 5.36 (dd, 1H, $J_{1,2}$ 8.1 Hz, $J_{2,3}$ 8.8 Hz, H-2), 6.84–8.10 (m, 20H, 4Ph); ^{13}C NMR (126 MHz, $CDCl_3$): δ −1.6 (3Me of TMSEt), 18.0 (C-2 of TMSEt), 19.3 (C of TBDPS), 26.6 (3Me of TBDPS), 66.2 (C-5), 67.6 (C-1 of TMSEt), 68.6 (C-6), 73.8 (C-3), 75.1 (C-2), 81.2 (C-4), 101.3 (C-1), 101.5 ($O_2\underline{C}HPh$), 126.2, 127.1, 127.2, 127.4, 127.69, 127.72, 128.1, 128.2, 128.5, 128.6, 129.0, 129.2, 129.3, 129.6, 129.7, 129.8, 129.9, 130.0, 130.2, 130.3, 132.4, 132.76, 132.82, 133.6, 134.1, 134.35, 134.44, 134.8, 134.9, 135.3, 135.6, 136.2, 136.3, 136.7, 165.1 (C=O of Bz); ESI-FT-MS, calculated for $C_{41}H_{50}O_7Si_2Na^+$ $(M + Na)^+$: 733.2987, found *m/z*: 733.2966.

4.2.11 2-(Trimethylsilyl)ethyl 2-*O*-benzoyl-4,6-*O*-benzylidene-β-D-glucopyranoside (compound **14**)

Compound **13** (1 eq., 433 mg, 609 μmol) in DMF (4 mL) was mixed with acetic acid (2.11 eq., 73.4 μL, 1.28 mmol) and cooled to 0°C. To the stirred solution was added a solution of 1.0 M tetrabutylammonium fluoride (TBAF) in tetrahydrofuran (THF) (2 eq., 1.22 mL, 1.22 mmol), and the reaction mixture was stirred for 5 days at room temperature. The samples were extracted with water and ethyl acetate, and the volatile components of the ethyl acetate layer were removed in vacuo. The DMF was eliminated by co-evaporation with toluene. The resulting residue was purified by silica gel column chromatography, using ethyl acetate/toluene (1/9, v/v) as the mobile phase to give pure compound **14** (210 mg, 73%). $[\alpha]_D^{27}$ −41.7 (c 1.00, $CHCl_3$); ^{1}H NMR (500 MHz, $CDCl_3$): δ −0.08 (s, 9H, 3Me of TMSEt), 0.83 (ddd, 1H, $J_{H\text{-}1',\,H\text{-}2}$ 5.5 Hz, $J_{H\text{-}1,H\text{-}2}$ 10.4 Hz, J_{gem} 13.9 Hz, H-2 of TMSEt), 0.90 (ddd, 1H, $J_{H\text{-}1,H\text{-}2'}$ 6.5 Hz, $J_{H\text{-}1',H\text{-}2'}$ 10.8 Hz, J_{gem} 13.9 Hz, H-2′ of TMSEt), 2.70 (d, 1H, $J_{OH,3}$ 3.2 Hz, 3-OH), 3.51 (td, 1H, $J_{4,5} = J_{5,6}$ 9.7 Hz, $J_{5,6'}$ 4.9 Hz, H-5), 3.57 (ddd, 1H, $J_{H\text{-}1,H\text{-}2'}$ 6.4 Hz, $J_{H\text{-}1,H\text{-}2}$ 10.3 Hz, J_{gem} 9.7 Hz, H-1 of TMSEt), 3.66 (t, 1H, $J_{3,4} = J_{4,5}$ 9.3 Hz, H-4), 3.82 (t, 1H, $J_{5,6} = J_{gem}$ 10.3 Hz, H-6), 3.96 (ddd, 1H, $J_{H\text{-}1',\,H\text{-}2}$ 5.5 Hz, $J_{H\text{-}1',\,H\text{-}2'}$ 10.8 Hz, J_{gem} 9.6 Hz, H-1′ of TMSEt), 4.02 (td, 1H, $J_{2,3} = J_{3,4}$ 9.2 Hz, $J_{OH,3}$ 2.9 Hz, H-3), 4.38 (dd, 1H, $J_{5,6'}$ 5.0 Hz, J_{gem} 10.5 Hz, H-6′), 4.68 (d, 1H, $J_{1,2}$ 7.9 Hz, H-1), 5.15 (dd, 1H, $J_{1,2}$ 7.9 Hz, $J_{2,3}$ 9.1 Hz, H-2), 5.56 (s, 1H, $O_2C\underline{H}Ph$), 7.23−8.09 (m, 10H, 2Ph); ^{13}C NMR (126 MHz, $CDCl_3$): δ −1.5 (3Me of TMSEt), 18.1 (C-2 of TMSEt), 66.2 (C-5), 67.8 (C-1 of TMSEt), 68.7 (C-6), 72.6 (C-3), 75.0 (C-2), 81.0 (C-4), 101.0 (C-1), 101.9 ($O_2\underline{C}HPh$), 126.3, 128.33, 128.34, 129.3, 129.7, 129.9, 133.2, 136.9, 165.9 (C=O of Bz); ESI-FT-MS, calculated for $C_{25}H_{32}O_7SiNa^+$ $(M + Na)^+$: 495.1810, found *m/z*:

495.1801.

4.2.12 2-(Trimethylsilyl)ethyl *O*-(2-*O*-benzoyl-4,6-*O*-benzylidene-3-*O*-(*tert*-butyldiphenylsilyl)-β-D-glucopyranosyl)-(1→3)-2-*O*-benzoyl-4,6-*O*-benzylidene-β-D-glucopyranoside (compound **15**)

Compound **12** (1.2 eq., 339 mg, 482 μmol), compound **14** (1 eq., 190 mg, 402 μmol), MS4Å (530 mg), and NIS (2.4 eq., 217 mg, 965 μmol) were dissolved in dry dichloromethane (6 mL), under nitrogen. After cooling the solution to −30°C, TfOH (0.48 eq., 17 μL, 193 μmol) was added. This reaction solution was kept for 2 h at −30°C, and the reaction was terminated by adding Et_3N (160 μL). Compound **15** (458 mg) was obtained by purification according to the same procedure as applied to compound **8**, however, using ethyl acetate/toluene (1/19, v/v) as the mobile phase for the silica gel column chromatography. $[\alpha]_D^{27}$ −9.09 (c 1.00, $CHCl_3$); ^{1}H NMR (500 MHz, $CDCl_3$): δ −0.15 (s, 9H, 3Me of TMSEt), 0.70 (s, 9H, 3Me of TBDPS), 0.68–0.77 (m, 2H, H-2, H-2′ of TMSEt), 3.18 (td, 1H, $J_{4,5} = J_{5,6}$ 9.7 Hz, $J_{5,6'}$ 4.8 Hz, H-5^{II}), 3.40 (ddd, 1H, *J* 6.4 Hz, *J* 6.8 Hz, *J* 10.3 Hz, H-1 of TMSEt), 3.51 (td, 1H, $J_{4,5}$ 9.7 Hz, $J_{5,6}$ 4.8 Hz, 5-H^{I}), 3.56 (t, 1H, $J_{5,6} = J_{gem}$ 10.2 Hz, H-6^{II}), 3.70 (t, 1H, $J_{3,4} = J_{4,5}$ 9.2 Hz, H-4^{II}), 3.77–3.86 (m, 3H, H-1′ of TMSEt, H-6^{I}, and H-4^{I}), 3.89 (t, 1H, $J_{2,3} = J_{3,4}$ 8.3 Hz, H-3^{II}), 3.82 (dd, 1H, $J_{5,6'}$ 4.9 Hz, J_{gem} 10.4 Hz, 6-H′^{II}), 4.13 (t, 1H, $J_{2,3} = J_{3,4}$ 8.8 Hz, H-3^{I}), 4.35 (dd, 1H, $J_{5,6'}$ 4.9 Hz, J_{gem} 10.4 Hz, H-6′^{I}), 4.55 (d, 1H, $J_{1,2}$ 7.5 Hz, H-1^{I}), 4.77 (d, 1H, $J_{1,2}$ 7.2 Hz, H-1^{II}), 4.85 (s, 1H, $O_2C\underline{H}Ph^{II}$), 5.19 (dd, 1H, $J_{1,2}$ 7.7Hz, $J_{2,3}$ 8.3 Hz, H-2^{I}), 5.31 (t, 1H, $J_{1,2} = J_{2,3}$ 7.5 Hz, H-2^{II}), 5.55 (s, 1H, $O_2C\underline{H}Ph^{I}$), 6.76–7.80 (m, 30H, 6Ph); ^{13}C NMR (126 MHz, $CDCl_3$): δ −1.6 (3Me of TMSEt), 18.0 (C-2 of TMSEt), 19.1 ($OSi(Ph)_2\underline{C}Me_3$), 26.5 (3Me of TBDPS), 65.8 (C-5^{II}), 66.4 (C-5^{I}), 67.4 (C-1 of TMSEt), 68.5 (C-6^{II}), 68.8 (C-6^{I}), 73.77

(C-2^{II}), 73.84 (C-3^{II}), 75.4 (C-2^{II}), 77.8 (C-3^{I}), 79.4 (C-4^{I}), 80.7 (C-4^{II}), 100.4 (C-1^{II}), 100.9 (C-1^{I}), 101.2 ($O_2\underline{C}HPh^{II}$), 101.4 (O_2CHPh^{I}), 125.3, 126.0, 126.1, 126.2, 127.0, 127.1, 127.5, 127.6, 127.8, 128.16, 128.20, 128.53, 129.00, 129.03, 129.1, 129.2, 129.68, 129.73, 129.8, 129.9, 132.36, 132.37, 132.7, 134.2, 135.5, 136.0, 136.7, 137.2, 137.8, 164.4 (C=O of Bz^{I}), 164.6 (C=O of Bz^{II}); HMBC 2D-NMR (500 MHz, $CDCl_3$), δ 4.77 (H-1^{II}) →77.8 (C-3^{I}), indicates 1→3 linkage; ESI-FT-MS, calculated for $C_{61}H_{68}O_{13}Si_2Na^+$ $(M + Na)^+$: 1087.4091, found *m/z*: 1087.4080.

4.2.13 2-(Trimethylsilyl)ethyl *O*-(2-*O*-benzoyl-4,6-*O*-benzylidene-β-D-glucopyranosyl)-(1→3)-2-*O*-benzoyl-4,6-*O*-benzylidene-β-D-glucopyranoside (compound **16**)

To a stirred solution of compound **15** (1 eq., 429 mg, 403 μmol) in DMF (4 mL) was added acetic acid (2.11 eq., 49 μL, 850 μmol). The solution was cooled to 0°C, and the solution of 1.0 M TBAF in THF (2 eq., 806 μL, 806 μmol) was added. The reaction mixture was stirred for 14 days at room temperature. The sample was extracted with water and ethyl acetate, and the volatile components of the ethyl acetate layer were removed in vacuo. This mixture was co-evaporated with toluene to eliminate the DMF. The resulting residue was purified by silica gel column chromatography using ethyl acetate/toluene (1/9, v/v) as the mobile phase to give pure compound **16** [220 mg, 66% (two steps)]. $[\alpha]_D^{27}$ −20.8 (c 1.00, $CHCl_3$); ^{1}H NMR (500 MHz, $CDCl_3$): δ −0.14 (s, 9H, 3Me of TMSEt), 0.67–0.80 (m, 2H, H-2 and H-2′ of TMSEt), 2.53 (d, 1H, $J_{OH,3}$ 2.7 Hz, 3-OH), 3.37 (td, 1H, $J_{4,5} = J_{5,6}$ 10.1 Hz, $J_{5,6'}$ 5.1 Hz, H-5^{II}), 3.43 (td, 1H, *J* 6.7 Hz, *J* 9.9 Hz, H-1 of TMSEt), 3.59 (td, 1H, $J_{4,5}$ 9.8 Hz, $J_{5,6} = J_{5,6'}$ 4.9 Hz, H-5^{I}), 3.67 (t, 1H, $J_{3,4} = J_{4,5}$ 9.2 Hz, H-4^{II}), 3.68 (t, 1H, $J_{5,6} = J_{gem}$ 10.5 Hz, H-6^{II}), 3.78–3.87 (m, 4H, H-4^{I}, H-6^{1}, H-3^{II}, and H-1′ of TMSEt),

4.17 (dd, $J_{5,6'}$ 5.1 Hz, J_{gem} 10.4 Hz, H-6′^{II}), 4.19 (t, 1H, $J_{2,3} = J_{3,4}$ 8.8 Hz, H-3^{I}), 4.36 (dd, 1H, $J_{5,6'}$ 4.9 Hz, J_{gem} 10.5 Hz, H-6′^{I}), 4.59 (d, 1H, $J_{1,2}$ 7.5 Hz, H-1^{I}), 4.94 (d, 1H, $J_{1,2}$ 7.2 Hz, H-1^{II}), 5.08 (dd, 1H, $J_{1,2}$ 7.2 Hz, $J_{2,3}$ 7.8 Hz, H-2^{II}), 5.22 (dd, 1H, $J_{1,2}$ 7.6 Hz, $J_{2,3}$ 8.4 Hz, H-2^{I}), 5.34 (s, 1H, $O_2C\underline{H}Ph^{II}$), 5.55 (s, 1H, $O_2C\underline{H}Ph^{I}$), 7.11–7.92 (m, 20H, 4Ph); ^{13}C NMR (126 MHz, $CDCl_3$): δ −1.59 (3Me of TMSEt), 18.0 (C-2 of TMSEt), 66.0 (C-5^{II}), 66.4 (C-5^{I}), 67.5 (C-1 of TMSEt), 68.6 (C-6^{II}), 68.8 (C-6^{I}), 72.7 (C-3^{II}), 73.7 (C-2^{I}), 75.4 (C-2^{II}), 78.0 (C-3^{I}), 79.4 (C-4^{I}), 80.5 (C-4^{II}), 100.2 (C-1^{II}), 100.8 (C-1^{I}), 101.5 ($O_2\underline{C}HPh^{I}$), 101.7 ($O_2\underline{C}HPh^{II}$), 125.3, 126.1, 126.2, 128.16, 128.21, 128.24, 128.26, 128.27, 128.4, 128.5, 129.0, 129.18, 129.24, 129.3, 129.6, 129.7, 129.8, 132.9, 136.9, 137.2, 137.9, 164.6 (C=O of Bz^{II}), 165.6 (C=O of Bz^{I}); ESI-FT-MS, calculated for $C_{45}H_{50}O_{13}SiNa^+$ (M + Na)$^+$: 849.2913, found *m/z*: 849.2894.

4.2.14 2-(Trimethylsilyl)ethyl *O*-(2,4,6-tri-*O*-benzoyl-3-levulinyl-α-D-glucopyranosyl)-(1→3)-2,4,6-tri-*O*-benzoyl-β-D-glucopyranoside (compound **17**)

Compounds **7** (1.5 eq., 242 mg, 354 μmol), compound **9** (1 eq., 140 mg, 236 μmol), MS4Å (382 mg), and NIS (3 eq., 159 mg, 708 μmol) were dissolved in dry dichloromethane (2 mL), under argon gas. After cooling this solution to −30°C, TfOH (0.6 eq., 12.5 μL, 142 μmol) was added, and the reaction solution was stirred for 40 h at −30°C. The reaction was terminated by adding Et_3N (154 μL). Compound **17** (54 mg, 20%) was obtained by purification according to the same procedure as applied to compound **8**. ^{1}H NMR (400 MHz, $CDCl_3$): δ −0.12 (s, 9H, 3Me of TMSEt), 0.99–1.04 (m, 2H, H-2 and H-2′ of TMSEt), 1.92 (s, 3H, Me of Lev), 2.29 (m, 2H, $COC\underline{H}_2CH_2COCH_3$), 2.40 (m, 2H, $COCH_2C\underline{H}_2COCH_3$), 3.64 (dd, 1H, $J_{5,6}$ 3.1 Hz, J_{gem} 12.6 Hz, H-6^{II}), 3.69 (td, 1H, *J* 6.1 Hz, *J* 10.0 Hz, H-1 of TMSEt), 3.99–4.05 (m, 1H, H-

5^{I}), 4.06 (td, 1H, *J* 5.9Hz, *J* 10.2 Hz, H-1′ of TMSEt), 4.28 (dt, 1H, $J_{4,5}$ 10.2 Hz, $J_{5,6}$ = $J_{5,6'}$ 2.8 Hz, H-5^{II}), 4.33 (dd, 1H, $J_{5,6'}$ 2.6 Hz, J_{gem} 12.4 Hz, H-6′^{II}), 4.46 (dd, 1H, $J_{5,6}$ 6.0 Hz, J_{gem} 11.9 Hz, H-6^{I}), 4.54 (dd, 1H, $J_{5,6'}$ 4.0 Hz, J_{gem} 11.8 Hz, H-6′), 4.57 (t, 1H, $J_{2,3}$ = $J_{3,4}$ 9.0 Hz, H-3^{I}), 4.82 (d, 1H, $J_{1,2}$ 7.7 Hz, H-1^{I}), 5.13 (dd, 1H, $J_{1,2}$ 3.8 Hz, $J_{2,3}$ 10.4 Hz, H-2^{II}), 5.47 (t, 1H, $J_{3,4}$ = $J_{4,5}$ 9.8 Hz, H-4^{II}), 5.61 (dd, 1H, $J_{1,2}$ 7.6 Hz, $J_{2,3}$ 9.3 Hz, H-2^{I}), 5.62 (d, 1H, $J_{1,2}$ 3.4 Hz, H-1^{II}), 5.63 (dd, 1H, $J_{3,4}$ 8.5 Hz, $J_{4,5}$ 10.9 Hz, H-4^{I}), 5.81 (t, 1H, $J_{2,3}$ = $J_{3,4}$ 10.0 Hz, H-3^{II}), 7.33–8.20 (m, 30H, 6Ph); ^{13}C NMR (100 MHz, $CDCl_3$): δ 0.25 (3Me of TMSEt), 19.5 (C-2 of TMSEt), 29.4 ($CO\underline{C}H_2CH_2COCH_3$), 30.8 (Me of Lev), 39.3 ($COCH_2\underline{C}H_2COCH_3$), 63.2 (C-6^{II}), 65.2 (C-6^{I}), 69.0 (C-1 of TMSEt), 69.5 (C-5^{II}), 70.3 (C-4^{II}), 71.2 (C-3^{II}), 72.0 (C-2^{II}), 73.7 (C-5^{I}), 74.0 (C-2^{I} or C-4^{I}), 74.1 (C-2^{I} or C-4^{I}), 78.2 (C-3^{I}), 98.2 (C-1^{II}), 102.0 (C-1^{I}), 129.7, 129.8, 129.92, 129.99, 130.04, 130.1, 130.4, 131.07, 131.16, 131.24, 131.3, 131.5, 131.7, 134.5, 134.6, 134.91, 134.96, 135.02, 135.1, 166.1 (C=O of Bz), 166.4 (C=O of Bz), 166.5 (C=O of Bz), 166.8 (C=O of Bz), 167.5 (C=O of Bz), 167.6 (C=O of Bz), 172.9 ($\underline{C}OCH_2CH_2COCH_3$), 205.3 ($COCH_2CH_2\underline{C}OCH_3$); HMBC 2D-NMR (400 MHz, $CDCl_3$), δ 4.57 (H-3^{I}) →98.2 (C-1^{II}), indicates 1→3 linkage.

4.2.15 *O*-(2,4,6-tri-*O*-benzoyl-3-levulinyl-β-D-glucopyranosyl)-(1→6)-1,2:3,5-di-*O*-isopropyridene-α-D-glucofuranose (compound **18**)

Compound **19** (1 eq., 20 mg, 76.8 μmol; Tokyo Chemical Industry, Tokyo, Japan), compound **7** (1.1 eq., 58 mg, 85.0 μmol), MS4Å (78 mg), and NIS (2.2 eq., 38 mg, 169 μmol) were dissolved in dry dichloromethane (1 mL) under argon gas. After cooling this solution to −30°C, TfOH (0.44 eq., 3.0 μL, 33.8 μmol) was added. This reaction solution was stirred for 1 h at −30°C, and the reaction was terminated by adding Et_3N (36 μL).

Compound **18** (32 mg, 50%) was obtained by purification according to the same procedure as applied to compound **8**. $[\alpha]_D^{27}$ +18.7 (c 0.603, $CHCl_3$); ^1H NMR (400 MHz, $CDCl_3$): δ 1.08 (s, 3H, Me of isopropylidene at 3- and 5-OH), 1.15 (s, 3H, Me of isopropylidene at 3- and 5-OH), 1.27 (s, 3H, Me of isopropylidene at 1- and 2-OH), 1.36 (s, 3H, Me of isopropylidene at 1- and 2-OH), 1.87 (s, 3H, Me of Lev), 2.33 (m, 2H, $COC\underline{H}_2CH_2COCH_3$), 2.43 (m, 2H, $COCH_2C\underline{H}_2COCH_3$), 3.63–3.73 (m, 2H, H-$4^I$ and H-6^I), 4.01–4.16 (m, 4H, H-3^I, H-5^I, H-$6'^I$ and H-5^{II}), 4.42–4.49 (m, 2H, H-2^I and H-6^{II}), 4.60 (dd, 1H, *J* 3.4 Hz, *J* 8.3 Hz, H-$6'^{II}$), 4.87 (d, 1H, $J_{1,2}$ 7.8 Hz, H-1^{II}), 5.37 (dd, 1H, $J_{1,2}$ 7.9 Hz, $J_{2,3}$ 9.7 Hz, H-2^{II}), 5.51 (t, 1H, $J_{3,4} = J_{4,5}$ 9.7 Hz, H-4^{II}), 5.64 (t, 1H, $J_{2,3} = J_{3,4}$ 9.6 Hz, H-3^{II}), 5.87 (d, 1H, $J_{1,2}$ 3.7 Hz, H-1^I), 7.35–8.07 (m, 15H, 3Ph); ^{13}C NMR (100 MHz, $CDCl_3$): δ 23.6 (Me of isopropylidene at 3- and 5-OH), 23.7 (Me of isopropylidene at 3- and 5-OH), 26.5 (Me of isopropylidene at 1- and 2-OH), 27.1 (Me of isopropylidene at 1- and 2-OH), 28.0 ($CO\underline{C}H_2CH_2COCH_3$), 29.3 (Me of Lev), 37.8 ($COCH_2\underline{C}H_2COCH_3$), 63.1 (C-$6^{II}$), 69.7 (C-$4^{II}$), 70.3 (C-$6^I$), 71.6 (C-$4^I$), 71.8 (C-$2^{II}$), 72.1 (C-$3^I$), 72.5 (C-$3^{II}$), 74.9 (C-$5^{II}$), 79.1 (C-$5^I$), 84.0 (C-$2^I$), 100.9 (C of isopropylidene at 3- and 5-OH), 101.6 (C-1^{II}), 106.3 (C-1^I), 112.1 (C of isopropylidene at 1- and 2-OH), 128.3, 128.4, 128.5, 129.5, 129.6, 129.8, 129.90, 129.93, 133.1, 133.2, 133.5, 165.0 (C=O of Bz), 165.2 (C=O of Bz), 166.1 (C=O of Bz), 171.8 ($\underline{C}OCH_2CH_2COCH_3$), 205.3 ($COCH_2CH_2\underline{C}OCH_3$); HMBC 2D-NMR (400 MHz, $CDCl_3$), δ 4.87 (H-1^{II}) →70.3 (C-6^I), indicates 1→6 linkage; ESI-FT-MS, calculated for $C_{44}H_{48}O_{16}Na^+$ $(M + Na)^+$: 855.2835, found *m/z*: 855.2826.

4.2.16 Phenyl 2,3-di-*O*-benzoyl-4,6-di-*O*-levulinyl-1-thio-β-D-glucopyranoside (compound **20**)

To a stirred solution of compound **10** (1 eq., 310 mg, 860 μmol) in pyridine (15 mL) was added BzCl (3 eq., 300 μL, 2.58 mmol), and the reaction mixture was stirred for 2 h at room temperature. The reaction was terminated by adding ice water. The precipitated sample was washed with water and 2 M HCl, and dissolved in chloroform. The pyridine was removed by co-evaporation with toluene. To the reaction mixture was added acetic acid aqueous solution (80%, v/v) (100 mL), and the resulting solution was stirred for 3 h at 60°C. The sample was concentrated in vacuo, washed with water, and reconcentrated in vacuo. Levulinic acid anhydride, prepared from levulinic acid (6 eq., 600 mg, 5.17 mmol) as described in the section 4.2.3, was dissolved in pyridine/dichloromethane (1/1, v/v) (6 mL) and mixed with the concentrated sample. To the stirred solution was added DMAP (1 eq., 105 mg, 859 μmol), and the reaction mixture was further stirred for 2 h at room temperature. The reaction was terminated by adding ice water. The sample was extracted with 2 M HCl and chloroform. The volatile components of the chloroform layer was removed in vacuo, and the resulting residue was purified by silica gel column chromatography using ethyl acetate/toluene (1/4, v/v) as the mobile phase to give pure compound **20** (462 mg, 79%). $[\alpha]_D^{27}$ +76.7 (c 1.00, $CHCl_3$); ^{1}H NMR (500 MHz, $CDCl_3$): δ 2.00 (s, 3H, Me of Lev), 2.18 (s, 3H, Me of Lev), 2.30–2.90 (m, 8H, C$\underline{H_2}$ of Lev), 3.89 (ddd, 1H, $J_{4,5}$ 10.0 Hz, $J_{5,6}$ 5.5 Hz, $J_{5,6'}$ 2.4 Hz, H-5), 4.26 (dd, 1H, $J_{5,6}$ 5.5 Hz, J_{gem} 12.2 Hz, H-6), 4.32 (dd, 1H, $J_{5,6'}$ 2.4 Hz, J_{gem} 12.1 Hz, H-6′), 4.93 (d, 1H, $J_{1,2}$ 10.0 Hz, H-1), 5.25 (t, 1H, $J_{3,4} = J_{4,5}$ 9.8 Hz, H-4), 5.37 (t, 1H, $J_{1,2} = J_{2,3}$ 9.7 Hz, H-2), 5.66 (t, 1H, $J_{2,3} = J_{3,4}$ 9.5 Hz, H-3), 7.21–7.99 (m, 15H, 3Ph); ^{13}C NMR (126 MHz, $CDCl_3$): δ 27.77 (CH_2 of Lev), 27.84 (CH_2 of Lev), 29.4 (Me of Lev), 29.82 (Me of Lev), 37.76 (CH_2 of Lev),

37.9 (CH_2 of Lev), 62.5 (C-6), 68.50 (C-4), 70.4 (C-2), 74.2 (C-3), 76.1 (C-5), 86.1 (C-1), 127.8, 128.2, 128.31, 128.33, 128.38, 128.5, 128.75, 128.83, 128.89, 128.99, 129.08, 129.10, 129.13, 129.81, 129.83, 130.0, 131.8, 132.0, 132.5, 133.0, 133.3, 133.5, 165.0 (C=O of Bz), 165.7 (C=O of Bz), 171.3 ($\underline{C}OCH_2CH_2COCH_3$), 172.2 ($\underline{C}OCH_2CH_2COCH_3$), 205.7 ($COCH_2CH_2\underline{C}OCH_3$), 206.36 ($COCH_2CH_2\underline{C}OCH_3$); HMBC 2D-NMR (500 MHz, $CDCl_3$), δ 5.37 (H-2) →165.0 (C=O of Bz) and δ 5.66 (H-3) →165.7 (C=O of Bz), indicate 2-OH and 3-OH were protected by Bz, respectively, and δ 5.25 (H-4) →171.3 ($\underline{C}OCH_2CH_2COCH_3$), 4.26 (H-6) →172.2 ($\underline{C}OCH_2CH_2COCH_3$) and 4.32 (H-6′) →172.2 ($\underline{C}OCH_2CH_2COCH_3$) indicate 4-OH and 6-OH were protected by Lev, respectively; ESI-FT-MS, calculated for $C_{36}H_{36}O_{11}SNa^+$ $(M + Na)^+$: 699.1871, found *m/z*: 699.1860.

4.2.17 2-(Trimethylsilyl)ethyl *O*-(2,3-di-*O*-benzoyl-4,6-di-*O*-levulinyl-β-D-glucopyranosyl)-(1→3)-*O*-(2-*O*-benzoyl-4,6-*O*-benzylidene-β-D-glucopyranosyl)-(1→3)-2-*O*-benzoyl-4,6-*O*-benzylidene-β-D-glucopyranoside (compound **21**)

Compound **20** (1.2 eq., 215 mg, 318 μmol), compound **16** (1 eq., 217 mg, 262 μmol), MS4Å (432 mg), and NIS (2.4 eq., 142 mg, 0.629 mmol) were dissolved in dry dichloromethane (5 mL), under nitrogen. After cooling this solution to −30°C, TfOH (0.48 eq., 11 μL, 0.126 mmol) was added and kept at −40°C for 2 h. The reaction was terminated by adding Et_3N (104 μL). Compound **21** (170 mg, 47%) was obtained according to the same procedure as applied to compound **8**, however, using ethyl acetate/toluene (1/4, v/v) as the mobile phase for the silica gel column chromatography. $[\alpha]_D^{27}$ +29.7 (c 0.59, $CHCl_3$); ^1H NMR (500 MHz, $CDCl_3$): δ −0.13 (s, 1H, 3Me of

TMSEt), 0.65–0.77 (m, 2H, H-2 and H-2′ of TMSEt), 1.99 (s, 3H, Me of Lev), 2.07 (s, 3H, Me of Lev), 2.36–2.49 (m, 4H, $COC\underline{H_2}CH_2COCH_3$), 2.49–2.81 (m, 4H, $COCH_2C\underline{H_2}COCH_3$), 3.19 (t, 1H, $J_{3,4} = J_{4,5}$ 9.4 Hz, H-4^{I}), 3.35–3.44 (m, 2H, H-5^{I} and H-1 of TMSEt), 3.50–3.57 (m, 2H, H-5^{II} and H-6^{II}), 3.61 (t, 1H, $J_{5,6} = J_{gem}$ 10.2 Hz, H-6^{I}), 3.73 (ddd, 1H, $J_{4,5}$ 10.0 Hz, $J_{5,6}$ 2.4 Hz, $J_{5,6'}$ 4.5 Hz, H-5^{III}), 3.80 (td, 1H, J 6.0 Hz, J 10.2 Hz, 1-H′ of TMSEt), 4.01 (dd, 1H, $J_{2,3}$ 4.2 Hz, $J_{3,4}$ 8.2 Hz, H-3^{II}), 4.05–4.15 (m, 4H, H-3^{I}, H-4^{II}, H-$6'^{II}$, H-6^{III}), 4.18 (dd, 1H, $J_{5,6'}$ 4.5 Hz, J_{gem} 12.2 Hz, H-$6'^{III}$), 4.27 (dd, 1H, $J_{5,6'}$ 4.9 Hz, J_{gem} 10.4 Hz, H-$6'^{I}$), 4.45 (d, 1H, $J_{1,2}$ 7.7 Hz, H-1^{I}), 4.70 (s, 1H, $O_2C\underline{H}Ph^{II}$), 4.83 (t, 1H, $J_{1,2} = J_{2,3}$ 8.2 Hz, H-2^{I}), 4.90 (d, 1H, $J_{1,2}$ 4.6 Hz, H-1^{II}), 5.11 (t, 1H, $J_{1,2} = J_{2,3}$ 4.4 Hz, H-2^{II}), 5.13 (d, 1H, $J_{1,2}$ 8.0 Hz, H-1^{III}), 5.26 (t, 1H, $J_{3,4} = J_{4,5}$ 9.8 Hz, H-4^{III}), 5.41 (s, 1H, $O_2C\underline{H}Ph^{I}$) 5.42 (dd, 1H, $J_{1,2}$ 7.9 Hz, $J_{2,3}$ 9.7 Hz, H-2^{III}), 5.55 (t, 1H, $J_{2,3} = J_{3,4}$ 9.6 Hz, H-3^{III}), 7.12–8.06 (m, 30H, 6Ph); ^{13}C NMR (126 MHz, $CDCl_3$): δ −1.5 (3Me of TMSEt), 18.0 (C-2 of TMSEt), 27.8 ($CO\underline{C}H_2CH_2COCH_3$), 27.9 ($CO\underline{C}H_2CH_2COCH_3$), 29.5 ($COCH_2CH_2CO\underline{C}H_3$), 29.8 ($COCH_2CH_2CO\underline{C}H_3$), 37.8 ($COCH_2\underline{C}H_2COCH_3$), 37.9 ($COCH_2\underline{C}H_2COCH_3$), 62.0 (C-$6^{III}$), 65.4 (C-$5^{II}$), 66.4 (C-$5^{I}$), 67.5 (C-1 of TMSEt), 68.7 (C-6^{I}), 68.8 (C-6^{II} and C-4^{III}), 71.6 (C-5^{III}), 71.7 (C-2^{III}), 72.6 (C-2^{II}), 73.3 (C-3^{III}), 74.4 (C-2^{I}), 74.7 (C-4^{II}), 77.0 (C-3^{II}), 77.8 (C-3^{I}), 78.9 (C-4^{I}), 98.0 (C-1^{II}), 98.3 (C-1^{III}), 100.5 ($O_2\underline{C}HPh^{II}$), 100.8 (C-1^{I}), 101.8 ($O_2\underline{C}HPh^{I}$), 126.1, 126.3, 128.0, 128.2, 128.32, 128.38, 128.41, 128.6, 128.8, 129.02, 129.04, 129.1, 129.2, 129.3, 129.67, 129.70, 129.74, 129.8, 133.00, 133.04, 133.07, 133.2, 133.3, 137.2, 137.3, 164.5 (C=O of Bz), 164.7 (C=O of Bz), 165.0 (C=O of Bz), 165.7 (C=O of Bz), 171.3 ($\underline{C}OCH_2CH_2COCH_3$), 172.3 ($\underline{C}OCH_2CH_2COCH_3$), 205.8 ($COCH_2CH_2\underline{C}OCH_3$), 206.4 ($COCH_2CH_2\underline{C}OCH_3$); HMBC 2D-NMR (500 MHz, $CDCl_3$), δ 5.13 (H-1^{III}) →77.0 (C-3^{II}), indicates 1→3 linkage; ESI-FT-MS, calculated for $C_{75}H_{80}O_{24}SiNa^+$ $(M + Na)^+$: 1415.4701, found *m/z*: 1415.4669.

4.2.18 2-(Trimethylsilyl)ethyl *O*-(2,3-di-*O*-benzoyl-β-D-glucopyranosyl)-(1→3)-*O*-(2-*O*-benzoyl-4,6-*O*-benzylidene-β-D-glucopyranosyl)-(1→3)-2-*O*-benzoyl-4,6-*O*-benzylidene-β-D-glucopyranoside (compound **22**)

To stirred solution of compound **21** (70 mg, 50.2 μmol) in pyridine (1 mL) was added the solution of 1 M hydrazine monohydrate in pyridine/acetic acid (3/2, v/v) (1 mL). This solution was stirred for 1 h at room temperature and concentrated in vacuo. After co-evaporation with toluene, silica gel column chromatography using ethyl acetate/toluene (1/9, v/v) as the mobile phase was performed to give pure compound **22** (47 mg, 78%). $[\alpha]_D^{27}$ +29.2 (c 0.57, $CHCl_3$); ^{1}H NMR (500 MHz, $CDCl_3$): δ −0.14 (s, 9H, 3Me of TMSEt), 0.65–0.77 (m, 2H, H-2 and H-2′ of TMSEt), 2.06–2.17 (m, 1H, 6-OH), 3.06 (d, 1H, $J_{4,OH}$ 4.1 Hz, 4-OH), 3.33 (t, 1H, $J_{3,4} = J_{4,5}$ 9.3 Hz, H-4^{I}), 3.36–3.43 (m, 2H, H-5^{I} and H-1 of TMSEt), 3.46 (ddd, 1H, $J_{5,6}$ 9.4 Hz, J 5.1 Hz, J 3.4 Hz, H-5^{III}), 3.50 (dd, 1H, $J_{5,6}$ 9.6 Hz, $J_{5,6'}$ 4.6 Hz, H-5^{II}), 3.57 (t, 1H, $J_{5,6} = J_{gem}$ 10.1 Hz, H-6^{II}), 3.65 (t, 2H, $J_{5,6} = J_{gem}$ 10.1 Hz, H-6^{I} and H-6^{III}), 3.76–3.86 (m, 3H, H-4^{III}, H-6′^{III} and H-1′ of TMSEt), 3.96–4.03 (m, 2H, H-3^{II} and H-4^{II}), 4.09 (t, 1H, $J_{2,3} = J_{3,4}$ 8.9 Hz, H-3^{I}), 4.15 (dd, 1H, $J_{5,6'}$ 4.6 Hz, J_{gem} 10.1 Hz, H-6′^{II}), 4.28 (dd, 1H, $J_{5,6'}$ 4.7 Hz, J_{gem} 10.5 Hz, H-6′^{I}), 4.47 (d, 1H, $J_{1,2}$ 7.7 Hz, H-1^{I}), 4.86 (d, 1H, $J_{1,2}$ 5.4 Hz, H-1^{II}), 4.89 (s, 1H, $O_2C\underline{H}Ph^{II}$), 4.92 (dd, 1H, $J_{1,2}$ 7.9 Hz, $J_{2,3}$ 8.6 Hz, H-2^{I}), 5.00 (d, 1H, $J_{1,2}$ 7.9 Hz, H-1^{III}), 5.16 (t, 1H, $J_{1,2} = J_{2,3}$ 5.3 Hz, H-2^{II}), 5.21 (t, 1H, $J_{2,3} = J_{3,4}$ 9.3 Hz, H-3^{III}), 5.37 (dd, 1H, $J_{1,2}$ 7.9 Hz, $J_{2,3}$ 9.6 Hz, H-2^{III}), 5.43 (s, 1H, $O_2C\underline{H}Ph^{I}$), 7.10–7.98 (m, 30H, 6Ph); ^{13}C NMR (126 MHz, $CDCl_3$): δ −1.6 (3Me of TMSEt), 18.0 (C-2 of TMSEt), 62.0 (C-6^{III}), 65.7 (C-5^{II}), 66.4 (C-5^{I}), 67.5 (C-1 of TMSEt), 68.7 (C-6^{I}), 68.8 (C-6^{II}), 70.1 (C-4^{III}), 71.3 (C-2^{III}), 72.9 (C-2^{II}), 74.2 (C-2^{I}), 75.65 (C-3^{I}), 75.72 (C-5^{III}), 77.3 (C-3^{II}), 77.8 (C-3^{III}), 77.9 (C-4^{II}), 78.9 (C-4^{I}), 98.4 (C-

1^{III}), 98.8 (C-1^{II}), 100.8 (C-1^{I}), 101.0 ($O_2\underline{C}HPh^{II}$), 101.7 ($O_2\underline{C}HPh^{I}$), 126.0, 126.3, 128.1, 128.2, 128.3, 128.4, 128.5, 128.8, 129.0, 129.1, 129.3, 129.67, 129.69, 239.74, 129.76, 129.84, 130.0, 132.8, 132.99, 133.03, 133.2, 133.6, 137.2, 164.56 (C=O of Bz), 164.60 (C=O of Bz), 165.3 (C=O of Bz), 167.7 (C=O of Bz); ESI-FT-MS, calculated for $C_{65}H_{67}O_{20}Si$ $(M-H)^-$: 1195.4000, found *m/z*: 1195.4029.

4.2.19 2-(Trimethylsilyl)ethyl *O*-(2-*O*-benzoyl-4,6-*O*-benzylidene-3-*O*-(*tert*-butyldiphenylsilyl)-β-D-glucopyranosyl)-(1→6)-*O*-(2,3-di-*O*-benzoyl-β-D-glucopyranosyl)-(1→3)-*O*-(2-*O*-benzoyl-4,6-*O*-benzylidene-β-D-glucopyranosyl)-(1→3)-2-*O*-benzoyl-4,6-*O*-benzylidene-β-D-glucopyranoside (compound **1**)

Compound **12** (1.2 eq., 27.8 mg, 39.5 μmol), compound **22** (1 eq., 39.4 mg, 32.9 μmol), MS4Å (67.2 mg), and NIS (2.4 eq., 17.8 mg, 79.1 μmol) were dissolved in dry dichloromethane (2 mL), under nitrogen. After cooling this solution to −30°C, TfOH (0.48 eq., 1.4 μL, 15.8 μmol) was added, and this solution was kept at −30°C for 2 h. The reaction was terminated by adding Et_3N (13.2 μL). Compound **1** (12.5 mg, 23%) was obtained according to the same procedure as applied to compound **8**, however, using ethyl acetate/toluene (1/18, v/v) as the mobile phase in the silica gel column chromatography. $[\alpha]_D^{27}$ −6.05 (c 0.61, $CHCl_3$); ^{1}H NMR (500 MHz, $CDCl_3$): δ −0.14 (s, 9H, 3Me of TMSEt), 0.67–0.74 (m, 2H, H-2 and H-2′ of TMSEt), 0.77 (s, 9H, 3Me of TBDPS), 2.82 (d, 1H, $J_{4,OH}$ 3.3 Hz, 4-OH), 3.22 (td, 1H, $J_{4,5} = J_{5,6}$ 9.7 Hz, $J_{5,6'}$ 4.9 Hz, H-5^{IV}), 3.32–3.46 (m, 5H, H-4^{I}, H-5^{I}, H-5^{II}, H-5^{III} and H-1 of TMSEt), 3.59–3.70 (m, 4H, H-6^{I}, H-6^{II}, H-6^{III} and H-6^{IV}), 3.75–3.83 (m, 2H, H-4^{III} and H-1′ of TMSEt), 3.88–3.95 (m, 2H, H-3^{II} and H-$6'^{III}$), 4.00 (t, 1H, $J_{2,3} = J_{3,4}$ 8.9 Hz, H-3^{IV}), 4.01 (t, 1H, $J_{2,3} = J_{3,4}$ 9.2 Hz, H-3^{II}), 4.09 (t,

1H, $J_{2,3} = J_{3,4}$ 8.9 Hz, H-3^{I}), 4.11 (dd, 1H, *J* 4.8 Hz, *J* 10.1 Hz, H-6′^{II}), 4.21 (dd, 1H, $J_{5,6}$ 4.9 Hz, J_{gem} 10.3 Hz, H-6′^{IV}), 4.28 (dd, 1H, *J* 5.2 Hz, *J* 10.8 Hz, H-6^{I}), 4.37 (d, 1H, $J_{1,2}$ 7.9 Hz, H-1^{IV}), 4.47 (d, 1H, $J_{1,2}$ 7.7 Hz, H-1^{I}), 4.85 (d, 1H, $J_{1,2}$ 5.4 Hz, H-1^{II}), 4.86 (s, 1H, $O_2C\underline{H}Ph^{II}$), 4.89 (d, 1H, $J_{1,2}$ 7.8 Hz, H-1^{III}), 4.91 (dd, 1H, $J_{1,2}$ 7.9 Hz, $J_{2,3}$ 8.4 Hz, H-2^{I}), 5.04 (t, 1H, $J_{1,2} = J_{2,3}$ 5.2 Hz, H-2^{II}), 5.14 (s, 1H, $O_2C\underline{H}Ph^{IV}$), 5.15 (t, 1H, $J_{2,3} = J_{3,4}$ 9.3 Hz, H-3^{III}), 5.22 (dd, 1H, $J_{1,2}$ 7.9 Hz, $J_{2,3}$ 9.6 Hz, H-2^{III}), 5.33 (dd, 1H, $J_{1,2}$ 7.9 Hz, $J_{2,3}$ 8.6 Hz, H-2^{IV}), 5.45 (s, 1H, O_2CHPh^{I}), 6.82–7.95 (m, 50H, 10Ph); ^{13}C NMR (126 MHz, $CDCl_3$): δ −1.6 (3Me of TMSEt), 18.0 (C-2 of TMSEt), 19.3 (C of TBDPS), 26.7 (3Me of TBDPS), 65.6 (C-5^{II}), 66.2 (C-5^{IV}), 66.4 (C-5^{I}), 67.5 (C-1 of TMSEt), 68.4 (C-6^{IV}), 68.6 (C-6^{II}), 68.7 (C-6^{I}), 69.5 (C-6^{III}), 70.3 (C-4^{III}), 71.4 (C-2^{III}), 72.7 (C-2^{II}), 73.5 (C-3^{IV}), 73.8 (C-5^{III}), 74.2 (C-2^{I}), 75.0 (C-2^{IV}), 75.3 (C-3^{I}), 76.7 (C-3^{III}), 77.4 (C-3^{II}), 78.1 (C-4^{II}), 79.0 (C-4^{I}), 81.1 (C-4^{IV}), 98.46 (C-1^{II}), 98.51 (C-1^{III}), 100.5 ($O_2\underline{C}HPh^{II}$), 100.8 (C-1^{I}), 101.5 ($O_2\underline{C}HPh^{IV}$), 101.7 (O_2CHPh^{I}), 102.0 (C-1^{IV}), 126.25, 126.27, 127.2, 127.3, 127.8, 127.96, 128.06, 128.19, 128.24, 128.31, 128.34, 128.6, 128.7, 128.87, 128.91, 129.0, 129.16, 129.23, 129.32, 129.36, 129.37, 129.57, 129.65, 129.70, 129.87, 129.91, 129.95, 131.0, 132.2, 132.3, 132.7, 132.88, 132.94, 133.03, 133.2, 133.9, 135.7, 136.1, 136.7, 137.1, 137.4, 164.3 (C=O of Bz), 164.6 (C=O of Bz), 164.9 (C=O of Bz), 165.4 (C=O of Bz), 166.9 (C=O of Bz); HMBC 2D-NMR (500 MHz, $CDCl_3$), δ 4.37 (H-1^{IV}) →69.5 (C-6^{III}), indicates 1→6 linkage; ESI-FT-MS, calculated for $C_{101}H_{104}O_{26}Si_2Na^+$ $(M + Na)^+$: 1811.6247, found *m/z*: 1811.6232.

4.3 Results and discussion

4.3.1 Synthesis of monomeric units for the formation of β1-3-glucosidic linkage

Compounds **9**, **14** and **19** were tested as monomeric acceptors in the formation of β1-

3-glucosidic linkages (Fig. 4-4). Compounds **9** and **14** were synthesized, while compound **19** was commercially available. The phenylthio (SPh) group, being more stable than the frequently used acid-sensitive trichloroacetimidate group (Du *et al*. 2000; Ning *et al*. 2003; Zhao *et al*. 2003; Zeng and Kong 2003; Yang and Kong 2005; Tanaka *et al*. 2012; Miyagawa *et al*. 2015), was selected as the leaving group of the donor units.

Compound **9** was synthesized as shown in Fig. 4-5. First, the reaction conditions were investigated for the 3-position-specific introduction of a Lev group as an orthogonal protecting group (Fig. 4-2 and 4-3). Regioselectivity was controlled by using acid anhydride as an active ester for levulinylation to promote acylation of the secondary hydroxy group (Kattnig and Albert 2004). Compound **2**, prepared from D-glucopyranose as reported previously (Roy *et al*. 2008), was exposed to reaction with levulinic acid anhydride under three conditions: a) 0.1 eq. DMAP and DMF as nucleophile and solvent, respectively; b) pyridine as nucleophile and solvent; and c) 1.1 eq. pyridine and DMF as nucleophile and solvent, respectively. The reactions were terminated upon reaching a mole percent of 44–51% of products containing the single Lev group. Reaction times increased in the order of c, b, and a. Compound **3** (6-Lev, 18%) was the major compound under conditions b, but compound **4** (3-Lev, 16%) was produced as much as compound **3** (6-Lev, 16%) under conditions a. Under conditions c, compound **4** (3-Lev) reached the highest yield (28%), although the reaction proceeded slowly (Fig. 4-3), with the 3-position-specific acylation seemingly due to enhanced formation of bidentate hydrogen bonds between carboxylate ions and the 6- and 3-OH groups (Kattnig and Albert 2004). Compound **4** was prepared from compound **2** (14 g, 51.4 mmol) under conditions c. The remaining hydroxy groups were protected by Bz groups, and compound **7** (5.17 g, 3.24 mmol) was obtained in 14% yield in the two steps (Fig. 4-5). Compound **5** (2-Lev), a

byproduct in the levulinylation, was neither clearly removed from compound **4** nor from compound **7** after benzoylation, resulting in a low yield for compound **7**. Compound **7** (1.00 g, 1.43 mmol) was subjected to the conversion from the SPh group to a TMSEt group according to the reported method (Komba and Tsuzuki 2017; Tanaka *et al*., 2018), and compound **8** (449 mg, 629 μmol) was obtained in 44% yield. The unreacted compound **7** (269 mg, 385 μmol) was subjected to the same conversion to obtain additional compound **8** (95 mg, 135 μmol) in 35% yield. The combined compound **8** (528 mg, 747 μmol) was subjected to the removal of its 3-Lev group, which provided compound **9** (397 mg, 650 μmol) in 87% yield. The selective removal of the Lev group under the presence of the Bz groups progressed due to the reaction of hydrazine progressed under the neutral conditions by acetic acid (Adamo *et al*. 2011).

Compound **14** was synthesized according to Fig. 4-6. This entailed the initial, 4-step synthesis of compound **10** from D-glucopyranose by the method (Roy *et al*. 2008). Compound **11** was obtained quantitatively (3.17 g, 5.30 mmol) by introducing a TBDPS group at the 3-position of compound **10** (1.90 g, 5.27 mmol), although the reaction was proceeded slowly (8 days). In compound **10**, 3-OH was previously reported to possess higher reactivity than 2-OH (Tanaka *et al*. 2018). Due to the size of the TBDPS group, and the steric hindrance caused by the SPh group at the anomeric position of compound **10**, the difference of reactivity in 3-OH and 2-OH was enhanced, and the reaction proceeded at the 3-position rather than at the 2-position. Compound **12** (1.46 g, 2.07 mmol) was then obtained in 51% yield from compound **11** (2.43 g, 4.05 mmol) through protecting the unmodified 2-OH by the Bz group. This reaction proceeded as the Bz group is smaller than the TBDPS group. The Bz group helps β-anomeric glycosylation of the donor unit *via* neighboring group participation (Nukada *et al*. 1998). Compound **12** (858

mg, 1.22 mmol) was subjected to the conversion of the SPh group to the TMSEt group by using the method (Komba and Tsuzuki 2017; Tanaka *et al*., 2018), and compound **13** (505 mg, 720 μmol) was obtained in 59% yield. Compound **14** (210 mg, 445 μmol) was obtained in 73% yield by removal of the TBDPS group from compound **13** (433 mg, 609 μmol). Due to the high stability of the TBDPS group bound to secondary hydroxy group of compound **13**, this removal reaction was proceeded slowly (5 days). Although each reaction takes a long time (8 days for introduction and 5 days for removal), the high efficiency of introduction and removal of TBDPS group at 3-position is the advantage of the monomeric unit in β1-3-linkage synthesis.

4.3.2 Glycosylation of compounds **9**, **14**, and **19** as acceptors

The formation of β1-3-linkage by glycosylation was tested using the three monomeric acceptors, compounds **9**, **14**, and **19** (Fig. 4-7). For the efficiency of chemical route, compounds **7** and **12**, which were obtained as intermediates of compounds **9** (Fig. 4-5) and **14** (Fig. 4-6), respectively, were used as donors for the glycosylation (Fig. 4-7). The β1-3-linked disaccharide derivative (compound **15**) was synthesized by combining compounds **14** (190 mg, 402 μmol) and **12** (339 mg, 482 μmol), resulting in a mixture of compound **15** and the unreacted donor (compound **12**), while the acceptor (compound **14**) was completely consumed. The TBDPS group was removed from the 3-position of the non-reducing-end sugar residue of compound **15**, synthesizing compound **16** (220 mg, 266 μmol) in 66% yield in the two steps. In condensation using compounds **9** (140 mg, 236 μmol) and **19** (20 mg, 76.8 μmol) as acceptors and compound **7** (242 mg, 354 μmol for the former, and 20 mg, 76.8 μmol for the latter) as donor, compound **17** (54 mg, 47.2 μmol), a derivative of α1-3-linked disaccharide, and compound **18** (32 mg, 38.4 μmol), a

derivative of β1-6-linked disaccharide, were produced in 20% and 50% yields, respectively (Fig. 4-7). The anomer types were determined based on the $J_{1,2}$ in ^{1}H NMR, and $J_{1,2}$ of compounds **15**, **16**, **17**, and **18** were 7.2 Hz, 7.2 Hz, 3.4 Hz, and 7.8 Hz, respectively, indicating β-, β-, α-, and β-anomer, respectively. Although the 2-position of the donors (compounds **7** and **12**) is protected by the Bz group, which helps β-glycosylation *via* neighboring group participation (Fig. 4-8A) as described above, α-glycosylation proceeded in the reaction of compound **17** synthesis. This suggests that the bulky and electron-withdrawing Bz group at the 4-position of compound **9** prevents β-glycosylation of the neighboring 3-OH and accept only α-glycosylation. In addition, the anchimeric assistance (Nishimura *et al*. 1972; Zhang *et al*. 2021) caused by the Lev group at 3-position of compound **7** (Fig. 4-8B) was prioritized than the neighboring group participation of the Bz group at 2-position (Fig. 4-8A) as the reactivity of 3-OH of the acceptor (compound **9**) was decreased by neighboring Bz groups as suggested in previous reports (Tanaka *et al*. 2012; Miyagawa 2018). In the reaction of compounds **7** and **19**, although the donor (compound **7**) has the Lev group at 3-position, β-glycosylation was proceeded. This suggests that the effect of the neighboring group participation of the Bz group at 2-position (Fig. 4-8A) was greater than the anchimeric assistance of Lev group at 3-positon (Fig. 4-8B) due to the high reactivity of 6-OH in compound **23**, which is formed in the reaction as described in the following statement. Compound **19** is often used for 3-position-specific glycosylation, using trimethylsilyl trifluoromethanesulfonate as an acid catalyst (Ning *et al*. 2003; Zhao *et al*. 2003). However, a β1-6 disaccharide derivative (compound **18**) was produced, indicating that 3-OH glycosylation was prevented due to the rearrangement of the isopropylidene group to the 3, 5-position (Fig. 4-9). This is attributed to severe acidity caused by NIS/TfOH, used for SPh activation.

Similar rearrangements have been reported for boron trifluoride·diethyl ether complex-catalyzed reactions (Just *et al*. 1988; Cruz-Gregorio *et al*. 2005). In the reaction of compounds **12** and **14**, compound **14** possesses enough space to receive β-D-glucosyl at the 3-position, and its 3-OH group has higher reactivity than that of compound **9**. This seems to cause the forming of β1-3-glucosidic linkage in compound **15**.

4.3.3 Synthesis of the monomeric unit for the formation of β1-6-linkages and Glcβ1-6Glcβ1-3Glcβ1-3Glc derivative

Compound **20**, required for β1-6-linkage synthesis, was synthesized from compound **10** in three steps (Fig. 4-10). The 2- and 3-positions of compound **10** (310 mg, 860 μmol) were protected with Bz groups. Subsequently, the 4- and 6-positions were protected by converting the benzylidene group to Lev groups, providing compound **20** (462 mg, 679 μmol) in 79% yield. Condensation of compounds **20** (215 mg, 318 μmol) and **16** (217 mg, 262 μmol) was performed (Fig. 4-11). Compounds **20** and **16** acted as donor and 3-position-specific acceptor, respectively, to form a β1-3-linkage, obtaining the laminaritriose derivative compound **21** (170 mg, 123 μmol) in 47% yield. The Lev groups were removed from compound **21** (70 mg, 50.2 μmol), providing a 6-position-specific acceptor, compound **22** (47 mg, 39.2 μmol), in 78% yield. In the reaction of compounds **12** (27.8 mg, 39.5 μmol) and **22** (39.4 mg, 32.9 μmol), a β1-6-glucosidic linkage was freshly formed, resulting in compound **1** (12.5 mg, 7.57 μmol), in 23% yield. The results indicate that compound **20**, which can be synthesized from compound **10** in short steps (Fig. 4-10), acts as a donor in the synthesis of compounds that serve as acceptors toward the formation of β1-6-glucosidic linkages. 4^{III}-*O*-glycosylation was not observed, even though the 4-OH group of the non-reducing-end sugar residue of compound **22** was

unprotected because the primary hydroxy group is more reactive than the secondary hydroxy group due to space availability. Additionally, the reactivity of the 4-OH group was decreased due to the bulky, electron-withdrawing Bz group at the 3-position, promoting the effective formation of the β1-6-linkage in the β1-3/1-6-glucan main chain. Compound **1**, with its non-reducing end-unit derived from compound **12,** presumably acts as an acceptor, to form another β1-3-linkage in the subsequent glycosylation. The deprotection of compound **1** can be performed at high yield as reported previously using a solution of sodium methoxide in methanol for the Bz group, acetic acid for the benzylidene group, and a solution of trifluoroacetic acid in dichloromethane (Komba and Tsuzuki 2017).

In summary, two monomeric units, phenyl 2-*O*-benzoyl-4,6-*O*-benzylidene-3-*O*-(*tert*-butyldiphenylsilyl)-1-thio-β-D-glucopyranoside (compound **12**) and phenyl 2,3-di-*O*-benzoyl-4,6-di-*O*-levulinyl-1-thio-β-D-glucopyranoside (compound **20**) were chemically synthesized. These served as donors in the synthesis of acceptor compounds, which can be used to introduce β1-3- and β1-6-linkages, respectively, to their non-reducing ends. By the successive glycosylation reactions using the two compounds (compounds **12** and **20**), starting with a β1-3-specific acceptor (compound **14**), the tetrasaccharide derivative (compound **1**) was synthesized. Thus, the monomeric units synthesized in this study is suitable and effective for the sequential synthesis of β1-3- and β1-6-linkages. β1-3/1-6-Glucooligosaccharides with desired linkage sequences can be synthesized by selective use of the monomeric units in each glycosylation reaction.

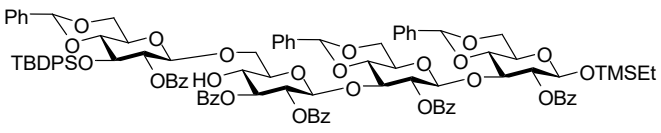

1

Fig. 4-1. Target compound
1: 6^{III}-*O*-D-glucosyl laminaritriose derivative.

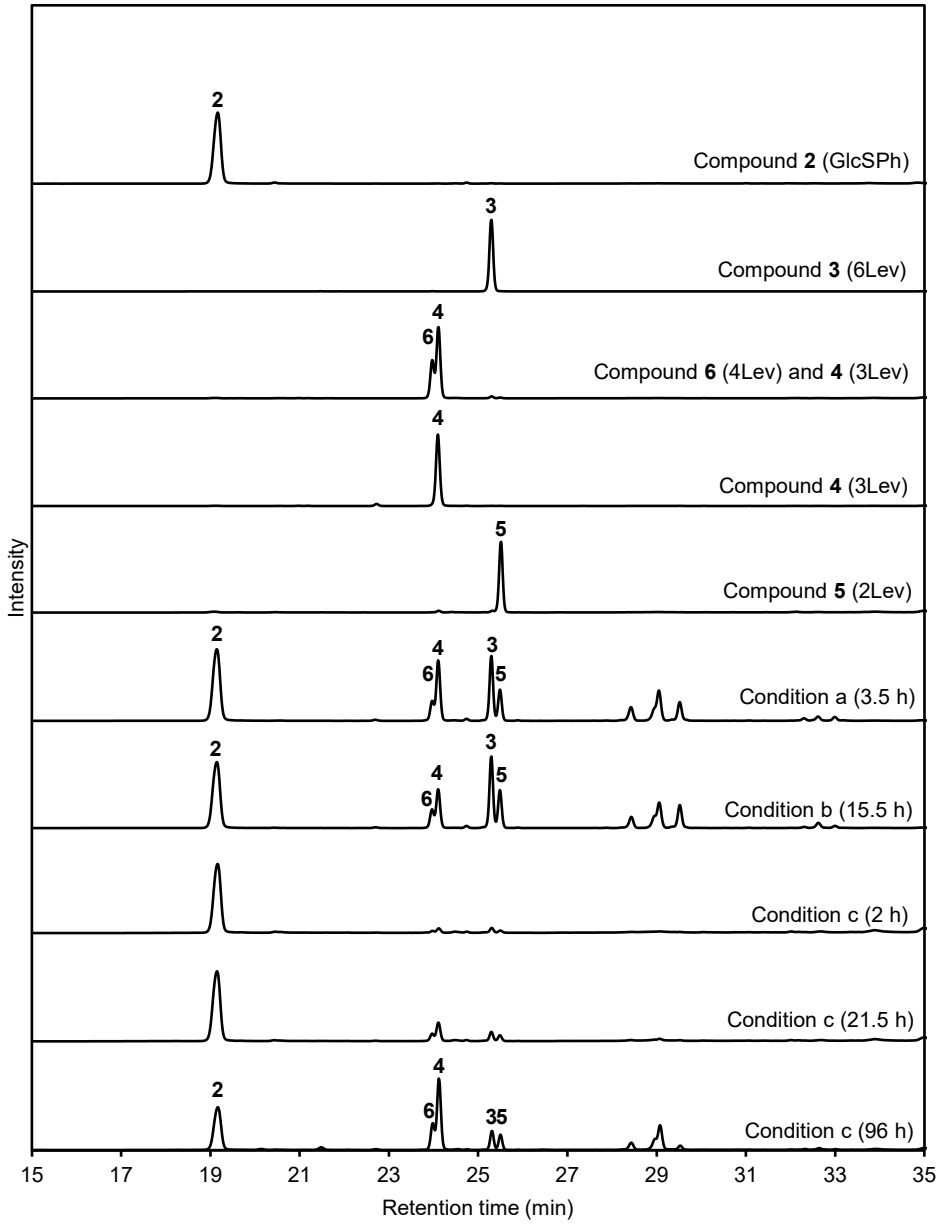

Fig. 4-2. HPLC chromatograms of regioselective levulinylation reactions shown in Fig. 4-3.

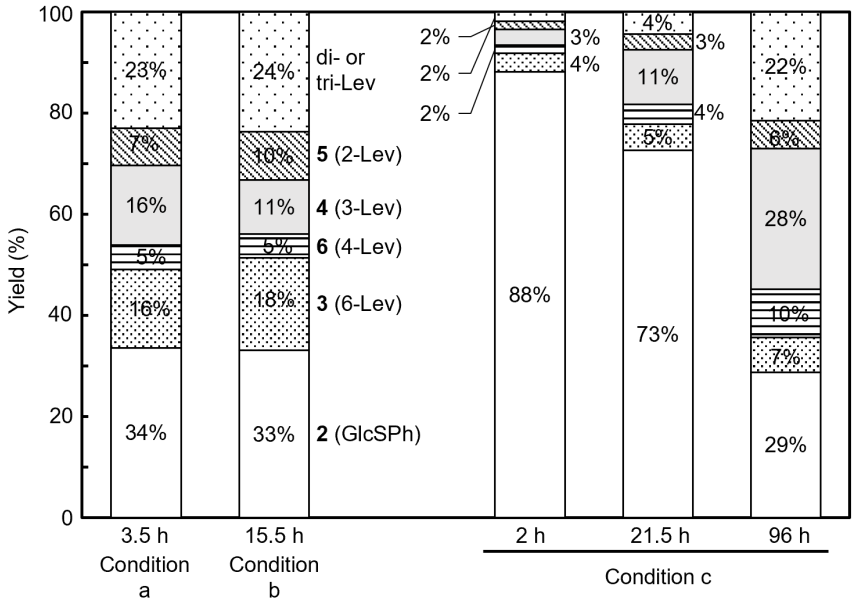

Fig. 4-3. The yield of regioselective levulinylation under each reaction conditions
The yield was calculated by analytical HPLC. Reagents and conditions: (a) levulinic acid anhydride, DMAP, DMF, 0˚C, 3.5 h. (b) levulinic acid anhydride, pyridine, 0˚C, 15.5 h. (c) levulinic acid anhydride, pyridine, DMF, 0˚C for 21.5 h and 27˚C for 74.5 h.

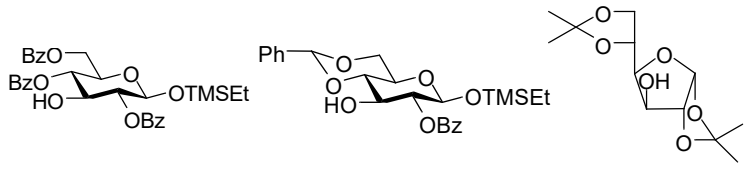

9 **14** **19**

Fig. 4-4. Tested monomeric acceptors for forming β1-3-linkage
9: 2-(trimethylsilyl)ethyl 2,4,6-tri-*O*-benzoyl-β-D-glucopyranoside. **14**: 2-(trimethylsilyl)ethyl 2-*O*-benzoyl-4,6-*O*-benzylidene-β-D-glucopyranoside. **19**: 1,2:5,6-di-*O*-isopropylidene-α-D-glucofuranose.

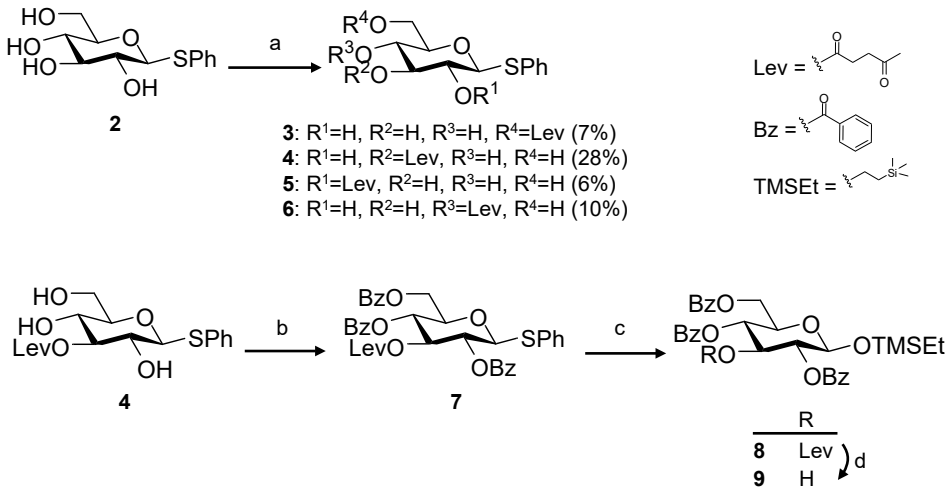

Fig. 4-5. Synthesis of monomeric units modified with levulinyl and benzoyl groups
Reagents and conditions: (a) levulinic acid anhydride, pyridine, DMF, 23˚C for 109.5 h. (b) BzCl, pyridine, room temperature, 1 h, 14% (2 steps). (c) TMSEtOH, NIS, TfOH, CH_2Cl_2, CH_3CN, −40˚C, 2 h, 44%. (d) hydrazine monohydrate, acetic acid, pyridine, room temperature, 5 min, 87%.

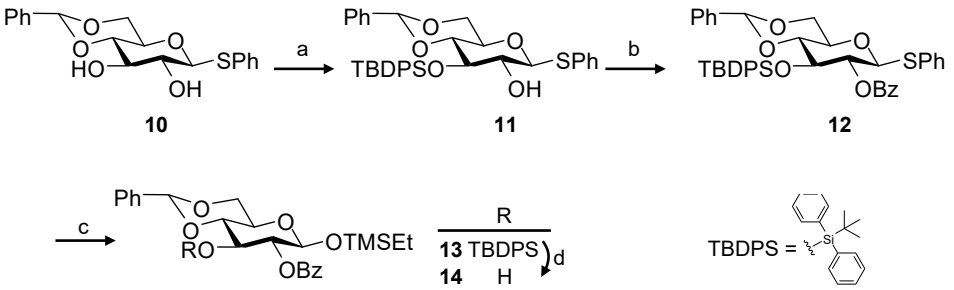

Fig. 4-6. Synthesis of monomeric units modified with benzylidene and silyl groups
Reagents and conditions: (a) TBDPS-Cl, imidazole, DMF, 4˚C, 8 days, quantitatively. (b) BzCl, pyridine, 60˚C, 7 days, 51%. (c) TMSEtOH, NIS, TfOH, CH_2Cl_2, CH_3CN, −40˚C, 1 h, 59%. (d) TBAF in THF, acetic acid, DMF, room temperature, 5 days, 73%.

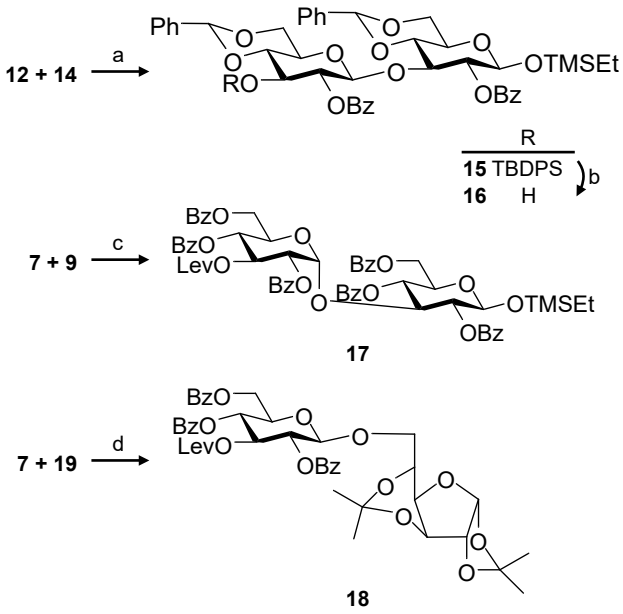

Fig. 4-7. Glycosylation reactions occurring with three acceptor units
Reagents and conditions: (a) TfOH, NIS, CH_2Cl_2, −30˚C, 2 h. (b) TBAF in THF, acetic acid, DMF, room temperature, 14 days, 66% (2 steps). (c) TfOH, NIS, CH_2Cl_2, −30˚C, 40 h, 20%. (d) TfOH, NIS, CH_2Cl_2, CH_3CN, −30˚C, 1 h, 50%.

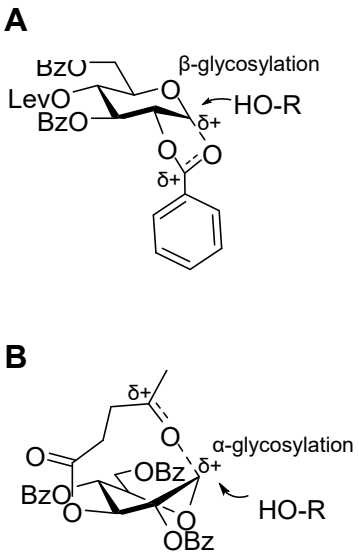

Fig. 4-8. The neighboring group participation of Bz group and the anchimeric assistance of Lev group in compound 7
(A) The neighboring group participation of Bz group at 2-position. (B) The anchimeric assistance of Lev group at 3-position.

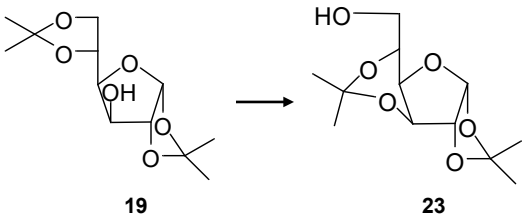

Fig. 4-9. Conversion of compound 3 in reaction d in Fig. 4-7
23: 1,2:3,5-di-*O*-isopropylidene-α-D-glucofuranose. This conversion occurred during the synthesis of compound **18**.

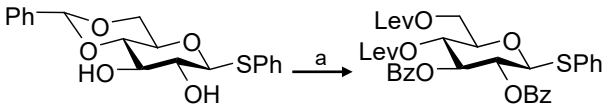

10 **20**

Fig. 4-10. Synthesis of monomeric unit for forming β1-6-linkage
(a) 1) BzCl, pyridine, room temperature, 2 h, 2) 80% (v/v) acetic acid aqueous solution, 60˚C, 3 h, 3) levulinic acid anhydride, DMAP, pyridine, CH_2Cl_2, room temperature, 2 h, 79% (3 steps).

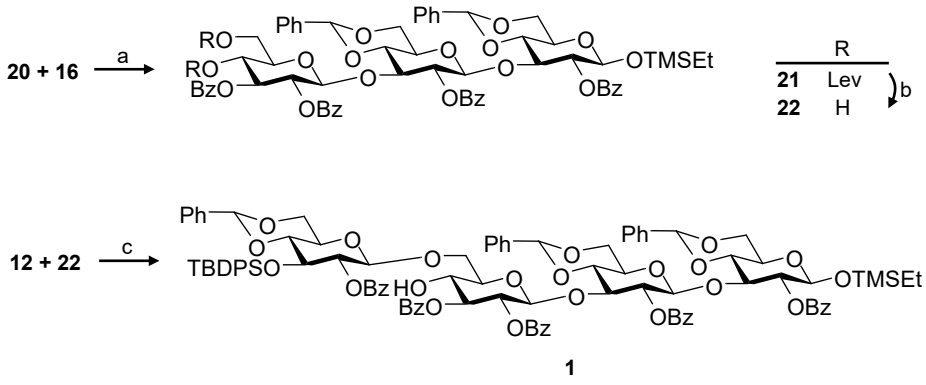

Fig. 4-11. Synthesis of compound 1 by using three monomeric units
Reagents and conditions: (a) TfOH, NIS, CH_2Cl_2, −40˚C, 2 h, 47%. (b) hydrazine monohydrate, acetic acid, pyridine, room temperature, 1 h, 78%. (c) TfOH, NIS, CH_2Cl_2, −30˚C, 2 h, 23%.

5. General discussion

In this study, two β1-3-glucan-degrading enzymes, GH3 β-glucosidase and GH55 endo-β-1,3-glucanase, from the pink snow mold fungus, *M. nivale,* were identified, and functionally and structurally characterized. GH3 β-glucosidase, MnBG3A, catalyzes strictly the hydrolysis of β1-3-and β1-6-D-glucosidic linkages and the formation of β1-6-linkage. It showed substrate and product inhibitions in pNP-Glc hydrolysis. The inhibition mechanism was proposed together with the allosteric effects of monosaccharides. GH55 endo-β-1,3-glucanase, MnLam55A, shows endo-type hydrolysis on laminarin at the non-reducing terminal β1-3-linkage of the laminarioligosaccharide moiety at the reducing end side of the main chain β1-6-linkage. The mechanism of this specific endo-type hydrolysis was demonstrated by the structural analysis of the degraded glucan and the analysis of possible glucan-binding mode on the protein structure solved. In addition to these analyses of β1-3-glucan-degrading enzymes, the method for the chemical synthesis of β1-3/1-6-glucooligosaccharides was developed. The availability of this method was evaluated by synthesizing tetrasaccharide derivative (Glcβ1-6Glcβ1-3Glcβ1-3Glc).

The characteristics of MnBG3A in hydrolysis, transglucosylation, and condensation are well similar to other fungal GH3 β-glucosidases, especially *A. aculeatus* AaBGL1 which have high sequence identity with MnBG3A. The inhibitions by substrate and product have also been reported for some fungal GH3 β-glucosidases (Krogh *et al*. 2010; Langston *et al*. 2006). Based on these functional similarities and the structural commonness of GH3 enzymes, the allosteric effects of monosaccharides found in this study might be common in other GH3 enzymes that show substrate inhibition. *A. oryzae* AoCel3A and *P. chrysosporium* PcBgl1A exhibit the decrease of reaction rate with the

increase of substrate concentration, which was explained by transglucosylation (Kawai *et al*. 2004; Langston *et al*. 2006). The reaction of these enzymes can be interfered with monosaccharides. It is still unknown what drives this kinetic behavior. To prove these mechanisms, verification in other GH3 enzymes, and structural analysis of monosaccharide and pNP-glycoside complexes are desired.

As described in chapter 3, GH55 contains both exo- and endo-β-1,3-glucanases and can be divided into three groups: group 1, bacterial exo-β-1,3-glucosidases; group 2, fungal exo-β-1,3-glucosidases; and group 3, fungal endo-β-1,3-glucanases. As for the substrate binding site, particularly for binding the glycan part, group 1 enzymes have only subsite −1 and lack the space to accommodate the D-glucosyl residue at subsite −2 (Bianchetti *et al*. 2015), but group 2 and 3 enzymes have subsites −1 and −2. The enzymes in each group have different lengths of C5-L3 loop. The putative GH55 enzymes which have the same length of C5-L3 with group 3 enzymes seemed to be endo-β-1,3-glucanases. To reveal the substrate binding mode and the existence of the predicted minus subsites of GH55 endo-β-1,3-glucanases, structural analysis of the complex with β1-3/1-6-glucooligosaccharides, which can be synthesized using the method established in chapter 4, and functional analysis of mutants with mutations in putative minus subsites are desired.

Based on the functional characteristics, the putative biological roles of these two enzymes in *M. nivale* are described in following statements. Around phytopathogenic fungi, β1-3-glucans are distributed to the fungal cell wall, fungal extracellular polysaccharides and host plant cells. Fungal extracellular polysaccharides are generally composed of β1-3-linked main chain and β1-6-D-glucosidic branches, such as scleroglucan and schizophyllan, and the fungal cell wall contains β1-3/1-6-glucans, which have similar structures to laminarin, but have β1-3-glucan branch linked by β1-6-linkages

(Fontaine *et al*. 2000; Aimanianda *et al*. 2017). In the host plant cells, two types of β1-3-glucans are present: linear β1-3/1-4-glucan, which is specifically distributed in grasses (Gómez *et al*. 1997), and callose, which is a linear β1-3-glucan that is involved in the plant immune system and protects the plant cell from pathogenic fungal invasion (Piršelová and Matušíková 2013).

Based on the published genome and transcriptome data of *M. nivale* (Tsers *et al*. 2023), I will discuss here the presumed carbohydrate metabolism pathway of this fungus involved in its growth and pathogenicity. Cairns *et al*. reported that *M. nivale* utilizes a variety of polysaccharides and monosaccharides (Cairns *et al*. 1995a). This fungus grown on sucrose as a carbon source expresses various types of extracellular glycoside hydrolases (Tsers *et al*. 2023): the degrading enzymes acting on chitin, cellulose, arabinan, α- and β-mannan, xylan, xyloglucan, β1-3-glucan, and so on. Chitin, α- and β-mannan, and β1-3-glucan are components of the fungal cell wall (Gow *et al*. 2017; Gow and Lenardon 2023), and cellulose, arabinan, xylan, xyloglucan, and β1-3/1-4-glucan are components of the plant cell wall (Scheller and Ulskov 2010). These enzymes are suggested to be involved in the degradation of fungal own and plant cell walls for the growth, the acquisition of carbon sources, and the invasion to plants. RNA levels of endo-β-1,3(4)-glucanase (MN608_09578), xyloglucan-specific endo-β-1,4-glucanase (MN608_09393), and endo-β-1,4-xylanase (MN608_10307) are upregulated by rye extract (Tsers *et al*. 2023), suggesting that *M. nivale* secretes these enzymes to degrade hemicellulose (β1-3/1-4-glucan, xylan, and xyloglucan) and to penetrate the cell wall of host plants.

β-Glucosidase has been implicated in the pathogenicity of *M. nivale* by Hofgaard *et al*. and Gorshkov *et al*. (Hofgaard *et al*. 2006; Gorshkov *et al*. 2020), although *M. nivale*

has possibility to secrete β-glucosidases other than MnBG3A through induction under the other conditions. During the invasion to the plant cell, MnBG3A is suggested to hydrolyze β1-3- and β1-4-glucooligosaccharides which released from plant β1-3/1-4-glucan degraded by endo-β-1,3(4)-glucanase. This enzyme also produces gentiobiose, the candidate of cellulase inducer (Kurasawa *et al*. 1992; Suto and Tomita 2001), in transglucosylation. Therefore, MnBG3A has possibilities to work with β-glucanases other than MnLam55A for infecting to plants.

Since MnLam55A specifically hydrolyzed laminarin but did not other β1-3-glucans without internal β1-6-linkages in their main chain, it presumably acts on fungal cell wall β1-3/1-6-glucan. To convert fungal cell wall β1-3/1-6-glucan degradable by MnLam55A, another endo-β-1,3-glucanase, which hydrolyzes β1-3-glucosidic linkage at non-reducing end side of β1-6-branch to convert the main chain of fungal cell wall glucan into linear β1-3/1-6-glucan, should be required (Fig. 5-1). As an example of such enzyme, the GH16 endo-β-1,3-glucanase from *P. chrysosporium*, PcLam16A, preferentially hydrolyzes β1-3-linkages at the non-reducing end side of the D-glucosyl residue at the root of the β1-6-D-glucosidic branches of *L. digitata* laminarin (Kawai *et al*. 2006). According to the recently published *M. nivale* genome data (Tsers *et al*. 2023), MN608_04815 is a homolog of PcLam16A. Since MnBG3A hydrolyzes laminaribiose and gentiobiose (Table 2-1), it can hydrolyze the end products of MnLam55A from β1-3/1-6-glucan. Therefore, MnLam55A and MnBG3A may contribute to the fungal growth and/or morphological changes by degrading the cell wall in the presence of initially acting endo-β-1,3-glucanases as illustrated in Fig. 5-1. These assumptions are also supported by the fact that these two enzymes were produced during the growth phase of *M. nivale* without the addition of any inducers. If these enzymes contribute to the degradation of the other

β1-3-glucans, the preprocessing by another endo-β-glucanase is also required. In this study, the laminarin- and pNP-Glc-hydrolyzing activities were not separated during the purification of each enzyme, and no other β1-3-glucanases were detected. As *M. nivale* has putative GH16 enzyme coding gene, MN608_0481, as described above, another endo-β-1,3-glucanase might be detected using β1-3-glucans with linear β1-3-linked main chain such as curdlan, paramylon, and scleroglucan as substrate.

From the GenBank database, putative GH55 endo-β-1,3-glucanases are found in several plant pathogenic fungi such as *Trichoderma* spp., *Fusarium graminearum, Fulvia fulva*, and *Ustilaginoidea virens*, grass endophytes such as *M. bolleyi* and *Epichloë festucae*, and model fungi such as *Aspergillus* spp. and *Neurospora crassa*. Since GH3 β-glucosidase is also distributed to various filamentous fungi, including those described above, these two β-glucan-degrading enzymes are suggested to have the general roles in filamentous fungi such as fungal growth and morphological changes. As the GH16 homologs are also present in the genome of the fungi described above, the putative cell wall glucan degradation scheme by GH16 endo-β-1,3-glucanase, GH55 endo-β-1,3-glucanase, and GH3 β-glucosidase may be common in these fungi. To elucidate the biological functions of these enzymes, further studies such as the identification and characterization of other endo-β-glucanases described above, the mutagenesis of *M. nivale*, and the expression analysis of the genes encoding these enzymes are needed.

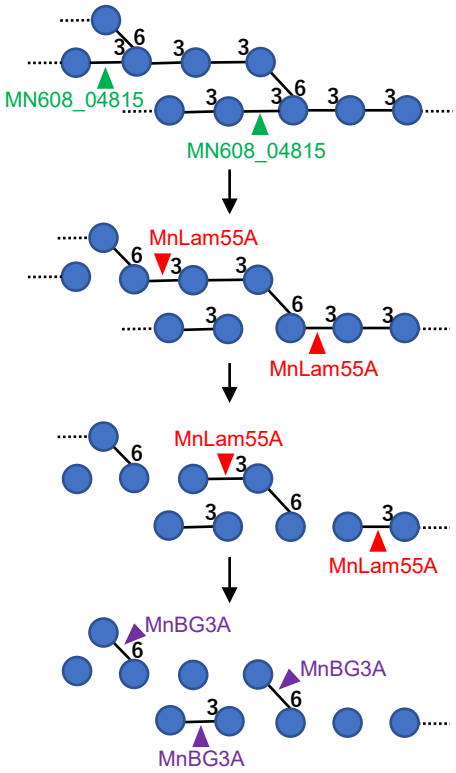

Fig. 5-1. Putative degradation scheme of the cell wall β1-3-glucan by *M. nivale*
Blue circles indicate D-glucose. Colored triangles indicate the cleavage linkages by each enzyme.

References

Adamo, R., Tontini, M., Brogioni, G., Romano, M.R., Costantini, G., Danieli, E., Proietti, D., Berti, F., and Costantino, P. (2011). Synthesis of laminarin fragments and evaluation of a β-(1,3) glucan hexasaccharide-CRM_{197} conjugate as vaccine candidate against *Candida albicans*. J. Carbohydr. Chem. *30*, 249–280.

Adams, P.D., Afonine, P.V., Bunkóczi, G., Chen, V.B., Davis, I.W., Echols, N., Headd, J.J., Hung, L.W., Kapral, G.J., Grosse-Kunstleve, R.W., McCoy, A.J., Moriarty, N.W., Oeffner, R., Read, R.J., Richardson, D.C., Richardson, J.S., Terwilliger, T.C., and Zwart, P.H. (2010). PHENIX: a comprehensive Python-based system for macromolecular structure solution. Acta Crystallogr. D Biol. Crystallogr. *66*, 213–221.

Agirre, J., Ariza, A., Offen, W.A., Turkenburg, J.P., Roberts, S.M., Mcnicholas, S., Harris, P.V., Mcbrayer, B., Dohnalek, J., Cowtan, K.D., Davies, G.J., and Wilson, K.S. (2016). Three-dimensional structures of two heavily *N*-glycosylated *Aspergillus* sp. family GH3 β-D-glucosidases. Acta Crystallogr. D Struct. Biol. *72*, 254–265.

Ahmad, S.K., Brinch, D.S., Friis, E.P., and Pedersen, P.B. (2004). Toxicological studies on lactose oxidase from *Microdochium nivale* expressed in *Fusarium venenatum*. Regul. Toxicol. Pharmacol. *39*, 256–270.

Aimanianda, V., Simenel, C., Garnaud, C., Clavaud, C., Tada, R., Barbin, L., Mouyna, I., Heddergott, C., Popolo, L., Ohya, Y., Delepierre, M., and Latge, J.P. (2017). The dual activity responsible for the elongation and branching of β-(1,3)-glucan in the fungal cell wall. mBio *8*, e00619-17.

Almagro Armenteros, J.J., Tsirigos, K.D., Sønderby, C.K., Petersen, T.N., Winther, O., Brunak, S., von Heijne, G., and Nielsen, H. (2019). SignalP 5.0 improves signal peptide predictions using deep neural networks. Nat. Biotechnol. *37*, 420–423.

Baba, Y., Sumitani, J., Tani, S., and Kawaguchi, T. (2015). Characterization of *Aspergillus aculeatus* β-glucosidase 1 accelerating cellulose hydrolysis with *Trichoderma* cellulase system. AMB Express *5*, 3.

Bianchetti, C.M., Takasuka, T.E., Deutsch, S., Udell, H.S., Yik, E.J., Bergeman, L.F., and Fox, B.G. (2015). Active site and laminarin binding in glycoside hydrolase family 55. J. Biol. Chem. *290*, 11819–11832.

Bowyer, P., Clarke, B.R., Lunness, P., Daniels, M.J., and Osbourn, A.E. (1995). Host range of a plant pathogenic fungus determined by a saponin detoxifying enzyme. Science *267*, 371–374.

Brown, G.D., and Gordon, S. (2005). Immune recognition of fungal β-glucans. Cell. Microbiol. *7*, 471–479.

Cairns, A.J., Howarth, C.J., and Pollock, C.J. (1995a). Submerged batch culture of the psychrophile *Monographella nivalis* in a defined medium; growth, carbohydrate utilization and responses to temperature. New Phytol. *129*, 299–308.

Cairns, A.J., Howarth, C.J., and Pollock, C.J. (1995b). Characterization of acid invertase from the snow mould *Monographella nivalis*: a mesophilic enzyme from a psychrophilic fungus. New Phytol. *130*, 391–400.

Chen, J., and Seviour, R. (2007). Medical importance of fungal β-(1→3), (1→6)-glucans.

Mycol. Res. *111*, 635–652.
Chen, V.B., Arendall III, W.B., Headd, J.J., Keedy, D.A., Immormino, R.M., Kapral, G.J., Murray, L.W., Richardson, J.S., and Richardson, D.C. (2010). MolProbity: all-atom structure validation for macromolecular crystallography. Acta Crystallogr. D Biol. Crystallogr. *66*, 12–21.
Crout, D.H., and Vic, G. (1998). Glycosidases and glycosynthetases in glycoside and oligosaccharide synthesis. Curr. Opin. Chem. Biol. *2*, 98–111.
Cruz-Gregorio, S., Sanchez, M., Clara-Sosa, A., Bèrnes, S., Quintero, L., and Sartillo-Piscil, F. (2005). Intramolecular hydrogen bonding (P=O--H) stabilizes the chair conformation of six-membered ring phosphates. J. Org. Chem. *70*, 7107–7113.
de la Cruz, J., Pintor-Toro, J.A., Benítez, T., Llobell, A., and Romero, L.C. (1995). A novel endo-β-1,3-glucanase, BGN13.1, involved in the mycoparasitism of *Trichoderma harzianum*. J. Bacteriol. *177*, 6937–6945.
David, A.S., Haridas, S., LaButti, K., Lim, J., Lipzen, A., Wang, M., Barry, K., Grigoriev, I.V., Spatafora, J.W., and May, G. (2016). Draft genome sequence of *Microdochium bolleyi*, a dark septate fungal endophyte of beach grass. Genome Announc. *4*, e00270-16.
Drula, E., Garron, M.L., Dogan, S., Lombard, V., Henrissat, B., and Terrapon, N. (2022). The carbohydrate-active enzyme database: functions and literature. Nucleic Acids Res. *50*, D571–D577.
Du, Y., Zhang, M., and Kong, F. (2000). Highly efficient and practical synthesis of 3,6-branched oligosaccharides. Org. Lett. *2*, 3797–3800.
Dubas, E., Golebiowska, G., Zur, I., and Wedzony, M. (2011). *Microdochium nivale* (Fr., Samuels & Hallett): cytological analysis of the infection process in triticale (×*Triticosecale* Wittm.) Acta Physiol. Plant. *33*, 529–537.
Emsley, P., and Cowtan, K. (2004). Coot: model-building tools for molecular graphics. Acta Crystallogr. D Biol. Crystallogr. *60*, 2126–2132.
Fontaine, T., Simenel, C., Dubreucq, G., Adam, O., Delepierre, M., Lemoine, J., Vorgias, C.E., Diaquin, M., and Latge, J.P. (2000). Molecular organization of the alkali-insoluble fraction of *Aspergillus fumigatus* cell wall. J. Biol. Chem. *275*, 27594–27607.
Fox, J.D., and Robyt, J.F. (1991). Miniaturization of three carbohydrate analyses using a microsample plate reader. Anal. Biochem. *195*, 93–96.
Fujimoto, Y., Hattori, T., Uno, S., Murata, T., and Usui, T. (2009). Enzymatic synthesis of gentiooligosaccharides by transglycosylation with β-glycosidases from *Penicillium multicolor*. Carbohydr. Res. *344*, 972–978.
Gams, W., and Müller, E. (1980). Conidiogenesis of *Fusarium nivale* and *Rhynchosporium oryzae* and its taxonomic implications. Neth. J. Pl. Path. *86*, 45–53.
Gibbons, J.G., Beauvais, A., Beau, R., McGary, K.L., Latgé, J.P., and Rokas, A. (2012). Global transcriptome changes underlying colony growth in the opportunistic human pathogen *Aspergillus fumigatus*. Eukaryot. Cell *11*, 68–78.
Glynn, N.C., Hare, M.C., Parry, D.W., and Edwards, S.G. (2005). Phylogenetic analysis

of EF-1 alpha gene sequences from isolates of *Microdochium nivale* leads to elevation of varieties *majus* and *nivale* to species status. Mycol. Res. *109*, 872–880.
Gómez, C., Navarro, A., Manzanares, P., Horta, A., and Carbonell, J.V. (1997). Physical and structural properties of barley (1→3),(1→4)-β-D-glucan. Part II. Viscosity, chain stiffness and macromolecular dimensions. Carbohydr. Polym. *32*, 17–22.
Gorshkov, V., Osipova, E., Ponomareva, M., Ponomarev, S., Gogoleva, N., Petrova, O., Gogoleva, O., Meshcherov, A., Balkin, A., Vetchinkina, E., Potapov, K., Gogolev, Y., and Korzun, V. (2020). Rye snow mold-associated *Microdochium nivale* strains inhabiting a common area: variability in genetics, morphotype, extracellular enzymatic activities, and virulence. J. Fungi *6*, 335.
Gow, N.A.R., Latge, J., and Munro, C.A. (2017). The fungal cell wall: structure, biosynthesis, and function. Microbiol. Spectr. *5*, FUNK-0035-2016.
Gow, N.A.R., and Lenardon, M.D. (2023). Architecture of the dynamic fungal cell wall. Nat. Rev. Microbiol. *21*, 248–259.
Hofgaard, I.S., Wanner, L.A., Hageskal, G., Henriksen, B., Klemsdal, S.S., and Tronsmo, A.M. (2006). Isolates of *Microdochium nivale* and *M. majus* differentiated by pathogenicity on perennial ryegrass (*Lolium perenne* L.) and *in vitro* growth at low temperature. J. Phytopathol. *154*, 267–274.
Horikoshi, K., Koffler, H., and Arima, K. (1963). Purification and properties of β-1,3-glucanase from the "lytic enzyme" of *Bacillus circulans.* Biochim. Biophys. Acta *73*, 267–275.
Hoshino, T., Xiao, N., and Tkachenko, O.B. (2009). Cold adaptation in the phytopathogenic fungi causing snow molds. Mycoscience *50*, 26–38.
Hrmova, M., and Fincher, G.B. (1997). Barley β-D-glucan exohydrolases. Substrate specificity and kinetic properties. Carbohydr. Res. *305*, 209–221.
Huggett, A.S.G., and Nixon, D.A. (1957). Use of glucose oxidase, peroxidase, and O-dianisidine in determination of blood and urinary glucose. Lancet *270*, 368–370.
Ihaka, R., and Gentleman, R. (1996). R: a language for data analysis and graphics. J. Comput. Graph. Stat. *5*, 299–314.
Ishida, T., Fushinobu, S., Kawai, R., Kitaoka, M., Igarashi, K., and Samejima, M. (2009). Crystal structure of glycoside hydrolase family 55 β-1,3-glucanase from the basidiomycete *Phanerochaete chrysosporium*. J. Biol. Chem. *284*, 10100–10109.
Jamalainen, E.A. (1974). Resistance in winter cereals and grasses to low-temperature parasitic fungi. Annu. Rev. Phytopathol. *12*, 281–302.
Jewell, L.E. (2013). Genetic and pathogenic differences between *Microdochium nivale* and *Microdochium majus*. Ph.D. thesis, The University of Guelph.
Jewell, L.E., and Hsiang, T. (2013). Multigene differences between *Microdochium nivale* and *Microdochium majus*. Botany *91*, 99–106.
Just, G., Wang, Z.Y., and Chan, L. (1988). *p,p′*-Dinitrobenzhydryl ethers, acid and base stable protecting groups, which are readily removable in the presence of benzyl and monomethoxytrityl functions. J. Org. Chem. *53*, 1030–1033.
Kabsch, W. (2010). XDS. Acta Crystallogr. Sect. D Biol. Crystallogr. *66*, 125–132.
Karkehabadi, S., Hansson, H., Mikkelsen, N.E., and Kim, S. (2018). Structural studies of

a glycoside hydrolase family 3 β-glucosidase from the model fungus *Neurospora crassa*. Acta Crystallogr. F Struct. Biol. Commun. *74*, 787–796.

Karkehabadi, S., Helmich, K.E., Kaper, T., Hansson, H., Mikkelsen, N., Gudmundsson, M., Piens, K., Fujdala, M., Banerjee, G., Scott-Craig, J.S., Walton, J.D., Phillips Jr, G.N., and Sandgren, M. (2014). Biochemical characterization and crystal structures of a fungal family 3 β-glucosidase, Cel3A from *Hypocrea jecorina.* J. Biol. Chem. *289*, 31624–31637.

Kasahara, S., Nakajima, T., Miyamoto, C., Wada, K., Furuichi, Y., and Ichishima, E. (1992). Characterization and mode of action of exo-1,3-β-D-glucanase from *Aspergillus saitoi*. J. Ferment. Bioeng. *74*, 238–240.

Katoh, K., Rozewicki, J., and Yamada, K.D. (2019). MAFFT online service: multiple sequence alignment, interactive sequence choice and visualization. Brief. Bioinform. *20*, 1160–1166.

Kattnig, E., and Albert, M. (2004). Counterion-directed regioselective acetylation of octyl β-d-glucopyranoside. Org. Lett. *6*, 945–948.

Kawai, R., Igarashi, K., Kitaoka, M., Ishii, T., and Samejima, M. (2004). Kinetics of substrate transglycosylation by glycoside hydrolase family 3 glucan (1→3)-β-glucosidase from the white-rot fungus *Phanerochaete chrysosporium*. Carbohydr. Res. *339*, 2851–2857.

Kawai, R., Igarashi, K., Yoshida, M., Kitaoka, M., and Samejima, M. (2006). Hydrolysis of β-1,3/1,6-glucan by glycoside hydrolase family 16 endo-1,3(4)-β-glucanase from the basidiomycete *Phanerochaete chrysosporium*. Appl. Microbiol. Biotechnol. *71*, 898–906.

Komba, S., and Tsuzuki, W. (2017). Synthesis of the branched tetrasaccharide repeating unit of *Lactobacillus fermentum* TDS030603 and its regioisomer. Chemistry Select *2*, 10146–10149.

Krogh, K.B.R.M., Harris, P.V., Olsen, C.L., Johansen, K.S., Hojer-Pedersen, J., Borjesson, J., and Olsson, L. (2010). Characterization and kinetic analysis of a thermostable GH3 beta-glucosidase from *Penicillium brasilianum*. Appl. Microbiol. Biotechnol. *86*, 143–154.

Kulys, J., Tetianec, L., and Schneider, P. (2001). Recombinant *Microdochium nivale* carbohydrate oxidase and its application in an amperometric glucose sensor. Biosenss. Bioelectron. *16*, 319–324.

Kurasawa, T., Yachi, M., Suto, M., Kamagata, Y., Takao, S., and Tomita, F. (1992). Induction of cellulase by gentiobiose and its sulfur-containing analog in *Penicillium purpurogenum*. Appl. Environ. Microbiol. *58*, 106–110.

Langston, J., Sheehy, N., and Xu, F. (2006). Substrate specificity of *Aspergillus oryzae* family 3 β-glucosidase. Biochim. Biophys. Acta *1764*, 972–978.

Letunic, I., and Bork, P. (2021). Interactive Tree Of Life (iTOL) v5: an online tool for phylogenetic tree display and annotation. Nucleic Acids Res. *49*, W293–W296.

Li, R., Li, Y., Kristiansen, K., and Wang, J. (2008). SOAP: short oligonucleotide alignment program. Bioinformatics *24*, 713–714.

Liu, Z., Xiong, Y., Yi, L., Dai, R., Wang, Y., Sun, M., Shao, X., Zhang, Z., and Yuan, S.

(2018). Endo-β-1,3-glucanase digestion combined with the HPAEC-PAD-MS/MS analysis reveals the structural differences between two laminarins with different bioactivities. Carbohydr. Polym. *194*, 339–349.

Marchessault, R.H., and Deslandes, Y. (1979). Fine structure of (1→3)-β-D-glucans: curdlan and paramylon. Carbohydr. Res. *75*, 231–242.

Martin, K.L., McDougall, B.M., Unkles, S.E., and Seviour, R.J. (2006). The three β-1,3-glucanases from *Acremonium blochii* strain C59 appear to be encoded by separate genes. Mycol. Res. *110*, 66–74.

Marin-Felix, Y., Hernández-Restrepo, M., Wingfield, M.J., Akulov, A., Carnegie, A.J., Cheewangkoon, R., Gramaje, D., Groenewald, J.Z., Guarnaccia, V., and Halleen, F. (2019). Genera of phytopathogenic fungi: GOPHY 2. Stud. Mycol. *92*, 47–133.

Matthews, B.W. (1968). Solvent content of protein crystals. J. Mol. Biol. *33*, 491–497.

McCoy, A.J., Grosse-Kunstleve, R.W., Adams, P.D., Winn, M.D., Storoni, L.C., and Read, R.J. (2007). Phaser crystallographic software. J. Appl. Crystallogr. *40*, 658–674.

Menshova, R.V., Ermakova, S.P., Anastyuk, S.D., Isakov, V.V., Dibrovskaya, Y.V., Kusaykin, M.I., Um, B.H., and Zvyagintseva, T.N. (2014). Structure, enzymatic transformation and anticancer activity of branched high molecular weight laminaran from brown alga *Eisenia bicyclis*. Carbohydr. Polym. *99*, 101–109.

Mesterházy, Á., Bartók, T., Kászonyi, G., Varga, M., Tóth, B., and Varga, J. (2005). Common resistance to different *Fusarium* spp. Causing *Fusarium* head blight in wheat. Eur. J. Plant Pathol. *112*, 267–281.

Millet, N., Moya-Nilges, M., Sachse, M., Locker, J.K., Latgé, J., and Mouyna, I. (2019). *Aspergillus fumigatus* exoβ(1-3)glucanases family GH55 are essential for conidial cell wall morphogenesis. Cell. Microbiol. *21*, e13102.

Mirdita, M., Schütze, K., Moriwaki, Y., Heo, L., Ovchinnikov, S., and Steinegger, M. (2022). ColabFold: making protein folding accessible to all. Nat. Methods *19*, 679–682.

Miwa, I., Okudo, J., Maeda, K., and Okuda, G. (1972). Mutarotase effect on colorimetric determination of blood glucose with β-D-glucose oxidase. Clin. Chim. Acta *37*, 538–540.

Miyagawa, A. (2018). Chemical synthesis of β-(1,3)-glucan oligosaccharide and its application. Trends Glycosci. Glycotechnol. *30*, E117–E127.

Miyagawa, A., Matsuda, T., and Yamamura, H. (2015). Synthesis of branched tetrasaccharide derivatives of schizophyllan-like β-glucan. J. Carbohydr. Chem. *34*, 215–246.

Mouyna, I., Hartl, L., and Latgé, J.P. (2013). β-1,3-Glucan modifying enzymes in *Aspergillus fumigatus*. Front. Microbiol. *4*, 81.

Nakajima, M., Yamashita, T., Takahashi, M., Nakano, Y., and Takeda, T. (2012). Identification, cloning, and characterization of β-glucosidase from *Ustilago esculenta*. Appl. Microbiol. Biotechnol. *93*, 1989–1998.

Ning, J., Zhang, W., Yi, Y., Yang, G., Wu, Z., Yi, J., and Kong, F. (2003). Synthesis of β-(1→6)-branched β-(1→3) glucohexaose and its analogues containing an α-(1→3) linked bond with antitumor activity. Bioorg. Med. Chem. *11*, 2193–2203.

Nishimura, D., Hasegawa, A., and Nakajima, M. (1972). Solvent effect and anchimeric assistance on α-glycosylation. Agric. Biol. Chem. *36*, 1767–1772.

Nobe, R., Sakakibara, Y., Fukuda, N., Yoshida, N., Ogawa, K., and Suiko, M. (2003). Purification and characterization of laminaran hydrolases from *Trichoderma viride*. Biosci. Biotechnol. Biochem. *67*, 1349–1357.

Nobe, R., Sakakibara, Y., Ogawa, K., and Suiko, M. (2004). Cloning and expression of a novel *Trichoderma viride* laminarinase AI gene (lamAI). Biosci. Biotechnol. Biochem. *68*, 2111–2119.

Nordkvist, M., Nielsen, P.M., and Villadsen, J. (2007). Oxidation of lactose to lactobionic acid by a *Microdochium nivale* carbohydrate oxidase: Kinetics and operational stability. Biotechnol. Bioeng. *97*, 694–707.

Nukada, T., Berces, A., Zgierski, M.Z., and Whitfield, D.M. (1998). Exploring the mechanism of neighboring group assisted glycosylation reactions. J. Am. Chem. Soc. *120*, 13291–13295.

Ooi, T., Sato, H., Matsumoto, K., and Taguchi, S. (2009). A unique post-translational processing of an exo-β-1,3-glucosidase of *Penicillium* sp. KH10 expressed in *Aspergillus oryzae*. Protein Expr. Purif. *67*, 126–131.

Pace, C.N., Vajdos, F., Fee, L., Grimsley, G., and Gray, T. (1995). How to measure and predict the molar absorption coefficient of a protein. Protein Sci. *4*, 2411–2423.

Pang, Z., Otaka, K., Maoka, T., Hidaka, K., Ishijima, S., Oda, M., and Ohnishi, M. (2005). Structure of β-glucan oligomer from laminarin and its effect on human monocytes to inhibit the proliferation of U937 cells. Biosci. Biotechnol. Biochem. *69*, 553–558.

Papageorgiou, A.C., Chen, J., and Li, D. (2017). Crystal structure and biological implications of a glycoside hydrolase family 55 β-1,3-glucanase from *Chaetomium thermophilum*. Biochim. Biophys. Acta Proteins Proteom. *1865*, 1030–1038.

Piršelová, B., and Matušíková, I. (2013). Callose: the plant cell wall polysaccharide with multiple biological functions. Acta Physiol. Plant. *35*, 635–644.

Pitson, S.M., Seviour, R.J., and McDougall, B.M. (1993). Noncellulolytic fungal β-glucanases: Their physiology and regulation. Enzyme Microb. Technol. *15*, 178–192.

Reese, E.T., and Mandels, M. (1959). β-D-1,3 glucanases in fungi. Can. J. Microbial. *5*, 173–185.

Rinaudo, M., and Vincendon, M. (1982). ^{13}C NMR structural investigation of scleroglucan. Carbohydr. Polym. *2*, 135–144.

Robert, X., and Gouet, P. (2014). Deciphering key features in protein structures with the new ENDscript server. Nucleic Acids Res. *42*, W320–W324.

Roy, S., Chakraborty, A., and Ghosh, R. (2008). Aryl 4,6-*O*-arylidene-1-thio-β-D-glycopyranoside-based new organogelators and their gels. Carbohydr. Res. *343*, 2523–2529.

Samuels, G.J., and Hallett, I.C. (1983). *Microdochium stoveri* and *Monographella stoveri*, new combinations for *Fusarium stoveri* and *Micronectriella stoveri*. Trans. Br. Mycol. Soc. *81*, 473–483.

Sandrock, R.W., DellaPenna, D., and VanEtten, H.D. (1995). Purification and characterization of β_2-tomatinase, an enzyme involved in the degradation of α-tomatine and isolation of the gene encoding β_2-tomatinase from *Septoria lycopersici*. Mol. Plant Microbe Interact. *8*, 960–970.

Schägger, H., Cramer, W.A., and von Jagow, G. (1994). Analysis of molecular masses and oligomeric states of protein complexes by blue native electrophoresis and isolation of membrane protein complexes by two-dimensional native electrophoresis. Anal. Biochem. *217*, 220–230.

Scheller, H.V., and Ulskov, P. (2010). Hemicelluloses. Annu. Rev. Plant Biol. *61*, 263–289.

Seidle, H.F., and Huber, R.E. (2005). Transglucosidic reactions of the *Aspergillus niger* family 3 β-glucosidase: Qualitative and quantitative analyses and evidence that the transglucosidic rate is independent of pH. Arch. Biochem. Biophys. *436*, 254–264.

Simpson, J.T., Wong, K., Jackman, S.D., Schein, J.E., Jones, S.J., and Birol, I. (2009). AbySS: a parallel assembler for short read sequence data. Genome Res. *19*, 1117–1123.

Smaali, M.I., Michaud, N., Marzouki, N., Legoy, M.D., and Maugard, T. (2004). Comparison of two β-glucosidases for the enzymatic synthesis of β-(1-6)-β-(1-3)-gluco-oligosaccharides. Biotechnol. Lett. *26*, 675–679.

Suto, M., and Tomita, F. (2001). Induction and catabolite repression mechanisms of cellulase in fungi. J. Biosci. Bioeng. *92*, 305–311.

Suzuki, K., Sumitani, J.I., Nam, Y.W., Nishimaki, T., Tani, S., Wakagi, T., Kawaguchi, T., and Fushinobu, S. (2013). Crystal structures of glycoside hydrolase family 3 β-glucosidase 1 from *Aspergillus aculeatus*. Biochem. J. *452*, 211–221.

Takada, G., Kawaguchi, T., Sumitani, J., and Arai, M. (1998). Expression of *Aspergillus aculeatus* No. F-50 cellobiohydrolase I (*cbhI*) and β-glucosidase 1 (*bgl1*) genes by *Saccharomyces cerevisiae*. Biosci. Biotechnol. Biochem. *62*, 1615–1618.

Takahashi, M., Konishi, T., and Takeda, T. (2011). Biochemical characterization of *Magnaporthe oryzae* β-glucosidases for efficient β-glucan hydrolysis. Appl. Microbiol. Biotechnol. *91*, 1073–1082.

Takeo, K., and Tei, S. (1986). Synthesis of the repeating units of schizophyllan. Carbohydr. Res. *145*, 293–306.

Tanaka, H., Amaya, T., and Takahashi, T. (2003). Parallel synthesis of multi-branched oligosaccharides related to elicitor active pentasaccharide in rice cell based on orthogonal deprotection and glycosylation strategy. Tetrahedron Lett. *44*, 3053–3057.

Tanaka, H., Kawai, T., Adachi, Y., Hanashima, S., Yamaguchi, Y., Ohno, N., and Takahashi, T. (2012). Synthesis of β(1,3) oligoglucans exhibiting a Dectin-1 binding affinity and their biological evaluation. Bioorg. Med. Chem. *20*, 3898–3914.

Tanaka, N., Nakajima, M., Aramasa, H., Nakai, H., Taguchi, H., Tsuzuki, W., and Komba, S. (2018). Synthesis of three deoxy-sophorose derivatives for evaluating the requirement of hydroxy groups at position 3 and/or 3’ of sophorose by 1,2-β-oligoglucan phosphorylases. Carbohydr. Res. *468*, 13–22.

Tronsmo, A.M., Hsiang, T., Okuyama, H., and Nakajima, T. (2001). Low temperature diseases caused by *Microdochium nivale*. In Low temperature plant microbe interactions under snow, Iriki N, Gaudet DA, Tronsmo AM, Matsumoto N, Yoshida M, Nishimune A ed. (Hokkaido National Agricultural Experimental Station), pp. 75–86.

Trott, O., and Olson, A.J. (2010). AutoDock Vina: improving the speed and accuracy of docking with a new scoring function, efficient optimization and multithreading. J. Comput. Chem. *31*, 455–461.

Tsers, I., Marenina, E., Meshcherov, A., Petrova, O., Gogoleva, O., Tkachenko, A., Gogoleva, N., Gogolev, Y., Potapenko, E., Muraeva, O., Ponomareva, M., Korzun, V., and Gorshkov, V. (2023). First genome-scale insights into the virulence of the snow mold causal fungus *Microdochium nivale*. IMA Fungus *14*, 2.

Usui, T., Yamaoka, N., Matsuda, K., Tuzimura, K., Sugiyama, H., and Seto, S. (1973). ^{13}C nuclear magnetic resonance spectra of glucobioses, glucotrioses, and glucans. J. Chem. Soc., Perkin 1, 2425–2432.

Varghese, J.N., Hrmova, M., and Fincher, G.B. (1999). Three-dimensional structure of a barley β-D-glucan exohydrolase, a family 3 glycosyl hydrolase. Structure *7*, 179–190.

Vetvicka, V., and Yvin, J.C. (2004). Effects of marine β-1,3 glucan on immune reactions. Int. Immunopharmacol. *4*, 721–730.

Walton, J.D. (1994). Deconstructing the cell wall. Plant Physiol. *104*, 1113–1118.

Xu, F., Golightly, E.J., Fuglsang, C.C., Schneider, P., Duke, K.R., Lam, L., Christensen, S., Brown, K.M., Jørgensen, C.T., Brown, S.H. (2001). A novel carbohydrate:acceptor oxidoreductase from *Microdochium nivale*. Eur. J. Biochem. *268*, 1136–1142.

Yang, G., and Kong, F. (2000). Synthesis of a glucoheptaose - the repeating unit of lentinan. Synlett *10*, 1423–1426.

Yang, G., and Kong, F. (2005). Synthesis of heptasaccharide and nonasaccharide analogues of the lentinan repeating unit. Carbohydr. Res. *340*, 39–48.

Zeng, Y., and Kong, F. (2003). Synthesis of 3,6-branched β-D-glucose oligosaccharides. J. Carbohydr. Chem. *22*, 881–890.

Zerbino, D., and Birney, E. (2008). Velvet: algorithms for de novo short read assembly using de Bruijn graphs. Genome Res. *18*, 821–829.

Zhang, Y., He, H., Chen, Z., Huang, Y., Xiang, G., Li, P., Yang, X., Lu, G., and Xiao, G. (2021). Merging reagent modulation and remote anchimeric assistance for glycosylation: highly stereoselective synthesis of α-glycans up to a 30-mer. Angew. Chem. Int. Ed. Engl. *60*, 12597–12606.

Zhang, Y., Kong, H., Fang, Y., Nishinari, K., and Phillips, G.O. (2013). Schizophyllan: A review on its structure, properties, bioactivities and recent developments. Bioact. Carbohydr. Diet. Fibre *1*, 53–71.

Zhang, Y., Li, S., Wang, X., Zhang, L., and Cheung, P.C.K. (2011). Advances in lentinan: Isolation, structure, chain conformation and bioactivities. Food Hydrocoll. *25*, 196–206.

Zhao, W., Yang, G., and Kong, F. (2003). Synthesis of two heptasaccharide analogues of the lentinan repeating unit. Carbohydr. Res. *338*, 2813–2823.

Zhou, X., Long, Q., Li, D., Gao, J., Sun, Q., Sun, S., Su, Y., Wang, P., Peng, W., and Li, M. (2021). Convergent synthesis of branched β-glucan tridecasaccharides ready for conjugation. Synthesis *53*, 2435–2448.

ACKNOWLEDGEMENTS

First of all, I would like to express my sincere gratitude to my first advisor, Professor Haruhide Mori for his kindly suggestion throughout my project and giving me words of encouragement supervision. Besides, I deeply appreciate Associate Professor Wataru Saburi for guidance and his help in progressing my research.

I would also like to thank Professor Haruhide Mori, Professor Hideyuki Matsuura, Professor Masayuki Okuyama and Associate Professor Wataru Saburi for their guidance and encouragement in preparing this paper.

I would like to thank Dr. Ryozo Imai, Institute of Agrobiological Science, National Agriculture and Food Research Organization, for his advice on the execution of research related to snow mold. I am grateful to Dr. Shiro Komba, Institute of Food Research, National Agriculture and Food Research Organization, for his guidance and advice on the chemical synthesis of oligosaccharides and analysis of chemicals. Regarding the X-ray crystal structure analysis of proteins, I would like to thank Professor Emeritus Min Yao, Graduate School of Life Science, Hokkaido University, Associate Professor Jian Yu, Institute for Protein Research, Osaka University, Associate Professor Keitaro Yamashita, Research Center for Advanced Science and Technology, the University of Tokyo, and Assistant Professor Takayoshi Tagami, Research Faculty of Agriculture, Hokkaido University. Regarding the whole genome sequencing of *M. nivale*, I am grateful to Professor Tom Hsiang, School of Environmental Sciences, University of Guelph, and Dr. Linda Elizabeth Jewell, St. John's Research and Development Center, Agriculture and Agri-Food Canada. I would like to thank Dr. Eri Fukushi, GC-MS & NMR Room, Research Faculty of Agriculture, Hokkaido University for her cooperation in the measurement of NMR. I am grateful to Associate Professor Naoki Kitaoka, Research Faculty of Agriculture, Hokkaido University, for his help on the optical rotation analysis. I would like to express my gratitude to Ms. Seiko Oka, Mr. Tomohiro Hirose, Ms. Nozomi Takeda, Ms. Nao Yamashita, and Ms. Harumi Hayashi, the Instrumental Analysis Division, Global Facility Center, Creative Research Institution, Hokkaido University for protein identification analysis, N-terminal amino acid sequence analysis, amino acid analysis, and ESI-MS analysis. I would like to thank Professor Emeritus Hirokazu Matsui of the Research Faculty of Agriculture, Hokkaido University for giving us an opportunity to think deeply about how to live as a researcher. This work was partly supported by JST, the establishment of university fellowships towards the creation of science technology innovation, Grant Number JPMJFS2101.

I would like to express our sincere gratitude to all the graduates and current students of Biochemistry Laboratory. Finally, I would like to express my deep gratitude to my parents who warmly watched over my student life and supported me financially and mentally.

Tomoya Ota

謝辞

本研究を遂行するにあたり，懇切なるご指導ならびにご鞭撻を賜りました本学大学院農学研究院 生物化学研究室 森春英 教授，佐分利亘 准教授に心より厚く御礼申し上げます.

また，本論文を作成するにあたり，ご指導，ご鞭撻をいただきました北海道大学大学院農学研究院 森春英 教授，松浦英幸 教授，奥山正幸 教授，および佐分利亘 准教授に感謝いたします.

雪腐病菌に関わる研究につきましてご指導，ご助言を賜りました国立研究開発法人農業・食品産業技術総合研究機構 生物機能利用研究部門 今井亮三 博士に深く感謝申し上げます.

オリゴ糖の有機合成ならびに化合物の分析に関し多くのご指導，ご助言を賜りました国立研究開発法人農業・食品産業技術総合研究機構 食品研究部門 今場司朗 博士に心より感謝いたします.

タンパク質の X 線結晶構造解析につきましては，本学大学院先端生命科学研究院 姚閔 名誉教授，大阪大学蛋白質研究所 于健 特任准教授，東京大学先端科学技術研究センター 山下恵太郎 准教授，ならびに本学大学院農学研究院 田上貴祥 助教にご助言，ご協力いただき感謝いたします.

雪腐病菌のゲノム解析では，ゲルフ大学 Tom Hsiang 教授およびカナダ農務省 Linda Elizabeth Jewell 博士にご助言，ご協力いただき感謝申し上げます.

NMR の測定にご協力いただきました，本学大学院農学院 GC-MS & NMR 測定室 福士江里 博士に感謝申し上げます。

有機合成した化合物の旋光度の測定では，本学大学院農学研究院 北岡直樹 准教授にご協力いただき，感謝いたします.

LC-MS/MS によるタンパク質の同定，N 末端アミノ酸配列解析，アミノ酸組成分析，および質量分析では，本学創生研究機構 グローバルファシリティセンター 機器分析受託部門 岡征子 氏，廣瀬知弘 氏，武田希美 氏，山下奈緒 氏，林治美 氏にご協力いただき，厚く御礼申し上げます.

研究者としてのあり方を考えるきっかけを与えていただきました，本学大学院農学研究院 松井博和 名誉教授に感謝申し上げます.

本研究の一部は、JST 科学技術イノベーション創出に向けた大学フェローシップ創設事業 JPMJFS2101 の支援を受けたものです。厚く御礼申し上げます.

本学大学院農学院 生物化学研究室の卒業生と在校生の皆様には日々の研究活動や私生活で様々な形で支えていただきました．心より感謝申し上げます。

最後になりましたが，学生生活を温かく見守り，経済的・精神的に支えてくださった両親に深く感謝いたします。

太田 智也